RADIOLABELED BIVALENT PEPTIDE LIGANDS FOR PROSTATE CANCER IMAGING

A Dissertation

Presented to

the Faculty of the Graduate School

at the University of Missouri-Columbia

In Partial Fulfillment

of the Requirements for the Degree

Doctor of Philosophy

---

by

ZONGRUN JIANG

Dr. Silvia S. Jurisson and Dr. Charles J. Smith, Dissertation Supervisors

DECEMBER 2015

The undersigned, appointed by the dean of the Graduate School, have examined the dissertation entitled

presented by Zongrun Jiang,

a candidate for the degree of doctor of philosophy,

and hereby certify that, in their opinion, it is worthy of acceptance.

_____

Professor Silvia Jurisson

_____

Professor Charles Smith

_____

Professor Susan Lever

_____

Professor Mark Lee

ACKNOWLEDGMENTS

At this moment I would like to thank my advisors who supported me academically with their oversight and experience during my pursuit of the Degree Doctor of Philosophy in the University of Missouri-Columbia. I would like to thank my advisor Dr. Silvia Jurisson for your valuable suggestions and guidance. It was you who introduced me to the field of radiochemistry. Thank you for always being warm and helpful to me. I would also like to thank my advisor Dr. Jeff Smith, who led me to the field of radiopharmaceuticals and supported me to accomplish research projects step by step. I really appreciate all the effort you have made to train me into a good radiochemist. It is my honor working in your lab. I would like to thank the other members on my committee, Dr. Susan Lever and Dr. Mark Lee. I truly appreciate your time and warm advices.

I would also like to thank those who have helped me and worked with me closely in the laboratory. Dr. Prasad Bandari, thank you for showing me how to run the lab and helping me solve practical problems. I learned a lot from you and your rich research experience. Brie Wienhoff, thank you for helping me get familiar with everything in the lab and providing knowledge and supports of radioactivity safety. Dr. Kubra Durkan, thank you for your warm guidance and encouragement to cheer me up when I come across any setback.

I also own thanks to the collaboration and support I received from the research groups in the Harry S. Truman VA hospital Radiopharmaceutical Sciences Institute and the MU Chemistry department for their help in my research projects. Tammy Rold, I always feel cozy to talk with you not only because of your professional support but also your constant cheerfulness. I really appreciate your help and valuable advice on my *in vivo* studies. Ashley F. Szczodroski, thank you for helping me with imaging studies. Thank you to Dr. Fabio Gallazzi for his help with characterization of my samples with mass spectrum.

Finally, I am grateful to my parents who understand and encourage me to finish this doctoral career, to my friends who are always there ready for sharing joys and sorrows, and to all the people who care for me.

The work was supported with resources and the use of facilities at the Harry S. Truman Memorial Veterans' Hospital in Columbia (HSTMVH), MO, 65201 and the University of Missouri, School of Medicine, Columbia, MO 65211, USA and the University of Missouri, Department of Chemistry, Columbia, MO 65211, USA.

TABLE OF CONTENTS

CHAPTER 2: COPPER-64 NODAGA DUPA/BBN(7-14)NH_2 BIVALENT LIGAND FOR POTENTIAL DIAGNOSTIC IMAGING OF PROSTATE CANCER

CHAPTER 3: COPPER-64 NOTA RGD/RM2 BIVALENT LIGAND FOR POTENTIAL DIAGNOSTIC IMAGING OF PROSTATE CANCER

CHAPTER 4: GALLIUM-67/GALLIUM-68/COPPER-64 DOTA RGD/RM2 BIVALENT LIGAND FOR POTENTIAL DIAGNOSTIC IMAGING OF PROSTATE CANCER

LIST OF FIGURES

Figure Page

LIST OF TABLES

LIST OF ABBREVIATION

Abbreviation	Definition
3D	Three-dimensional
5-Ava	5-aminovaleric acid
6-Ahx	6-aminohexanoic acid
A	Alanine
BBN	Bombesin
BFCA	Bifunctional chelate approach
BSA	Bovine serum albumin
CT	Computed tomography
DIPEA	Dissopropylethylamine
DMF	Dimethylformamide
DOTA	1,4,7,10-tetraazacyclododecane-1,4,7,10-tetraacetic acid
DTPA	Diethylenetriaminepentaacetic acid
EDC	1-ethyl-3-[3-dimethylaminopropyl]carbodiimide hydrochloride
EDTA	Ethylenediamine tetraacetic acid
ESI-MS	Electrospray ionization-mass spectroscopy
Fmoc	9-Fluorenylmethyloxycarbonyl
G	Glycine
GRP	Gastrin releasing peptide
GRPR	Gastrin releasing peptide receptor
H	Histidine

HBTU	O-Benzotriazole-N,N,N’,N’-tetramethyl-uronium-hexafluoro-phosphate
HOBt	Hydroxybenzotriazole
IC_{50}	Half maximal inhibitory concentration
L	Lysine
M	Methionine
MES	2-[morpholino]ethanesulfonic acid
NODAGA	[2-(4,7-biscarboxymethyl)-1,4,7-(triazonan-1-yl)pentanedioic acid]
NOTA	1,4,7-triazacyclononane-1,4,7-triacetic acid
PBS	Phosphate buffered saline
PET	Positron-emission tomography
Q	Glutamine
SCID	Severe combined immunodeficient
SD	Standard deviation
SPECT	Single photon emission computed tomography
SPPS	Solid phase peptide synthesis
Sulfo-NHS	N-hydroxysulfosuccinimide
RP-HPLC	Reverse phase high performance liquid chromatography
$t_{1/2}$	Half-life
t_R	Retention time
TETA	1,4,8,11-tetraazacyclotetradecane-1,4,8,11-tetraacetic acid
TFA	Trifluoroacetic acid

UV	Ultraviolet
V	Valine
W	Tryptophan

RADIOLABELED BIVALENT PEPTIDE LIGANDS FOR PROSTATE CANCER IMAGING

Zongrun Jiang

Professor Silvia S. Jurisson, Dissertation Advisor

Professor Charles J. Smith, Dissertation Advisor

ABSTRACT

Peptide ligand has been a field of great interest for decades due to its capability of binding to specific receptors that are over-expressed in human tumors. Currently, the so-called bivalent peptide ligand, a radiotracer that has two types of targeting motifs for two different biomarkers, has become an active field of research. The synthesis, characterizations, and *in vitro/in vivo* biological evaluations of bivalent peptide ligands are discussed in this dissertation.

One biomarker of great interest is the gastrin-releasing peptide receptor (GRPR) due to its high expression on prostate cancer. The amphibian peptide, bombesin (BBN), is well known for its high affinity and specificity to GRPR. The peptide targeting motif for GRPR are BBN analogues, BBN(7-14)NH_2 and RM2, which have strong binding affinity to GRPR. BBN(7-14)NH_2 is an agonist peptide for GRPR. RM2 is an antagonist peptide for GRPR. The second biomarker of interest is the prostate specific membrane antigen (PSMA) due to its high expression on prostate cancer and low expression on normal tissues. For this target, a small molecule, DUPA (2-[3-(1,3-Bis-tert-butoxycarbonylpropyl)-ureido]pentanedioic acid), which is a urea derivative with strong binding affinity to PSMA, is used as the targeting motif. The third biomarker of interest

is the $\alpha_V\beta_3$ integrin due to its considerable expression in human prostate cancer and important role in modulation of cell migration and survival during angiogenesis, which facilitates invasion of the tumors cells across the blood vessels. The targeting motif used for the integrin receptor is c(RGDyK) or RGD, a cyclic peptide, which has high binding affinity to the $\alpha_V\beta_3$ integrin. The goal of the thesis was to produce, characterize, radiolabeled with suitable radionuclides ($^{67/68}$Ga/^{64}Cu), and *in vitro/ in vivo* evaluate bivalent ligands that contain two of the targeting motifs.

My first aim was to synthesize and investigate a GRPR/PSMA dual targeting bivalent ligand. The bivalent ligand conjugate, [DUPA-6-Ahx-(NODAGA)-5-Ava-BBN(7-14)NH_2], was synthesized, purified by reversed-phase high performance liquid chromatography (RP-HPLC), confirmed via electrospray ionization mass spectrometry (ESI-MS), and then metallated with $^{nat/64}CuCl_2$. The metallated ligand, [DUPA-6-Ahx-(^{nat}Cu-NODAGA)-5-Ava-BBN(7-14)NH_2], was evaluated *in vitro* via competitive displacement binding assays (IC_{50} = 11.1 ± 0.46 nM in PC-3 cells, IC_{50} = 1.16 ± 1.35 nM in LNCaP cells). MicroPET/CT images of PC-3 tumor-bearing severe combined immunodeficient (SCID) and LNCaP tumor-bearing athymic nude mice were obtained at 18 h post-injection (p.i.) of [DUPA-6-Ahx-(^{nat}Cu-NODAGA)-5-Ava-BBN(7-14)NH_2]. The study demonstrated the capability of the bivalent ligand to target both biomarkers. However, further optimizations of the ligand are warranted for superior pharmacokinetics *in vivo*.

My second aim was to synthesize and investigate a GRPR/$\alpha_v\beta_3$ dual targeting bivalent ligand. The first bivalent ligand, [RGD-Glu-(NO2A)-6-Ahx-RM2], was synthesized, purified via RP-HPLC, characterized via ESI-MS, and then metallated with $^{nat/64}$Cu. The ^{nat}Cu-metallated ligand was evaluated *in vitro* via competitive displacement binding assays (IC_{50} = 3.09 ± 0.34 nM in PC-3 cells, IC_{50} = 518 ± 37.5 nM in U87-MG cells). *In vivo* biodistribution studies of [RGD-Glu-(^{64}Cu-NO2A)-6-Ahx-RM2] were conducted in normal CF-1 mice and PC-3 tumor-bearing SCID mice. The results showed high tumor uptake and retention in PC-3 tumor-bearing SCID mice (4.86 ± 1.01 %ID/g at 1 h p.i., 4.26 ± 1.23 %ID/g at 24 h p.i.). High contrast microPET images of the tracer in

PC-3 tumor-bearing mice were obtained at 4 h p.i., indicating the strong capability of the tracer to target PC-3 tumor cells *in vivo*.

The second bivalent ligand for GRPR/$\alpha_v\beta_3$ dual targeting , [RGD-Glu-(DO3A)-6-Ahx-RM2] was synthesized, purified by RP-HPLC, characterized with ESI-MS, and metallated with $^{nat/67/68}$Ga or $^{nat/64}$Cu. The *in vitro* investigations of the binding affinities of the natural-metallated ligands for the GRPR or the $\alpha_v\beta_3$ integrin were performed via competitive displacement binding assays in human prostate PC-3 and glioblastoma U87-MG cell lines. Following stability investigations via RP-HPLC, the *in vivo* evaluations of the Ga^{67}/Cu^{64}-radiolabeled ligands were performed in CF-1 mice and SCID mice bearing PC-3 tumors. The *in vitro* studies of the natural-metallated ligands showed high binding affinities for the GRPR (7.78 ± 2.42, 8.64 ± 2.16 nM; Ga, Cu respectively) and moderate binding affinity for the $\alpha_v\beta_3$ integrin receptor (307 ± 0.0, 308 ± 42.6 nM; Ga, Cu respectively). *In vivo* biodistribution studies displayed high tumor uptake (7.44 ± 1.09, 10.85 ± 4.02%ID/g at 1 h post-intravenous injection; ^{67}Ga, ^{64}Cu respectively) and prolonged tumor retention (4.89 ± 1.11, 4.09 ± 0.96%ID/g at 24 h post-intravenous injection; ^{67}Ga, ^{64}Cu respectively) in PC-3 tumor-bearing mice. Micro-single photon emission computed tomography (microSPECT) and micro-positron emission computed tomography (microPET) molecular imaging studies produced high-quality, high-contrast images in PC-3 tumor-bearing mice at 18 h post-intravenous injection. Both radiolabeled ligands shows satisfactory tumor uptake and retention in PC-3 tumor-bearing mice. However, [RGD-Glu-(^{67}Ga-DO3A)-6-Ahx-RM2] demonstrates superior pharmacokinetic profiles to [RGD-Glu-(^{64}Cu-DO3A)-6-Ahx-RM2], presumably due to more favorable *in vivo* stability. The comparative studies on [RGD-Glu-(^{64}Cu/^{67}Ga-DO3A)-6-Ahx-RM2] demonstrated poor *in vivo* stability of ^{64}Cu-labeled DOTA conjugate and favorable pharmacokinetics of the ^{67}Ga-labeled tracer. As a result, superior in vivo behaviors of [RGD-Glu-(^{68}Ga-DO3A)-6-Ahx-RM2] are expected for future studies.

Chapter 1: INTRODUCTION

1.1 RADIOPHARMACEUTICALS

The development of radiopharmaceuticals has greatly changed the way of diagnosis and the treatment of disease nowadays. With the growing number of novel and sophisticated radiopharmaceuticals being designed, synthesized, and evaluated, the area of nuclear medicine has been established as a relatively new field of medicine, which is a highly interdisciplinary area incorporating chemistry, biology, and pathology. Radiopharmaceuticals are basically any drug that contains radioactive nuclides whose nuclear emissions are captured by clinical detection instrumentation for imaging and therapy of the disease. The drug or ligand with the radionuclide attached composes the radiopharmaceutical (also termed radioligand), which possesses the property to bind to certain places of interest in the body. As a result, the radionuclide is delivered and accumulates where the drug binds *in vivo*. Determined by the advanced clinical imaging modalities, the *in vivo* localization and distribution of the radioisotope delivered into the patient by the radiopharmaceutical provides the capability of demonstrating important information related with a specific biological process or the mapping of cancer cells. Single photon emission computed tomography (SPECT) and positron emission tomography (PET) are two primary clinical detection modalities that have been largely utilized to generate three dimensional spatial distribution of radionuclide density *in vivo* in combination with computed tomography (CT) in order to specifically investigate either a biological target or process. SPECT is a nuclear medicine tomographic imaging technique using gamma cameras to measure gamma rays emitted by the gamma emitting radionuclide delivered by the radiopharmaceutical into the patient generally through

injection into the bloodstream. PET is another important and useful nuclear medicine tomographic imaging technique using gamma cameras to measure pairs of annihilation photons emitted indirectly by the positron emitting radionuclide delivered by the radiopharmaceutical into the patient, generally through injection into the bloodstream. CT is a computed tomographic technique using combination of many X-ray images taken from different angles to generate cross-sectional images of places of interest. Three-dimensional images of the radioligand concentration within the body can be consequently determined by SPECT or PET with the aid of a CT X-ray scan performed on the patient at the same time. It is the effort in research towards exploiting biological targeting radioligands with new structures in combination with the improvement of imaging instrumentation that has the potential to push the further development of the field of nuclear medicine to satisfy the growing needs from patient care with regards to both diagnosis and therapy.

The history of radiopharmaceutical design in the past decades has been driven by our increasingly advanced understanding of not only physiological processes, but also the disease processes at molecular level. The understanding is due to the cellular or sub-cellular discoveries via flourishing research in biochemistry, pharmacology, immunology, and molecular biology. The focus of the research in radioligands has been emphasized on the choice and production of radionuclides, the synthesis and biological studies of the biomolecules as targeting vectors towards places of interest *in vivo*, and the development of chelation technologies or radiometal conjugation techniques. The first radiopharmaceutical applied in clinical nuclear imaging can be traced back to 1925 when Dr. Hermann Blumgart and Dr. Otto Yens monitored blood flow via injecting 1-6 mCi of

bismuth-214 (^{214}Bi), also known as Radium C. In 1936, phosphorous-32 (^{32}P) became the first nuclear medicine isotope used in therapeutic application by Dr. John Lawrence to treat leukemia. The focus of nuclear medicine was on whole organ targeting up until the radioligand, a coordination complex containing a radionuclide, was developed. For example, technetium-99m labeled DTPA (diethylenetriaminepentaacetic acid) was developed by W. Eckelman and P. Richards in 1970. In the 1970's, the receptor-specific radiopharmaceutical, a radioisotope incorporated molecular targeting vector for receptor-specific uptake, began to receive the greatest amount of attention for research [1]. The investigations of these radioligands pushed the development of nuclear medicine in tumor targeting based on specific antigens, receptors, metabolic pathways, and DNA.

This dissertation emphasizes the imaging of cancer cells using radiopharmaceuticals. The general design of a radiotracer capable of selectively binding to tumor cells is discussed. By utilizing bioactive molecules as targeting vectors or ligands to bind to the biomarkers that are overexpressed on tumors, most of the dose is delivered to and retained at tumors while minimizing the radiolysis effect in parallel normal tissues. One important method of the various ways of coupling the radionuclide to the targeting vector is using the bifunctional chelate approach (BFCA), where a bifunctional chelating agent is employed to coordinate the radiometal meanwhile linking to the targeting motif [2]. Additionally, linkers or spacers are also used to link the chelator and the targeting motif in order to maintain the biological activity of the targeting motif via keeping the radionuclide an appropriate distance from the targeting vector. Furthermore, the hydrophilicity of the tracer can be adjusted by selecting certain pharmacokinetic modifiers as linkers to optimize the pharmacokinetics of the radioligand

[3, 4]. The basic structure of the radiopharmaceutical based on the design mentioned above is shown in Figure 1.1. The considerations of the construction for each part of this system involves many factors. First of all, the choice of radionuclide must be focused on selecting radioisotopes with appropriate nuclear properties for the designed applications, including the decay mode, emission energies, and the physical half-life. Secondly, the targeting vector is supposed to be a biomolecule with strong and specific binding affinity to the targeted receptors or biomarkers expressed on the places of interest such as cancer, so that the radioactive effects on normal tissues can be minimized. Thirdly, the selection of the bifunctional chelating agent and the spacer are also a very important aspect with respect to *in vivo* stability and pharmacokinetics of the radiotracer. Further considerations on the design of the radioligand in my research will be discussed in greater detail.

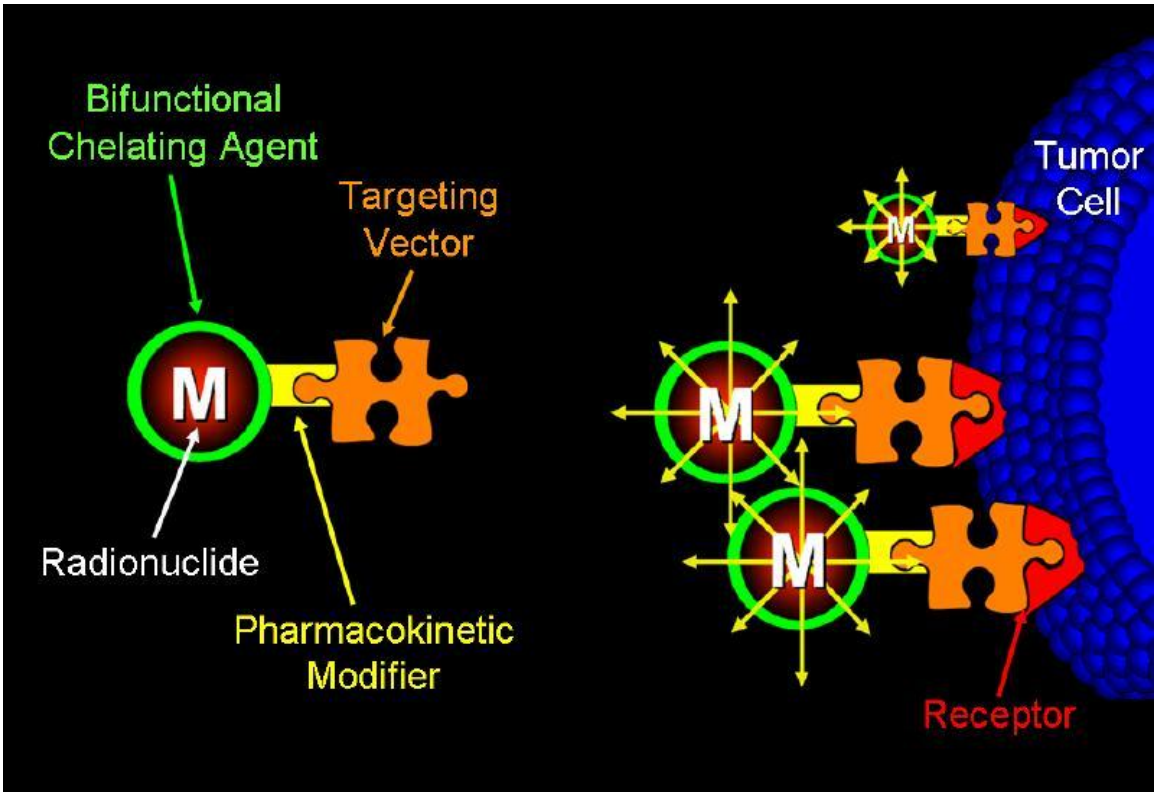

Fig. 1.1: Schematic of the structure and targeting of a site-directed radiopharmaceutical.

1.2 DIAGNOSTIC RADIONUCLIDES – COPPER-64 AND GALLIUM-68

The choice of radionuclides used for diagnostic applications of SPECT/CT or PET/CT is affected by various factors including the means of production, physical half-life, energy of emission, type of energetic emission, and the chemistry required to incorporate the radioisotope onto the targeting vectors. For diagnostic purposes, nuclides with penetrating emissions such as gamma (γ) ray emitters or positron (β^+) emitters which can produce pairs of annihilation photons emitted in opposite directions through electron-positron annihilation. For therapeutic purposes, nuclides with emissions such as alpha (α) or beta (β^-) are preferred to deliver a dose to the lesion [5, 6]. However, the majority of current radiopharmaceuticals are intended for imaging purposes, especially for specific targeting of tumor cells when coupled into a biological targeting vector such as an antibody or a peptide, which can selectively bind to and accumulate at certain biomarkers expressed on the tumor cells.

Positron emission tomography (PET) is a nuclear imaging technique that features the opportunity of quantifying the tracer uptake with high sensitivity and a resolution superior to SPECT (single photon emission tomography). A radiopharmaceutical that is labeled with a positron emitter is required for PET use in molecular imaging. ^{11}C and ^{18}F are the most common isotopes used both in the literature and in clinical studies. For example, ^{18}F-Fluorodeoxyglucose (Figure 1.2) is a FDA approved diagnostic radiopharmaceutical routinely used for its capability of mimicking glucose *in vivo* to display changes in glucose metabolism [7]. However, the development of ^{11}C [$t_{1/2}$=20.4 min] or ^{18}F [$t_{1/2}$=109.8 min] labeled ligands is limited by the short half-lives of the two isotopes and comparably difficult chemistry of the incorporation of them with

biologically-functional molecules. For example, the short half-life of ^{11}C makes it unsuitable for evaluating the drug candidates in longer biological processes lasting from hours to days. In addition, the relatively complex chemistry of incorporating ^{11}C and ^{18}F into molecules of interest can lower the radiolabeling yield.

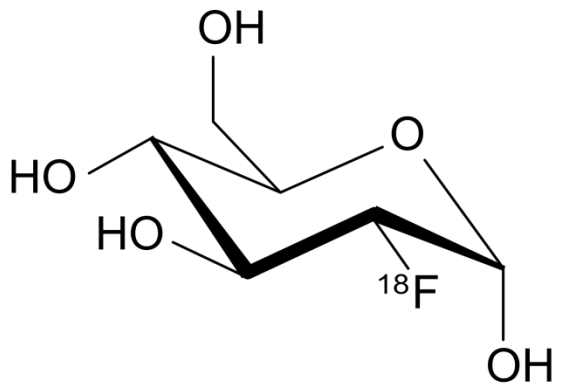

Fig. 1.2: Chemical structure of ^{18}F-Fluorodeoxyglucose.

With the growth of PET in clinical use over the past decade, there has been a rising interest in ^{68}Ga in recent years for the following reasons. First of all, similar to the production of ^{99m}Tc from the $^{99}Mo/^{99m}Tc$ generator, ^{68}Ga can be obtained from the $^{68}Ge/^{68}Ga$ generator, which is superior to the majority of positron emitters that are generated from a cyclotron for the reason of much lower cost and more convenience of the generator over the cyclotron. A radionuclide generator is composed of a relatively long-lived parent nuclide and a short-lived daughter nuclide that is the decay product of the parent nuclide [8]. The parent nuclide in the $^{68}Ge/^{68}Ga$ generator is ^{68}Ge, with a long half-life of 271 days, making it possible to act as a continuous ^{68}Ga source to support production of ^{68}Ga radiolabeled pharmaceuticals for PET use [9]. The separation methods of ^{68}Ga from ^{68}Ge have also been established based on their sufficiently different

chemical properties and classified into two main strategies. One is to use organic phenolic groups to form stable complexes with Ge(IV). The ^{68}Ga can be eluted with HCl in the forms of $^{68}GaCl^-_4$. The other is to use inorganic oxide matrices, such as Al_2O_3, SnO_2, Sb_2O_5, ZrO_2, and TiO_2, with ^{68}Ga eluted in HCl or EDTA (ethylenediamine tetraacetic acid) [10]. Secondly, ^{68}Ga is a good candidate for clinical application in PET due to its optimal nuclear characteristics. As a positron emitter, ^{68}Ga decays by positron emission [$E_{\beta+\ max}$=1.9 MeV, $E_{\beta+\ avg}$=0.74 MeV] in 89% yield. Moreover, the 68 min half-life of ^{68}Ga is compatible with drug process and imaging for small molecules and peptides that show much faster clearance from the normal tissues with comparison to large biological molecules such as antibodies. The high yield of the positron emission of ^{68}Ga, along with its convenient half-life, makes it a suitable positron emitter for PET imaging applications [11]. Thirdly, the coordination chemistry of gallium(III) has been well studied due to its great potential to be used in PET imaging. As a metal in the III A group of the periodic table, gallium only exists in the +3 oxidation state under physiological conditions. Ga^{3+} is determined to be a hard acid and prefers to coordinate with ionic and hard Lewis bases like nitrogen and oxygen atoms in carboxylate, phosphonate, and amino groups [12]. With an ionic radius of 62 pm, Ga^{3+} prefers the coordination number of 6 and is only stable under acidic conditions in solution [13]. Hydrolysis reactions of Ga^{3+} to form insoluble hydroxides of Ga^{3+} like $Ga(OH)_3$ can occur at higher pH values including physiological conditions. As a result, the simple and direct ^{68}Ga radiolabeling of molecules in water is prevented [14]. However, the bifunctional chelating agents can coordinate Ga^{3+} under acidic conditions to produce complexes that are thermodynamically and kinetically stable at physiological pH *in vitro*

and *in vivo* [10]. A bifunctional chelating agent is a molecule that comprises a chelator with the capacity of strongly complexing metals and a part of the molecule that can be used to attach the agent onto the targeting vector, such as peptides and antibodies. Based on this functionality, the bifunctional chelating agents can be conjugated to the targeting vector commonly through carboxylate, phenol or isothiocyante groups and then complex radionuclides to form radiopharmaceuticals.

^{64}Cu shows potential to be both a diagnostic radionuclide for PET imaging and radiotherapeutic radionuclide of great interest due to its good nuclear characteristics. As a radionuclide that is capable of being produced in large scale with high specific activity via the ^{64}Zn(n, p)^{64}Cu or ^{64}Ni(p, n)^{64}Cu in a medical cyclotron, it decays by positron [$E_{\beta^+_{max}}$=0.65MeV (17.9%)], beta emission [$E_{\beta^-_{max}}$=0.57MeV (39%)], and electron capture (43.1%). It has a half-life of 12.7 hours, which is sufficiently long for drug preparation, quality control, drug delivery, drug clearance, and patient imaging [8, 15]. The solution chemistry of Cu(II) has also been well studied for its potential use in nuclear imaging. As a metal in the II B group of the periodic table, copper can exist in +2 or +1 oxidation state under physiological conditions. However, Cu^{2+} is more prevalent in the solution chemistry of copper with bifunctional chelating agents. Many chelators such as macrocyclic or linear polyamino carboxylates can complex with Cu(II) at pH~7. Copper prefers to bind to nitrogen-containing functional groups to form complexes with coordination numbers ranging from four to six. Kinetic inertness is considered more important for Cu than thermodynamic stability in terms of *in vivo* stability of ^{64}Cu-labeled compounds. The instability of Cu compounds results from the reduction of Cu(II) to Cu(I) *in vivo* and the subsequent decomposition of Cu from the complexes due to the

competitive chelation by proteins such as superoxide dismutase (SOD). The transchelation of Cu from the ligands to SOD causes Cu accumulation in the liver, which emphasizes the importance of choosing the right chelating agent to provide strong *in vivo* stability for ^{64}Cu-labeled radiopharmaceuticals [16].

This work involves studies using ^{64}Cu, ^{68}Ga, and ^{67}Ga (as the substitute for ^{68}Ga) in biological evaluation of the radiotracer and their production and decay properties are generalized in Table 1.1.

Table 1.1. Selected radionuclide production and decay properties

Radionuclide	**Production**	**Decay**	**$E_\lambda/E_{\beta^-}/E_{\beta^+}/E_\alpha$ (keV)**	**$t_{1/2}$**
Ga-68	^{68}Ge/^{68}Ga generator	EC, β^+	λ: 1077.4 β^+: 1899.1	67.6 min
Ga-67	Cyclotron	EC	λ: 887.7 β^-: 907.2	3.3 d
Cu-64	Cyclotron	EC, β^-, β^+	λ: 1345.8 β^-: 578 β^+: 651	12.7 h

1.3 PROSTATE CANCER

Prostate cancer, also known as the carcinoma of the prostate, is the malignant alteration of gland cells of the human prostate. It is one of the most common cancers diagnosed and the second common cause of cancer related death in men in the United States. According to the American Cancer Society, prostate cancer is expected to account

for an estimated 220,800 new cases and continues to be a severe burden [17]. The disease often eventually evolves to be refractory to androgen deprivation therapy and achieves metastasis, which is the primary reason for the complications and mortalities associated with prostate cancer. Although the survival rate of the disease, which is localized to the prostate gland, is high there is a dramatic rise in mortality once the cancer has spread beyond the prostate. As a result, the early detection and staging of prostate cancer is important [18, 19]. Current methods for the clinical diagnosis of prostate cancer include digital rectal exam (DRE), blood analysis of blood-serum levels of prostate-specific antigen (PSA), and diagnostic anatomical imaging generally with magnetic resonance imaging (MRI), computed tomography (CT), or ultrasound (US). These diagnostic approaches are often considered to be inadequate for early diagnosis due to disadvantages such as invasiveness, non-specificity, and false positives. For example, serum PSA levels, combined with DRE, are common tests for early detection of prostate cancer. However, the lack of specificity of PSA in discriminating prostate cancer from benign prostatic hyperplasia has led to a high number of false diagnosis and unnecessary biopsies [20-25]. Consequently, the challenges for the early detection and staging of prostate tumors, excruciating pain, and increasing costs of palliative therapy associated with the chronic and metastatic stages of the disease motivate the efforts to exploit novel and more effective methods for early diagnosis, staging to differentiate indolent from aggressive tumors, and therapy.

1.4 PEPTIDE BASED RADIOPHARMACEUTICALS

The high expression of peptide receptors in human tumors has attracted great attention for the past decade. Modified regulatory peptide analogues have been synthesized and radiolabeled to act as targeting vectors for selectively binding to the cell membrane receptors of cancer cells. Using small biological molecules like peptides to target specific receptors *in vivo* has been of great interest due to their advantages over the usage of larger biomolecules such as antibodies due to favorable pharmacokinetics and tissue distribution pattern, rapid clearance from the blood and non-target tissues, good permeability to rapidly reach targets, and low toxicity and immunogenicity [26, 27]. The use of radiolabeled somatostatin analogues to target the somatostatin receptors that are overexpressed in human neuroendocrine tumors has shown successful results and stimulated the development of strategies for targeting the bombesin receptors [28].

1.5 BOMBESIN AND GASTRIN RELEASING PEPTIDE RECEPTOR

Bombesin (BBN) is a 14 amino acid counterpart for the human gastrin releasing peptide (GRP) that is a regulatory peptide playing an important role in cancer growth along with physiological effects. GRP is a 27 amino acid peptide that was isolated from porcine stomach in 1979 [29]. GRP and BBN share the final 7 amino acids, -Trp-Ala-Val-Gly-His-Leu-Met-NH_2, in the amidated C terminus sequence. Studies have showed that bombesin probably stimulated cancer growth through binding the bombesin receptors on the surface of cancer cells in an autocrine fashion [30]. The investigation of the BBN receptors was initiated by the isolation of the tetradecapeptide bombesin in 1971 [31]. Currently, there are four receptor subtypes in the bombesin receptor family: the

neuromedin B (NMB) subtype (BB1), the GRP subtype (BB2), the orphan receptor subtype (BB3), and the bombesin (BBN) receptor subtype (BB4) [32]. Among the four subtypes that have been already identified in the bombesin receptor family, the GRP receptor (GRPR), a seven-transmembrane G-protein coupled receptor also known as BB2, has been well studied and characterized with the development of a number of radioligands to target tumors that have high expression of GRPR, such as prostate cancer, breast carcinomas, small cell lung cancers (SCLCs), and renal cell carcinomas [33-37]. In addition to prostate tumor cells, GRPR is also expressed in the vast majority of lymph node metastases and in 52.9% of bone metastases of prostate cancer [38]. To date, design and development of radiolabeled agents for the bombesin receptor family have largely focused upon the GRP (BB2) receptor subtype. One of the frequently studied targeting agents for the GRPR is BBN(7-14)NH_2, whose final 7 amino acid sequence, -Trp-Ala-Val-Gly-His-Leu-Met-NH_2, has been determined to be necessary for high binding affinity to GRPR (Fig. 1.3) [39-43]. The other targeting motif used in this research is RM2 (Fig. 1.4) which is an antagonist analogue of BBN with high binding affinity to GRPR. The studies of BBN antagonists have shown superior biodistribution and imaging as compared to BBN agonists. For example, RM2, as an antagonist analog of BBN, has recently been investigated to show improved uptake and retention in tumor [44-48].

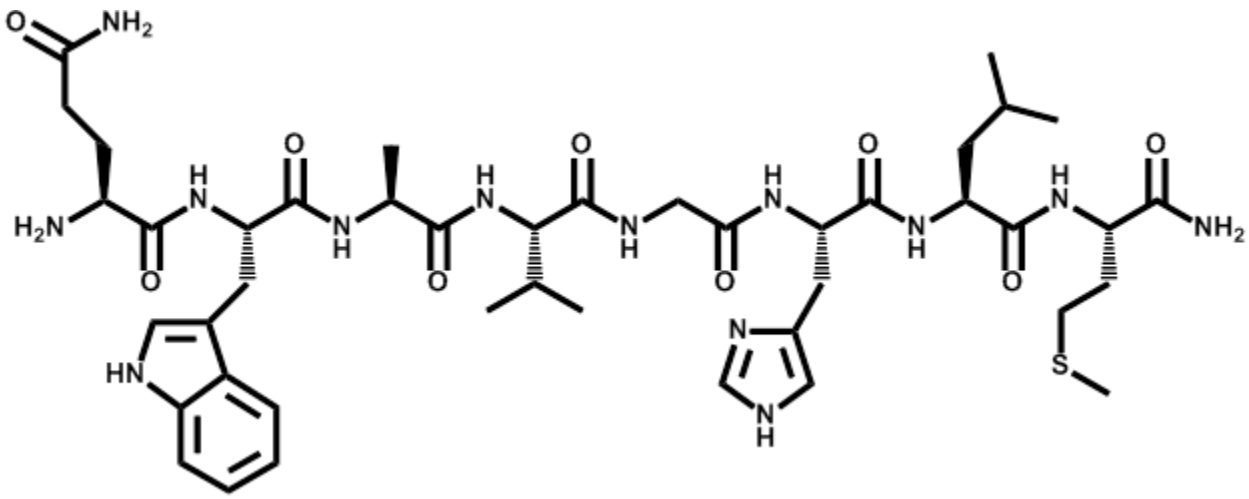

Fig. 1.3: Chemical structure of BBN(7-14)NH_2 agonist.

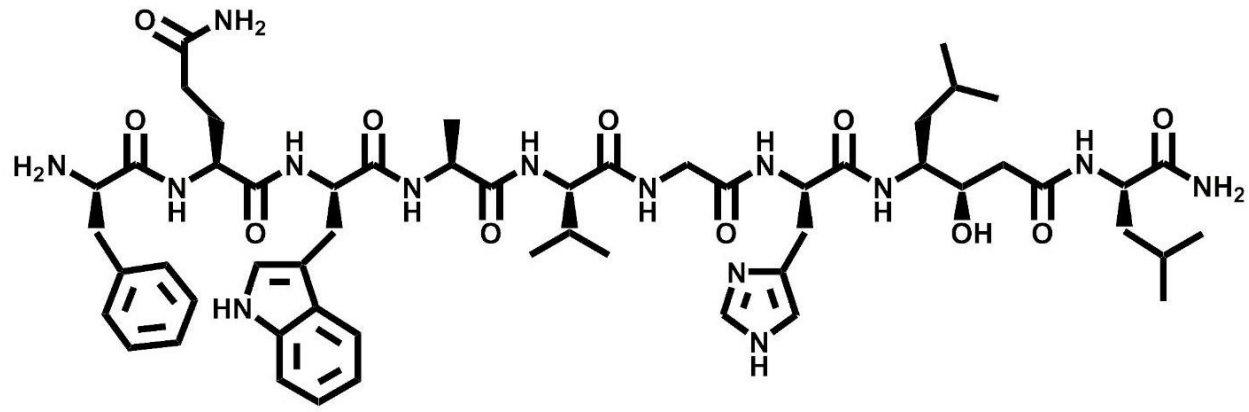

Fig. 1.4: Chemical structure of RM2 antagonist.

Recently, numerous BBN analogue conjugates have been generated and radiolabeled with ^{99m}Tc, ^{111}In, ^{64}Cu, and other radionuclides in order to evaluate their potential of targeting GRPR-expressing tumors for therapeutic and diagnostic applications in patients [49-55].A large body of work has been reported for monovalent ligands based on BBN analogues. For example, in 2003, a novel series of ^{111}In-labeled BBN analogs, [^{111}In-DOTA-X-BBN(7-14)NH_2] (X=0, β-Ala, 5-Ava, 8-Aoc, 11-Aun) were synthesized, characterized, and evaluated *in vitro* and *in vivo* (DOTA=1,4,7,10-tetraazacyclododecane-1,4,7,10-tetraacetic acid). The results showed that the complexes in which X=5-Ava or 8-Aoc were present exhibited high binding affinity to the GRPR and high retention on PC-3 human prostate cancer xenografts in SCID (severe combined immunodeficient) mice. However, the *in vivo* biodistribution studies also showed high uptake and retention of the conjugates in liver and pancreas [49]. A series of ^{99m}Tc-labeled BBN analogs have also been developed, characterized, and evaluated [50]. Since this time, other DOTA-linker-BBN(7-14)NH_2 conjugates have been synthesized for radiolabeling studies with ^{64}Cu. However, the *in vivo* kinetic stability of DOTA-chelated to ^{64}Cu was inadequate [51-53]. As a result, a series of NOTA (NOTA= 1,4,7-triazacyclononane-1,4,7-triacetic acid) conjugated, ^{64}Cu-radiolabeled BBN ligands, [^{64}Cu-NO2A-(X)-BBN(7–14)NH_2] (X=β-Ala, 5-Ava, 6-Ahx, 8-Aoc, 9-Anc or AMBA), were synthesized and evaluated. These new radioligands presented with high uptake of tracer in GRPR positive tissues with little retention in non-target tissues, indicating the superiority of NOTA as a chelate to stabilize ^{64}Cu *in vivo* [40-43].

1.6 DUPA AND PROSTATE SPECIFIC MEMBRANE ANTIGEN

The second targeting vector being studied in this application is DUPA (DUPA=2-[3-(1,3-Bis-tert-butoxycarbonylpropyl)-ureido]pentanedioic acid, Fig. 1.5), which is a urea derivative with high binding affinity for PSMA. PSMA, also known as folate hydrolase I or glutamate carboxypeptidase II, is a 750-amino acid cell membrane protein, which was originally defined by the antibody (MAb)7E11 in 1987 [56]. It is an ideal target for nuclear medicine due to its many biological characteristics. First, as a non-secreted protein anchored to the plasma membrane of prostate epithelial cells, PSMA shows over-expression on prostate cancer cells. Studies also have shown that it is highly expressed in lymph node and bone metastases of prostate cancer [38, 57]. However, the expression of PSMA in normal human tissues is 100 to 1000 fold less than that in prostate cancer [58]. PSMA expression also has been reported in the neovasculature of most solid tumors including renal carcinoma, colorectal carcinoma, glioblastoma multiforme, pancreatic duct carcinoma, and breast carcinoma [59]. Second, when ligand binding occurs, PSMA is internalized via clathrin-coated pits and subsequent endocytosis, which favors the transportation of the bound radionuclides into the cells [60]. Finally, there are studies showing that PSMA expression levels increase as the stage and grade of the tumor increase, showing the potential of PSMA in the application for tumor staging [61, 62].

Considerable work has been reported for the development of small molecule inhibitors for PSMA so far. In 2004, a series of urea-based inhibitors of PSMA were synthesized, and the biological evaluations of these inhibitors showed the necessity for one of the glutamic acid moieties to remain intact to maintain their inhibitory potency

[63]. In 2005, ^{11}C and ^{125}I radiolabeled urea derivatives were produced for evaluation in severe combined immunodeficient mice bearing MCF-7 (breast, PSMA-negative), PC-3 (prostate, PSMA-negative), and LNCaP (prostate, PSMA-positive) xenografts, and whose results showed the feasibility of using urea derivatives as potential targeting vectors for PSMA [64]. Afterwards, other radionuclides such as ^{99m}Tc, ^{18}F, ^{123}I and ^{68}Ga were also applied to radiolabel a variety of urea derivatives [65-68]. In 2009, the DUPA molecule was radiolabeled with ^{99m}Tc and the imaging and biodistribution studies showed high uptake and retention of the tracer on LnCaP cell tumor xenografts [69]. These studies on glutamate-urea based inhibitors showed the potency of DUPA as an efficient targeting vector for PSMA.

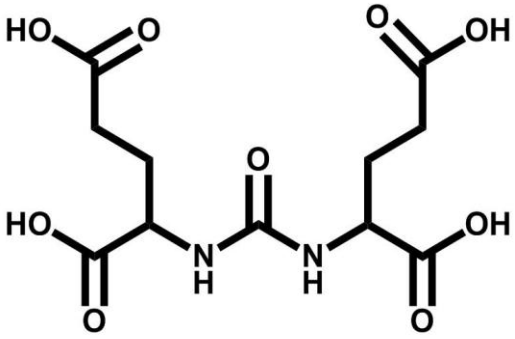

Fig. 1.5: Chemical structure of DUPA

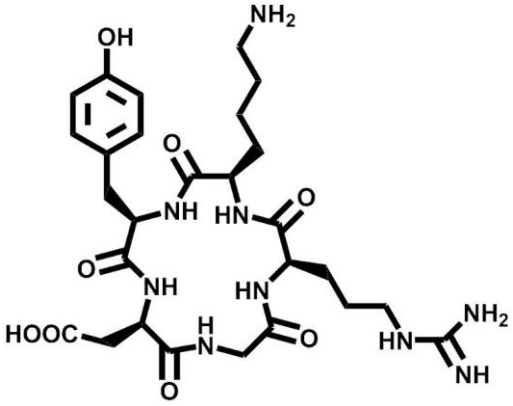

Fig. 1.6: Chemical structure of RGD

1.7 RGD AND $\alpha_v\beta_3$ INTEGRIN

The third targeting vector of great interest is the RGD peptide sequence, a cyclic five amino acid moiety abbreviated as c(RGDyK), with strong binding affinity to $\alpha_v\beta_3$, a member of the integrins (Fig. 1.6). The integrin family is composed of heterodimericly structured transmembrane receptors, which play an important role in cell adhesion due to its capability of connecting cells to proteins of the extracellular matrix. The integrin is a combination of two parts, the α subunit and β subunit, each of which is a type I membrane glycoprotein. Each subunit of the integrin consists of a large extracellular domain, a transmembrane helix, and a short cytoplasmic tail. 24 heterodimers, which are formed by 18 α and 8 β subunits that have been identified up till now, have been found and investigated [70-72]. The RGD peptide sequence has been confirmed to be an essential binding motif for seven integrin receptors, including $\alpha_v\beta_3$, that is moderately expressed in a number of cancers such as malignant melanoma, glioblastoma, breast, and androgen-independent prostate cancer cells [73, 74]. Despite its moderate expression on tumors, $\alpha_v\beta_3$ remains an attractive target of great interest due to its important roles in the modulation of cell migration and survival during angiogenesis, which potentially facilitates metastatic invasion of the tumors cells across the blood vessels [75-77]. Angiogenesis, a process of formation of new blood vessels in avascular tissues, is upregulated in a number of diseases including tumor growth as well as tumor metastasis. The integrins, as a member of cell adhesion receptors, take the responsibility of mediating migration of endothelial cells into the basement membrane and regulating growth, survival, and differentiation of endothelial cells during angiogenesis [78, 79].

Up till now, a variety of modified $\alpha_v\beta_3$-integrin targeting probes based on the RGD sequence for SPECT and PET diagnostic application has been developed and evaluated biologically. For example, in 2004, ^{18}F-radiolabeled RGD peptide was produced and initially evaluated for imaging brain tumor angiogenesis [80]. In 2007, a radiolabeled RGD peptide was used to target the integrin of tumors [81]. Patterns of $\alpha_v\beta_3$ expression in breast cancer were studied via ^{18}F-galacto-RGD in PET imaging in 2008 [82]. Other peptide ligands based on RGD were synthesized and labeled with other radionuclides including ^{68}Ga for mapping $\alpha_v\beta_3$ expression *in vivo* [83, 84]. With the exploitation of RGD-motif peptides, important strategies for improving pharmacokinetics were proposed and supported via comparative studies [85]. The strategies include introduction of hydrophilic linkers as pharmacokinetic modifiers and multimerisation of RGD to from multimers, which triggered the research on multimeric RGD peptides. The studies showed the multimerisation of RGD provides increased binding affinity and superior *in vivo* behaviors such as tumor uptake and retention [86-91].

1.8 BIFUNCTIONAL CHELATORS – NOTA, NODAGA, DOTA

The BFCAs used in this dissertation are cyclic polyaminocarboxylates with the capability of coordinating the metals efficiently. Several carboxylate groups of the chelators can be involved in coordination with the metals to form complexes, while the remaining carboxylate can be used to form an amide bond with a primary amino residue of the peptide targeting vector thus linking the chelator onto the main structure of the ligand [92]. The three cyclic polyaminocarboxylate chelators that will be discussed herein are listed in Figure 1.7 (NOTA, 1,4,7-triazacyclononane-1,4,7-triacetic acid), Figure 1.8

(NODAGA, [2-(4,7-biscarboxymethyl)-1,4,7-(triazonan-1-yl)pentanedioic acid]), and Figure 1.9 (DOTA, 1,4,7,10-tetraazacyclododecane-1,4,7,10-tetraacetic acid).

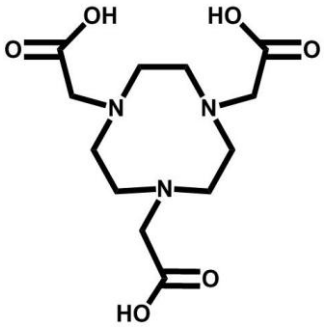

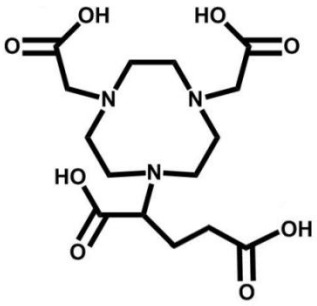

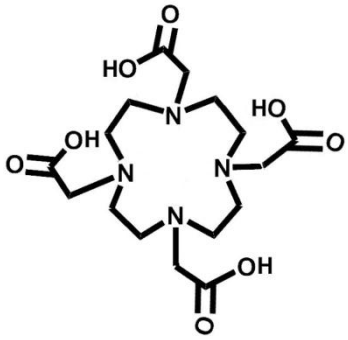

Fig. 1.7: NOTA structure **Fig. 1.8:** NODAGA structure **Fig. 1.9:** DOTA structure

1.9 BIVALENT PEPTIDE LIGAND

Bivalent ligands are a combination of two targeting vectors (peptides or small molecules) having very high affinity for multiple receptor subtypes. Compared to bivalent ligands, monovalent ligands (which oftentimes target only a single receptor subtype) have several disadvantages. First, the number of effective receptors may differ significantly during tumor development causing significantly reduced uptake and retention of targeting vector. Second, the binding affinity can be relatively low for monovalent species as compared to bivalent targeting ligands. Third, pharmacokinetic considerations (clearance properties and excretion rates) may limit the diagnostic imaging utility of a specific monovalent targeting ligand. Consequently, the development of bivalent ligands is important for producing a multipurpose ligand, having the ability to effectively target prostate cancer cells with expression or co-expression of two biomarkers. Bivalent ligands are superior to monovalent ligands due to its capability of being used as universal ligands for targeting multiple peptide receptors. Moreover,

bivalent ligands have the potential for targeting prostate tumor cells at all stages of the disease.

For the reasons mentioned above, the development of multivalent regulatory peptide probes that are new and innovative targeting vectors with high selectivity and affinity for multi-receptor subtypes on human prostate cancer is a new avenue and impetus for diagnostic molecular imaging of tumors expressing multiple receptors. The first bivalent peptide ligand for GRPR/PSMA targeting was synthesized in our lab and evaluated *in vitro* and *in vivo* [93]. Reports on the synthesis and biological evaluation of heterodimeric regulatory peptide probes of RGD/BBN conjugates for targeting both $\alpha_v\beta_3$ and GRPR receptors with ^{68}Ga- or ^{64}Cu-radiolabeled [NOTA-RGD-BBN(7-14)NH_2] have shown improved retention of ^{64}Cu tracer on PC-3 tumor cells at 20 h post injection as compared to the monomeric BBN or RGD conjugates [94, 95]. Radiolabeled NOTA and DOTA conjugates of RGD-RM2 bivalent peptide antagonists, [RGD-Glu-(^{64}Cu-NO2A)-6-Ahx-RM2] and [RGD-Glu-(^{177}Lu/^{111}In-DO3A)-6-Ahx-RM2], have been also synthesized and biologically investigated on PC-3 tumor cells to display superior biological behaviors *in vivo* and imaging [96, 97].

1.10 REFERENCES

1. SNMMI. Historical Timeline. 2009
2. Moi, M. K., DeNardo, S. J., Meares, C. F., Stable bifunctional chelates of metals used in radiotherpy. Cancer Research (Supplement), 1990. **50**: p. 789-793.
3. Weiner, R. E., Thakur, M. L., Radiolabeled Peptides in Oncology: Role in Diagnosis and Treatment. BioDrugs, 2005. **19**: p. 145-163.
4. Liu, S., Edwards, D. S., ^{99m}Tc-labeled small peptides as diagnostic radiopharmaceuticals. Chemical Reviews, 1999;99: 2235.
5. Heeg, M. J. and Jurisson, S. S., The Role of Inorganic Chemistry in the Development of Radiometal Agents for Cancer Therapy. Accounts of Chemical Research, 1999. **32**(12): p. 1053-1060.
6. Kassis, A. I. and Adelstein, S. J., Considerations in The Selection of Radionuclides for Cancer Therapy, in Handbook of Radiopharmaceuticals, M.J. Welch and C.S. Redvanly, Editors. 2003, John Wiley and Sons, Ltd: West Sussex. p. 767-793.
7. Jr., L.G.W., Organic Chemistry. 3rd edition ed. 1995, Upper Saddle River, New Jersey: Prentice Hall, Inc.
8. Anderson, C. J. and M. J. Welch, Radiometal-labeled agents (non-technetium) for diagnostic imaging. Chemical Reviews, 1999. **99**(9): p. 2219.
9. Rösch F., ^{68}Ge/ ^{68}Ga generators: past, present, and future. Recent Results Cancer Res, 2013. **194**: p. 3-16
10. M. Isabel M. Prata, Gallium-68: A New Trend in PET Radiopharmacy. Current Radiopharmaceuticals, 2012. **5**: p. 142-149.
11. Fani, M., André, J. P., Maecke, H. R., ^{68}Ga-PET: a powerful generator-based alternative to cyclotron-based PET radiopharmaceuticals. Contr Med Mol Imag, 2008. **3**: p. 67-77.
12. Pearson, R.G., Hard and Soft Acids and Bases. J Am Chem Soc, 1963. **85**: p. 3533-3539
13. Harris, W. R., Pecoraro, V. L., Thermodynamic binding constants for gallium transferrin. Biochemistry, 1983. **22**: p. 292-299.
14. Dymov, A. M., Seventin, A. P., Analytical Chemistry of Gallium. Ann Arbor Science Publishers, Michigan, 1970.
15. Anderson, C. J., Ferdani, R., Copper-64 radiopharmaceuticals for PET imaging of cancer: advances in preclinical and clinical research. Cancer Biother Radiopharm, 2009. **24**(4): p. 379-93
16. Cutler, C. S., Hennkens, H. M., Sisay, N., Huclier-Markai, S., Jurisson, S. S., Radiometals for combined imaging and therapy. Chem Rev, 2013. **113**: p. 858.
17. American Cancer Society. Cancer facts & figures. 2015.
18. Yong, C., Onukwugha, E., Mullins, C. D., Clinical and economic burden of bone metastasis and skeletal-related events in prostate cancer. Curr Opin Oncol, 2014. **26**: p. 274.
19. Jayasekera, J., Onukwugha, E., Bikov, K., Mullins, C. D., Seal, B., Hussain, A., The economic burden of skeletal-related events among elderly men with metastatic prostate cancer. Pharmaco Economics, 2014. **32**: p. 173.

20. Howrey, B. T., Kuo, Y. F., Lin, Y. L., Goodwin, J. S., The impact of PSA screening on prostate cancer mortality and overdiagnosis of prostate cancer in the United States. J Gerontol A: Biol Med Sci, 2013. **68**: p. 56.
21. Hayes, J. H., Barry, M. J., Screening for prostate cancer with the prostate-specific antigen test: a review of current evidence. JAMA, 2014. **311**: p. 1143.
22. Sullivan, P. W., Nelson, J. B., Mulani, P. M., Sleep, D., Quality of life as a potential predictor for morbidity and mortality in patients with metastatic hormone-refractory prostate cancer. Qual Life Res, 2006. **15**: p. 1297.
23. D'Amico, A. V., Prostate-cancer mortality after PSA screening. N Engl J Med, 2012. **366**: p. 2229.
24. Duffy, M. J., Prostate-specific antigen: does the current evidence support its use in prostate cancer screening? Ann Clin Biochem, 2011. **48**: p. 310.
25. Zappa, M., Puliti, D., Hugosson, J., Schröder, F. H., van Leeuwen, P. J., et al., A different method of evaluation of the ERSPC Trial confirms that prostate-specific antigen testing has a significant impact on prostate cancer mortality. Eur Urol, 2014. **66**: p. 401.
26. Reubi, J. C., Peptide receptors as molecular targets for cancer diagnosis and therapy. Endocr Rev, 2003. **24**: p. 389–427.
27. Reubi, J. C., Maecke, H. R., Peptide-based probes for cancer imaging. J Nucl Med, 2008. **49**: p. 1735–8.
28. de Jong, M., Breeman, W. A., Kwekkeboom, D. J., Valkema, R., Krenning, E. P., Tumor imaging and therapy using radiolabeled somatostatin analogues. Acc Chem Res, 2009. **42**: p. 873.
29. McDonald, T. J., Jörnvall, H., Nilsson, G., Vagne, M., Ghatei, M., Bloom, S. R., Mutt, V., Characterization of a gastrin releasing peptide from porcine non-antral gastric tissue. Biochem Biophys Res Comm, 1979. **90**: p. 227.
30. Siegfried, J. M., Krishnamachary, N., Gaither, A., Gubish, C., Hunt, J. D., Shriver, S. P., Evidence for autocrine actions of neuromedin B and gastrin-releasing peptide in non-small cell lung cancer. Pulm Pharmacol Ther, 1999. 12(5): p. 291-302.
31. Anastasi, A., Erspamer, V., Nucci, M., Isolation and amino acid sequences of alytesin and bombesin, two analogous active tetradecapeptides from the skin of European discoglossid Frogs. Arch Biochem Biophys, 1972. **148**: p. 443.
32. Jensen, R. T., Battey, J. F., Spindel, E. R., Benya, R. V., International union of pharmacology. LXVIII. Mammalian bombesin receptors: nomenclature, distribution, pharmacology, signaling, and functions in normal and disease states. Pharmacol Rev, 2008. **60**: p. 1–42.
33. Markwalder, R., Reubi, J. C., Gastrin-releasing peptide receptors in the human prostate: Relation to neoplastic transformation. Cancer Res, 1999. **59**: p. 1152.
34. Smith, C. J., Volkert, W. A., Hoffman, T. J., Gastrin releasing peptide (GRP) receptor targeted radiopharmaceuticals: a concise update. Nucl Med Biol, 2003. **30**: p. 861.
35. Varvarigou, A., Bouziotis, P., Zikos, C., Scopinaro, F., De Vincentis, G., Gastrin-releasing peptide (GRP) analogues for cancer imaging. Cancer Biother. Radiopharm, 2004. **19**: p. 219.

36. Schroeder, R. P., van Weerden, W. M., Krenning, E. P., Bangma, C. H., Berndsen, S., et al., Gastrin-releasing peptide receptor-based targeting using bombesin analogues is superior to metabolism-based targeting using choline for in vivo imaging of human prostate cancer xenografts. Eur J Nucl Med Mol Imaging, 2011. **38**: p. 1257.
37. Yu, Z., Ananias, H. J., Carlucci, G., Hoving, H. D., Helfrich, W., et al., An update of radiolabeled bombesin analogs for gastrin-releasing peptide receptor targeting. Curr Pharm Des, 2013. **19**: p. 3329.
38. Ananias, H. J., van den Heuvel, M. C., Helfrich, W., de Jong, I. J., Expression of the gastrin-releasing peptide receptor, the prostate stem cell antigen and the prostate-specific membrane antigen in lymph node and bone metastases of prostate cancer. Prostate, 2009. **69**: p. 1101.
39. Johnson, C. V., Shelton, T., Smith, C. J., Ma, L., Perry, M. C., Volkert, W. A., Hoffman, T. J., Evaluation of combined ^{177}Lu-DOTA-8-Aoc-BBN(7-14)NH_2 GRP receptor-targeted radiotherapy and chemotherapy in PC-3 human prostate tumor cell xenografted SCID mice. Cancer Biother Radiopharm, 2006. **21**: p. 155.
40. Prasanphanich, A. F., Nanda, P. K., Rold, T. L., Ma, L., Lewis, M. R., Garrison JC, Hoffman TJ, Sieckman GL, Figueroa SD, Smith CJ.., [64Cu-NOTA-8-Aoc-BBN(7-14)NH_2] targeting vector for position-emission tomography imaging of gastrin-releasing peptide receptor-expressing tissues. Proc Nat Acad Sci USA, 2007. **104**: p. 12462.
41. Prasanphanich, A. F., Retzloff, L., Lane, S. R., Nanda, P. K., Sieckman, G. L., Rold, T. L., Ma, L., Figueroa, S. D., Sublett, S. V., Hoffman, T. J., Smith, C. J., In vitro and in vivo analysis of [^{64}Cu-NO2A-8-Aoc-BBN(7-14)NH_2]: a site-directed radiopharmaceutical for positron-emission tomography imaging of T-47D human breast cancer tumors. Nucl Med Biol, 2009. **36**: p. 171–81.
42. Lane, S. R., Nanda, P., Rold, T. L., Sieckman, G. L., Figueroa, S. D., Hoffman, T. J., Jurisson, S. S., Smith, C. J., Optimization, biological evaluation and microPET imaging of copper-64-labeling bombesin agonists, [^{64}Cu-NO2A-(X)-BBN(7-14)NH_2], in a prostate tumor xenografted mouse model. Nucl Med Biol, 2010. **37**: p. 751.
43. Jackson, A. B., Nanda, P. K., Rold, T. L., Sieckman, G. L., Szczodroski, A. F., Hoffman, T. J., Chen, X., Smith, C. J., ^{64}Cu-NO2A-RGD-Glu-6-Ahx-BBN(7-14)NH_2: a heterodimeric targeting vector for positron emission tomography imaging of prostate cancer. Nucl Med Biol, 2012. **39**: p. 377.
44. Abiraj, K., Mansi, R., Tamma, M. L., Fani, M., Forrer, F., Nicolas, G., Cescato, R., Reubi, J. C., Maecke, H. R., Bombesin antagonist based radioligands for translational nuclear imaging of gastrin-releasing peptide receptor-positive tumors. J Nucl Med, 2011. **52**: p. 1970.
45. Dumont, R. A., Tamma, M., Braun, F., Borkowski, S., Reubi, J. C., Maecke, H., Weber, W. A., Mansi, R., Targeted radiotherapy of prostate cancer with a gastrin-releasing peptide receptor antagonist is effective as monotherapy and in combination with rapamycin. J Nucl Med, 2013. **54**: p. 762.
46. Cescato, R., Maina, T., Nock, B., Nikolopoulou, A., Charalambidis, D., Piccand, V., Reubi, J. C., Bombesin receptor antagonists may be preferable to agonists for tumor targeting. J Nucl Med, 2008. **49**: p. 318.

47. Ginj, M., Zhang, H., Waser, B., Cescato, R., Wild, D., Wang, X., Erchegyi, J., Rivier, J., Mäcke, H. R., Reubi, J. C., Radiolabeled somastostatin receptor antagonists are preferable to agonists for in vivo peptide receptor targeting of tumors. Proc Natl Acad Sci USA, 2006. 103: p. 16436.
48. Anderson, C. J., Welch, M. J., Radiometal-labeled agents (non-technetium) for diagnostic imaging. Chem Rev, 1999. **99**: p. 2219.
49. Hoffman, T. J., Gali, H., Smith, C. J., Sieckman, G. L., Hayes, D. L., Owen, N. K., Volkert, W. A., Novel Series of ^{111}In-Labeled Bombesin Analogs as Potential Radiopharmaceuticals for Specific Targeting of Gastrin-Releasing Peptide Receptors Expressed on Human Prostate Cancer Cells. J Nucl Med, 2003. **44**: p. 823.
50. Smith, C. J., Gali, H., Sieckman, G. L., Higginbotham, C., Volkert, W. A., Hoffman, T. J., Radiochemical Investigations of ^{99m}Tc-N_3S-X-BBN[7-14]NH_2:An in Vitro/in Vivo Structure-Activity Relationship Study Where X = 0-, 3-, 5-, 8-, and 11-Carbon Tethering Moieties. Bioconjugate Chemistry, 2003. **14**: p. 93.
51. Rogers, B. E., Bigott, H. M., Bigott H. M., McCarthy, D. W., Della Manna, D., Kim, J., Sharp, T. L., Welch, M. J., MicroPET Imaging of a Gastrin-Releasing Peptide Receptor-Positive Tumor in a Mouse Model of Human Prostate Cancer Using a 64Cu-Labeled Bombesin Analogue. Bioconjugate Chemistry, 2003. **14**: p. 756.
52. Chen, X., Park, R., Hou, Y., Tohme, M., Shahinian, A. H., Bading, J. R., Conti, P. S., MicroPET and autoradiographic imaging of GRP receptor expression with ^{64}Cu-DOTA-[Lys^3] bombesin in human prostate adenocarcinoma xenografts. J Nucl Med, 2004. **45**: p. 1390.
53. Parry, J. J., Kelly, T. S., Andrews, R., Rogers, B. E., In vitro and in vivo evaluation of ^{64}Cu-labeled DOTA-linker-bombesin(7-14) analogues containing different amino acid linker moieties. Bioconjug Chem, 2007. **18**: p. 1110.
54. Smith C. J., Sieckman, G. L., Owen, N. K., Hayes, D. L., Mazuru, D. G., Kannan, R., Volkert, W. A., Hoffman, T. J., Radiochemical investigations of gastrin-releasing peptide receptor-specific [^{99m}Tc(X)$(CO)_3$-Dpr-Ser-Ser-Ser-Gln-Trp-Ala-Val-Gly-His-Leu-Met-(NH_2)] in PC-3, tumor-bearing, rodent models: syntheses, radiolabeling, and in vitro/in vivo studies where Dpr = 2,3-diaminopropionic acid and X = H_2O or P(CH_2OH)$_3$. Cancer Res, 2003. **63**: p. 4082–8.
55. Scopinaro, F., De Vincentis, G., Varvarigou, A. D., Laurenti, C., Iori, F., Remediani, S., Chiarini, S., Stella, S., ^{99m}Tc-bombesin detects prostate cancer and invasion of pelvic lymph nodes. Eur J Nucl Med Mol Imaging, 2003. **30**: p. 1378–82.
56. Horoszewicz, J. S., Kawinski, E., Murphy, G. P. Monoclonal antibodies to a new antigenic marker in epithelial prostatic cells and serum of prostatic cancer patients. Anticancer Res, 1987. **7**: p. 927.
57. Perner, S., Hofer, M. D., Kim, R., Shah, R. B., Li, H., Möller, P., Hautmann, R. E., Gschwend, J. E., Kuefer, R., Rubin, M. A., Prostate-specific membrane antigen expression as a predictor of prostate cancer progression. Hum Pathol, 2007. **38**: p. 696.

58. Sokoloff, R. L., Norton, K. C., Gasior, C. L., Marker, K. M., Grauer, L. S., A dual-monoclonal sandwich assay for prostate-specific membrane antigen: Levels in tissues, seminal fluid and urine. Prostate, 2000. **43**: p. 150.
59. Bostwick, D. G., Pacelli, A., Blute, M., Roche, P., Murphy, G. P., Prostate specific membrane antigen expression in prostatic intraepithelial neoplasia and adenocarcinoma: a study of 184 cases. Cancer, 1998. **82**: p. 2256.
60. Rajasekaran, S. A., Anilkumar, G., Oshima, E., Bowie, J. U., Liu, H., Heston, W., Bander N. H., Rajasekaran, A. K., A novel cytoplasmic tail MXXXL motif mediates the internalization of prostate-specific membrane antigen. Mol Biol Cell, 2003. **14**: p. 4835.
61. Chang, S. S., Overview of prostate-specific membrane antigen. Rev Urol, 2004. **6**: p. S13.
62. Laidler, P., Dulińska, J., Lekka, M., Lekki, J., Expression of prostate specific membrane antigen in androgen-independent prostate cancer cell line PC-3. Arch Biochem Biophys, 2005. **435**: p. 1.
63. Kozikowski, A. P., Zhang, J., Synthesis of Urea-Based Inhibitors as Active Site Probes of Glutamate Carboxypeptidase II: Efficacy as Analgesic Agents. Journal of Medicinal Chemistry, 2004. **47**: p. 1729.
64. Foss, C. A., Mease, R. C., Fan, H., Wang, Y., Ravert, H. T., Dannals, R. F., Olszewski, R. T., Heston, W. D., Kozikowski, A. P., Pomper, M. G., Radiolabeled Small-Molecule Ligands for Prostate-Specific of Prostate Cancer. Clin Cancer Res, 2005. **11**: p. 4022
65. Barrett, J., LaFrance, N., Coleman, R. E., Goldsmithet, S., et al., Targeting metastatic prostate cancer [PCa] in patients with ^{123}I-MIP1072 and ^{123}I-MIP1095. J Nucl Med, 2009. **50**: p. 522.
66. Osborne, J. R., Akhtar, N. H., Vallabhajosula, S., Nikolopoulou, A., Maresca, K. P., et al., Tc-99m labeled small-molecule inhibitors of prostate-specific membrane antigen (PSMA): New molecular imaging probes to detect metastatic prostate adenocarcinoma (PC). J Clin Oncol, 2012. **30**(Suppl 5): Abstract p. 173.
67. Afshar-Oromieh, A., Haberkorn, U., Eder, M., Eisenhut, M., Zechmann, C. M., [^{68}Ga] Gallium-labelled PSMA ligand as superior PET tracer for the diagnosis of prostate cancer: comparison with ^{18}F-FECH. Eur J Nucl Med Mol Imaging, 2012. **39**: p. 1085–6.
68. Eder, M., Schafer, Schäfer, M., Bauder-Wüst, U., Hull, W. E., Wängler, C., Mier, W., Haberkorn, U., Eisenhut, M., ^{68}Ga-Complex Lipophilicity and the Targeting Property of a Urea-Based PSMA Inhibitor for PET Imaging. Bioconjug Chem, 2012. **23**: p. 688.
69. Kularatne S. A., Wang, K., Santhapuram, H. K., Low, P. S., Prostate-Specific Membrane Antigen Targeted Imaging and Therapy of Prostate Cancer Using a PSMA Inhibitor as a Homing Ligand. Molecular Pharmaceuticals, 2009. **6**: p. 780.
70. Hynes, R. O., Integrins: Bidirectional, allosteric signaling machines. Cell, 2002. **110**: p. 673–687.
71. Tamkun, J. W., DeSimone, D. W., Fonda, D., Patel, R. S., Buck, C., Horwitz, A. F., Hynes, R. O., Structure of integrin, a glycoprotein involved in the transmembrane linkage between fibronectin and actin. Cell, 1986. **46**: p. 271–282.

72. Humphries, M. J., McEwan, P. A., Barton, S. J., Buckley, P. A., Bella, J., Mould, A. P., Integrin structure: Heady advances in ligand binding, but activation still makes the knees wobble. Trends Biochem Sci, 2003. **28**: p. 313–320.
73. Meyer, A., Auernheimer, J., Modlinger, A., Kessler, H., Targeting RGD recognizing integrins: Drug development, biomaterial research, tumor imaging and targeting. Curr Pharm Des, 2006. **12**: p. 2723–2747.
74. Sutherland M., Gordon, A., Shnyder, S. D., Patterson, L. H., Sheldrake, H. M., RGD-binding integrins in prostate cancer: expression patterns and therapeutic prospects against bone metastasis. Cancers, 2012. **4**: p. 1106–45.
75. Ruoslahti, E., Pierschbacher, M. D., New perspectives in cell adhesion: RGD and integrins. Science, 1987. **238**: p. 491.
76. Romanov, V. I., Goligorsky, M. S., RGD-recognizing integrin mediate interactions of human prostate carcinoma cells with endothelial cells in vitro. Prostate, 1999. **39**: p. 108.
77. Gladson, C. L., Cheresh, D. A., Glioblastoma expression of vitronectin and the αvβ3 integrin. Adhesion mechanism for transformed glial cells. J Clin Invest, 1991. **88**: p. 1924.
78. Folkman, J., Klagsbrun, M., Angiogenic factors. Science, 1987. **235**: p. 442–447.
79. Risau, W., Mechanisms of angiogenesis. Nature, 1997. **386**: p. 671–674.
80. Chen, X., Park, R., Shahinian, A. H., Tohme, M., Khankaldyyan, V., Bozorgzadeh, M. H., Bading, J. R., Moats, R., Laug, W. E., Conti, P. S., ^{18}F-labeled RGD peptide: initial evaluation for imaging brain tumor angiogenesis. Nucl Med Biol, 2004. **31**: p. 179-89.
81. Dijkgraaf, I., Kruijtzer, J. A., Frielink, C., Corstens, F. H., Oyen, W. J., Liskamp, R. M., Boerman, O. C., αvβ3 Integrin-targeting of intraperitoneally growing tumors with a radiolabeled RGD peptide. Int J Cancer, 2007. **120**: p. 605–10.
82. Beer A. J., Niemeyer, M., Carlsen, J., Sarbia, M., Nährig, J., Watzlowik, P., Wester, H. J., Harbeck, N., Schwaiger, M., Patterns of αvβ3 expression in primary and metastatic human breast cancer as shown by ^{18}F-galacto-RGD PET. J Nucl Med, 2008. **49**: p. 255–9.
83. Schottelius M., Laufer, B., Kessler, H., Wester, H. J., Ligands for mapping αvβ3-integrin expression in vivo. Acc Chem Res, 2009. **42**: p. 969–80.
84. Blom E., Velikyan, I., Estrada, S., Hall, H., Muhammad, T., Ding, C., Nair, M., Långström, B., ^{68}Ga-Labeling of RGD peptides and biodistribution. Int J Clin Exp Med, 2012. **5**: p. 165–72.
85. Line B. R., Mitra, A., Nan, A., Ghandehari, H., Targeting tumor angiogenesis: comparison of peptide and polymer-peptide conjugates. J Nucl Med, 2005. **46**: p. 1552–60.
86. Wu Y., Zhang, X., Xiong, Z., Cheng, Z., Fisher, D. R., Liu, S., Gambhir, S. S., Chen, X., MicroPET Imaging of glioma integrin αvβ3 expression using 64Cu-labeled tetrameric RGD peptide. J Nucl Med, 2005. **46**: p. 1707–18.
87. Liu S., Radiolabeled multimeric cyclic RGD peptides as Integrin αvβ3 targeted radiotracers for tumor imaging. Mol Pharm, 2006. **3**: p. 472–87.
88. Wu, Z., Li, Z. B., Chen, K., Cai, W., He, L., Chin, F. T., Li, F., Chen, X., MicroPET of tumor integrin αvβ3 expression using ^{18}F-labeled PEGylated tetrameric RGD peptide (^{18}F-FPRGD4). J Nucl Med, 2007. **48**: p. 1536.

89. Li, Z., Cai, W., Cao, Q., Chen, K., Wu, Z., He, L., Chen, X., ^{64}Cu-labeled tetrameric and octameric RGD peptides for small-animal PET of tumor αvβ3 integrin expression. J Nucl Med, 2007. **48**: p. 1162.
90. Shi, J., Kim, Y. S., Zhai, S., Liu, Z., Chen, X., Liu, S., Improving tumor uptake and pharmacokinetics of ^{64}Cu-labeled cyclic RGD peptide dimers with Gly(3) and PEG(4) linkers. Bioconjug Chem, 2009. **20**: p. 750.
91. Dijkgraaf, I., Terry, Y. A. S., McBride W. J., Goldenberg D. M., Laverman, P., et al., Imaging integrin αvβ3 expression in tumors with an ^{18}F-labeled dimeric RGD peptide. Contrast Media Mol Imaging, 2013. **8**: p. 238.
92. Sosabowski, J. K., Mather, S. J., Conjugation of DOTA-like chelating agents to peptides and radiolabeling with trivalent metallic isotopes. Nat Protoc, 2006. **1**: p. 972–976.
93. Bandari, R. P., Jiang, Z., Stott Reynolds, T., Bernskoetter, N., Szczodroski, A. F., Bassuner, K. J., Kirkpatrick, D. L., Rold, T. L., Sieckman, G. L., Hoffman, T. J., Connors, J. P., Smith, C. J., Synthesis and biological evaluation of copper-64 radiolabeled [DUPA-6-Ahx-(NODAGA)-5-Ava-BBN(7-14)NH_2], a novel bivalent targeting vector having affinity for two distinct biomarkers (GRPr/PSMA) of prostate cancer. Nucl Med Biol, 2014. **41**: p. 355-63
94. Liu, Z., Niu, G., Wang, F., Chen, X., ^{68}Ga-labeled NOTA-RGD-BBN peptide for dual integrin and GRPR-targeted tumor imaging. European J Nucl Mol Imag, 2009. **36**: p. 1483.
95. Andrew, B. J., Nanda, P. K., Rold, T. L., Sieckman, G. L., Szczodroski, A. F., Hoffman, T. J., Chen, X., Smith, C. J., ^{64}Cu-NO2A-RGD-Glu-6-Ahx-BBN(7-14)NH_2: a heterodimeric targeting vector for positron emission tomography imaging of prostate cancer. Nucl Med Biol, 2012. **39**: p. 377.
96. Durkan, K., Jiang, Z., Rold, T. L., Sieckman, G. L., Hoffman, T. J., Bandari, R. P., Szczodroski, A. F., Liu, L., Miao, Y., Reynolds, T. S., Smith, C. J., A heterodimeric [RGD-Glu-[64Cu-NO2A]-6-Ahx-RM2] $\alpha_V\beta_3$/GRPr-targeting antagonist radiotracer for PET imaging of prostate tumors. Nucl Med Biol, 2014. **41**: p. 133.
97. Stott Reynolds, T. J., Schehr, R., Liu, D., Xu, J., Miao, Y., Hoffman, T. J., Rold, T. L., Lewis, M. R., Smith, C. J., Characterization and evaluation of DOTA-conjugated Bombesin/RGD-antagonist for prostate cancer tumor imaging and therapy. Nucl Med Biol, 2015. **42**: p. 99.

Chapter 2: COPPER-64 NODAGA DUPA/BBN(7-14)NH_2 BIVALENT LIGAND FOR POTENTIAL DIAGNOSTIC IMAGING OF PROSTATE CANCER

2.1 INTRODUCTION

As ideal biomarkers for molecular targeting using radiolabeled peptides or small molecules, prostate-specific membrane antigen (PSMA) and gastrin releasing peptide receptors (GRPR) are co-expressed in very high numbers on human cancers including prostate cancer [1, 2]. The GRPR is one of the four known mammalian bombesin receptor subtypes, which are G protein-coupled, 7-transmembrane receptors with the capability of being endocytosed upon binding by an effective agonist ligand [3, 4]. BBN, a 14 amino acid amphibian peptide analog of gastrin releasing peptide (GRP), shares with the mammalian regulatory peptide GRP a homologous, 7 amino acid amidated C-terminus that is essential for high-affinity binding to GRPR [5]. PSMA, also known as folate hydrolase I or glutamate carboxypeptidase II, is a 750 amino acid integral membrane protein present in the neovasculature of most solid tumors but absent in normal vascular endothelium of normal tissues [6, 7]. For prostate cancer, although PSMA is mainly expressed in the epithelium, upregulation and translocation of PSMA from internal organelles to the cell surface generally occurs as all prostate cancer progress to the androgen-independent, metastatic disease stage [8-10]. Furthermore, PSMA undergoes internalization via clathrin-coated pits and has a tendency to be recycled to the surface of prostate cancer cells for additional internalization events [11, 12].

In this project, a C-terminal amidated BBN, BBN(7-14)NH_2 (Fig. 1.3), was used as the GRPR targeting motif, and a urea derivative with high binding affinity for PSMA,

DUPA (Fig. 1.5), was used as the PSMA targeting motif to form the bivalent ligand. ^{64}Cu, a radionuclide with ideal nuclear characteristics, was used to radiolabel the bivalent ligand to produce the tracer for biological evaluations. NODAGA (Fig. 1.8), a NOTA (Fig. 1.7) derivative, was used as the chelating agents for complexing ^{64}Cu to the bivalent ligand via conjugation onto the ligand with a functional group.

2.1.1 Specific Aims

The goal of the project was to produce, purify, characterize, and evaluate, both *in vitro* and *in vivo*, a GRPR/PSMA dual-targeting peptide conjugate ligand suitable for metallation of copper-64.

2.2 EXPERIMENTAL

2.2.1 Materials

Amino acids and resins for solid-phase and manual peptide synthesis were purchased from either Novabiochem/EMD Biosciences, Inc. (La Jolla, CA), Advanced ChemTech (Louisville, KY), or Chem-Impex International (Wood Dale, IL). $^{64}CuCl_2$ was purchased as a 0.1 M HCl solution from the University of Wisconsin-Madison (Madison, WI). All other reagents or solvents were purchased from Fisher Scientific (Pittsburgh, PA, USA) or Sigma-Aldrich Chemical Company (St. Louis, MO, USA) and used without further purification. ^{125}I-[Tyr^4]-BBN was purchased from Perkin-Elmer (Waltham, MA, USA). PC-3 and LNCaP cells were obtained from American Type Culture Collection and were maintained by the University of Missouri Cell and Immunobiology Core Facility (Columbia, MO).

2.2.2 Synthesis of [DUPA-6-Ahx-K-5-Ava-BBN(7-14)NH_2] Precursor

A combination of solid phase and manual peptide synthesis was used to synthesize the bivalent GRPR/PSMA-targeting precursor, [DUPA-6-Ahx-K-5-Ava-BBN(7-14)NH_2]. Briefly, manual resin-based peptide synthesis was employed to prepare the GRPR/PSMA-targeting precursor using traditional F-moc chemistry. 6-Ahx and 5-Ava represent the pharmacokinetic modifiers 6-aminohexanoic acid and 5-aminovaleric acid, BBN(7-14)NH2 = Q-W-A-V-G-H-L-M-NH_2, and DUPA precursor denotes 2-[3-(1,3-Bis-tert-butoxycarbonylpropyl)-ureido]pentanedioic acid. Briefly, Rink Amide-MBHA resin (0.1 mmol) and F-moc protected amino acids with appropriate side-chain protections (0.2 mmol) were utilized for synthesis. After being swelled with a combination of methylene chloride (3 ml) and dimethyl formamide (DMF, 3 ml), the resin was mixed with a solution of 20% piperidine in DMF (3 × 3 ml) and bubbled with nitrogen for 5 min. Then, the resin was washed with DMF (3 × 3 ml) and isopropyl alcohol (i-PrOH, 3 × 3 ml). The Kaiser Test was employed to assess the formation of the free, N-terminal, primary amines. Upon swelling the resin once again in DMF, a solution of F-moc protected amino acids (0.2 mmol), O-Benzotriazole-N,N,N’,N’-tetramethyl-uronium-hexafluoro-phosphate (HBTU) (0.2 mmol), Hydroxybenzotriazole (HOBt) (0.2 mmol) and N,N-Diisopropylethylamine (DIPEA) (0.4 mmol) in DMF was added to the resin. The resin was bubbled by nitrogen gas for 2 h, followed by washing with DMF (3 × 3 ml) and i-PrOH, (3 × 3 ml). The coupling efficiency was assessed by the Kaiser Test, and the above coupling procedure was repeated 12 additional times to produce the bivalent ligand precursor. The peptide was cleaved from the resin via a cocktail of water, triisopropylsilane (TIS), and trifluoracetic acid (TFA) in a ratio of 2.5:2.5:95 and then

precipitated in methyl-t-butyl ether. The crude peptide conjugate was purified by RP-HPLC (reversed phase high performance liquid chromatography, t_R = 11.3 min). Solvents were removed in vacuo using a SpeedVac concentrator (Labconco, Kansas City, MO). The purified peptides were characterized by ESI-MS (Electrospray ionization-mass spectroscopy).

2.2.3 Synthesis of [DUPA-6-Ahx-(NODAGA)-5-Ava-BBN(7-14)NH_2]

The new NODAGA conjugate was produced by conjugating a derivative of NOTA (1,4,7-triazacyclononane-1,4,7-triacetic acid), NODAGA (2-(4,7-biscarboxymethyl)-1,4,7-(triazonan-1-yl)pentanedioic acid), onto the ε-amine of lysine (K) on the bivalent peptide precursor [DUPA-6-Ahx-K-5-Ava-BBN(7-14)NH_2] via an active ester using a modified procedure that has been previously described [13, 14]. Briefly, [DUPA-6-Ahx-K-5- Ava-BBN(7-14)NH_2] (2.7 μmol) was dissolved in 0.1 M sodium phosphate buffer and the pH was adjusted to 7.4 using 10% NaOH. NODAGA-NHS (27 μmol), dissolved in 200 μL of 0.1 M sodium phosphate buffer (pH = 7.0), was mixed with the peptide solution. The reaction mixture was stirred for 6 h at 5–10 ℃, followed by stirring overnight at ambient temperature. The bivalent NODAGA conjugate was purified by RP-HPLC (t_R = 12.2 min). The new bivalent conjugate was confirmed by ESI-MS.

2.2.4 Metallation of [DUPA-6-Ahx-(NODAGA)-5-Ava-BBN(7-14)NH_2] with ^{nat}Cu and ^{64}Cu

[DUPA-6-Ahx-(^{nat}Cu-NODAGA)-5-Ava-BBN(7-14)NH_2] was produced by adding 7.4 mM natural $CuCl_2$•$2H_2O$ in 0.05 N HCl (90 nmol) to purified [DUPA-6-Ahx-(NODAGA)-5-Ava-BBN(7-14)NH_2] peptide conjugate (80 nmol, 250 μl 0.4M

ammonium acetate). The pH of the reaction mixture was adjusted to approximately 7.0 by the addition of 1% NaOH. The mixture was incubated for 1 h at 70 ℃ and then 50 µl of 10 mM DTPA (diethylenetriaminepentaacetic acid) solution was added to scavenge unbound metal. The metallated conjugate, [DUPA-6-Ahx-(^{nat}Cu-NODAGA)-5-Ava-BBN(7-14)NH_2], was purified by RP-HPLC (t_R = 11.6 min) and characterized by ESI-MS prior to *in vitro* receptor binding assays.

Likewise, the radiolabeled ligand, [DUPA-6-Ahx-(^{64}Cu-NODAGA)-5-Ava-BBN(7-14)NH_2], was synthesized by the reaction of [DUPA-6-Ahx-(NODAGA)-5-Ava-BBN(7-14)NH_2] (50 µg, 200 µl 0.4 M ammonium acetate) with $^{64}CuCl_2$ (185 MBq, 2.02 $\times 10^{-11}$ mol, 9.16 $\times 10^{18}$ Bq/mol) in 0.05 N HCl for 1 h at 70 ℃ (pH = 7.0). Fifty µl of 10 mM DTPA solution was added to scavenge any remaining copper metal ion. The ^{64}Cu-radiolabeled peptide was purified via RP-HPLC (t_R = 11.6 min) and collected into 100 µl of 1mg/ml BSA (bovine serum albumin) and ascorbic acid (25 µg) prior to *in vitro*, *in vivo*, and imaging assays. Acetonitrile was removed under a steady stream of nitrogen and the radiochemical purity was assessed by RP-HPLC (t_R = 11.6 min).

2.2.5 RP-HPLC and MS Analysis of Non-metallated and Metallated [DUPA-6-Ahx-(NODAGA)-5-Ava-BBN(7-14)NH_2]

The reversed-phase high-performance liquid chromatography (RP-HPLC) purifications of the peptide conjugate and metallated complexes were performed on an SCL-10A HPLC system (Shimadzu, Kyoto, Japan) employing a binary gradient system [solvent A = 99.9% DI water with 0.1% trifluoroacetic acid (TFA); solvent B = 99.9% acetonitrile containing 0.1% TFA]. A linear gradient of 75:25A/B to 65:35A/B over 15 min and 65:35A/B to 5:95A/B over 2 min was used for purification. Samples were

observed using an in-line Shimadzu SPD-10A UV-vis tunable absorbance detector (λ = 280 nm) as well as an in-line EG&G Ortec NaI solid crystal scintillation detector (EG&G, Salem, MA, USA). EZStart software (7.4; Shimadzu) was used for data acquisition of both signals. A semi-preparative C-18 reversed-phase column (Phenomenex Jupiter Proteo, 250 × 10.00 mm, 10 µm; Phenomenex, Torrance, CA, USA) maintained at 34 ℃ via an Eppendorf TC-50 column heater was used for purification of [DUPA-6-Ahx-K-5-Ava-BBN(7-14)NH_2] precursor and [DUPA-6-Ahx-(NODAGA)-5-Ava-BBN(7-14)NH_2]. [DUPA-6-Ahx-($^{nat/64}$Cu-NODAGA)-5-Ava-BBN(7-14)NH_2] were purified using an analytical C-18 reversed-phase column (Phenomenex Jupiter Proteo, 250 × 4.60 mm, 5 µm). Purified peptide conjugates were lyophilized in a CentriVap system (Labconco, Kansas City, MO, USA). Electrospray-ionization mass spectrometry (ESI-MS) for characterization of precursor peptide, non-metallated and metallated peptide conjugate was performed at the MS facility, Department of Chemistry, University of Missouri (Columbia, MO).

2.2.6 *In Vitro* Competitive Displacement Binding Assays of [DUPA-6-Ahx-(^{nat}Cu-NODAGA)-5-Ava-BBN(7-14)NH_2] in GRPR-positive PC-3 cells and PSMA-positive LNCaP Cells

Competitive displacement binding assays of [DUPA-6-Ahx-(^{nat}Cu-NODAGA)-5-Ava-BBN(7-14)NH_2] were conducted in GRPR-positive PC-3 cells and PSMA-positive LNCaP homogenized cell membranes using [^{125}I-(Tyr^4)-BBN] and [+N-acetyl aspartyl ^{3}H-glutamate] (NAAG) as the radioligands.

The IC_{50} (half maximal inhibitory concentration) value of [DUPA-6-Ahx-(^{nat}Cu-NODAGA)-5-Ava-BBN(7-14)NH_2] was determined using GRPR-expressing, human PC-3 prostate cancer cells (~3 × 10^4 cells/tube, suspended in DMEM/F-12 K media containing 0.01 M MEM and 2% BSA, pH = 5.5) incubated with ~20,000 cpm of ^{125}I-[Tyr^4]-BBN and increasing concentrations of the cold metal labeled conjugate (10^{-12} M to 10^{-5} M) for 1 h at 37 ℃ in a 5% CO_2-enriched atmosphere. The medium was aspirated after incubation, and the cells washed three times with cold cell medium (pH = 7, 0.2% BSA in DMEM + HEPES). A Packard Riastar multiwall gamma counting system was utilized to measure cell-associated radioactivity. The percent of bound radioligand was plotted against increasing concentrations of the metallated conjugate to determine the IC_{50} value. The dissociation curves and IC_{50} values were generated via Prism Software (version 5.0). The experiments were carried out in triplicate, and the average of the trials was used as the final IC_{50} value.

For the PSMA-positive LNCaP homogenized cell membranes, the binding affinity of [DUPA-6-Ahx-(^{nat}Cu-NODAGA)-5-Ava-BBN(7-14)NH_2] was also measured via the N-acetylated-a-linked acidic dipeptidase (NAALADase) assay with only minor modification [15]. Briefly, LNCaP tissue culture homogenized cell membranes were incubated with increasing concentrations of [DUPA-6-Ahx-(^{nat}Cu-NODAGA)-5-Ava-BBN(7-14)NH_2] (1×10^{-13}–1×10^{-5} M) in 50 μL of Tris–HCl buffer (50 mM, pH = 7.4) for 45 min. After the addition of [N-acetyl aspartyl ^{3}H-glutamate], the reaction mixture was allowed to incubate for an additional 15 min at 37 ℃. Then, 50 ml of cold sodium phosphate buffer (0.1 M, pH = 7.4) was added to stop the enzymatic reaction. Cation exchange chromatography was performed to resolve [N-acetyl aspartyl ^{3}H-glutamate]

and [^{3}H-glutamate] with AG 50 W-X8 columns (200–400 mesh) which were pre-equilibrated with 0.2 M HCl prior to loading of the reaction mixture. Fractions containing [^{3}H-glutamate] were eluted using 6 ml of 2 M HCl. Scintillation cocktail was added to each fraction and the amount of radioactivity in each was measured by liquid scintillation counting. The percent of bound radioligand was plotted against increasing concentrations of the metallated conjugate to determine the IC_{50} value. IC_{50} values were determined by curve fitting using Prism Software (version 5.0).

2.2.7 *In Vivo* Assays of [DUPA -6-Ahx-(^{64}Cu- NODAGA)-5-Ava-BBN(7-14)NH_2]

2.2.7.1 MicroPET/microCT Imaging Studies of [DUPA-6-Ahx-(^{64}Cu-NODAGA)-5-Ava-BBN(7-14)NH2] in GRPR-positive Tumors and PSMA-positive Tumors

All animal studies were conducted in compliance with the NIH guide for Care and Use of Laboratory Animals and the Policy and Procedures for Animal Research at the Harry S. Truman Memorial Veterans' Hospital. ICR SCID (Institute of Cancer Research Severe Combined Immunodeficient) female mice (4–5 weeks of age) and male athymic nude-Fox1^{nu} mice were supplied from Taconic Farms (Germantown, NY) or Harlan Laboratories (Madison, WI). The mice were housed in sterile micro-isolator cages in a temperature- and humidity-controlled room with a 12 h light/12 h dark schedule. The animals were fed autoclaved rodent chow (Ralston Purina Company, St. Louis, MO) and water *ad libitum*. For tumor inoculations, bilateral subcutaneous flank injections of approximately 5×10^{6} PC-3 cells per 100 µl of normal sterile saline were performed on the SCID mice, which were anesthetized with isoflurane (Baxter Healthcare Corp., Deerfield, IL, USA) at a rate of 2.5% with 0.4 L oxygen supplied through a non-

rebreathing anesthesia vaporizer. Tumors were allowed to grow 2-3 weeks post inoculation and developed to range in mass from 0.2 g to 0.4 g. Athymic nude mice were also anesthetized for injections with isoflurane (Baxter Healthcare Corp., Deerfield, IL) at a rate of 2.5% with 0.4 L oxygen through a non-rebreathing anesthesia vaporizer. LNCaP cells were injected bilaterally into the subcutaneous flank regions, with ~ 5×10^6 cells in a suspension of 100 μL normal sterile saline per injection site.

Maximum intensity microPET coronal and axial images were obtained on a Siemens INVEON small animal, dedicated PET/CT unit (Siemens, Nashville, TN, USA) at 18 h p.i. according to published procedure [2]. ~675 μCi (~25 MBq) of [DUPA -6-Ahx-(^{64}Cu-NODAGA)-5-Ava-BBN(7-14)NH_2] in 100 μl of isotonic saline was delivered to each PC-3 or LNCaP tumor-bearing mouse through the tail vein injection. The mice were euthanized via CO_2 administration. Micro-computed tomography (microCT) coronal images were also obtained on the Siemens INVEON small-animal CT unit following microPET imaging for fusing the anatomic and molecular data. The microCT images were acquired, and concurrent image reconstruction was achieved using a conebeam (Feldkamp) filtered, back-projection algorithm. The raw, reconstructed microSPECT datasets were imported into the INVEON Research Workstation software for subsequent image fusion with the microCT image data and 3D (three-dimensional) visualization.

2.3 RESULTS AND DISCUSSION

In this study, [DUPA-6-Ahx-K-5-Ava-BBN(7-14)NH_2] was synthesized by solid-phase peptide synthesis (SPPS). However, amino acid and 2-[3-(1,3-bis-tert-

butoxycarbonylpropyl)-ureido]pentanedioic acid 1-tert-butyl ester were manually added, and afterwards the deprotection was performed using using a cocktail of water, triisopropylsilane (TIS), and TFA. Then, NODAGA was conjugated to the ε-amine of lysine (K) to produce [DUPA-6-Ahx-(NODAGA)-5-Ava-BBN(7-14)NH_2] in high yield (~65%). The bivalent ligand, [DUPA-6-Ahx-(NODAGA)-5-Ava-BBN(7-14)NH_2], was purified by RP-HPLC, characterized by ESI-MS and then metallated with $^{nat/64}CuCl_2$ to produce [DUPA-6-Ahx-($^{nat/64}$Cu-NODAGA)-5-Ava-BBN(7-14)NH_2] the structure of which is shown in Fig. 2.1. The mass spectrometry results of each [DUPA-6-Ahx-K-5-Ava-BBN(7-14)NH_2] derivative, shown in Table 2.1, were consistent with the calculated molecular weights, which confirmed the identity of the expected products. The ^{64}Cu-radiolabeled conjugate was synthesized in high radiochemical yield (> 95%). According to the RP-HPLC chromatographic profile of [DUPA-6-Ahx-(^{64}Cu-NODAGA)-5-Ava-BBN(7-14)NH_2] (Fig. 2.2, Table 2.1), the ^{64}Cu-conjugate has similar retention time (t_R = 11.6 min) to ^{nat}Cu-conjugate, indicating structural similarity between the tracer and the cold ligand.

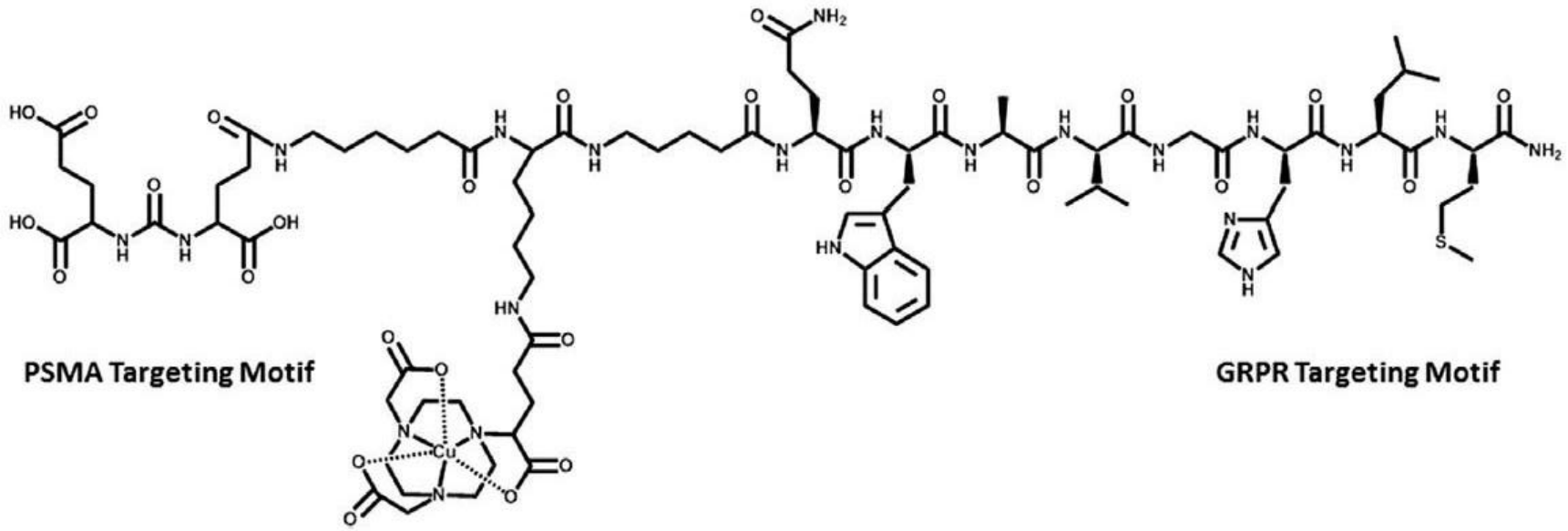

Fig. 2.1: Chemical structure of [DUPA-6-Ahx-(^{64}Cu-NODAGA)-5-Ava-BBN(7-14)NH_2]

Table 2.1. Mass spectrometry, IC_{50}, and RP-HPLC data for [DUPA-6-Ahx-K-5-Ava-BBN(7-14)NH_2], [DUPA-6-Ahx-(NODAGA)-5-Ava-BBN(7-14)NH_2], and [DUPA-6-Ahx-(^{nat}Cu-NODAGA)-5-Ava-BBN(7-14)NH_2].

Molecular formula [DUPA-6-Ahx-K-5-Ava-BBN(7-14)NH_2]	$C_{71}H_{111}N_{19}O_{20}S$
Molecular formula [DUPA-6-Ahx-(NODAGA)-5-Ava-BBN(7-14)NH_2]	$C_{86}H_{134}N_{22}O_{27}S$
Molecular formula [DUPA-6-Ahx-(^{nat}Cu-NODAGA)-5-Ava-BBN(7-14)NH_2]	$C_{86}H_{132}N_{22}O_{27}S$ Cu
Calculated molecular mass, [DUPA-6-Ahx-K-5-Ava-BBN(7-14)NH_2]	1581.80 Da
Calculated molecular mass, [DUPA-6-Ahx-(NODAGA)-5-Ava-BBN(7-14)NH_2]	1940.02 Da
Calculated molecular mass, [DUPA-6-Ahx-(^{nat}Cu-NODAGA)-5-Ava-BBN(7-14)NH_2]	2001.09 Da
ESI-MS molecular mass (M + H^+), [DUPA-6-Ahx-K-5-Ava-BBN(7-14)NH_2]	1582.64 Da
ESI-MS molecular mass (M + H^+), [DUPA-6-Ahx-(NODAGA)-5-Ava-BBN(7-14)NH_2]	1941.03 Da
ESI-MS molecular mass (M + H^+), [DUPA-6-Ahx-(^{nat}Cu-NODAGA)-5-Ava-BBN(7-14)NH_2]	2001.87 Da
[DUPA-6-Ahx-K-5-Ava-BBN(7-14)NH_2] RP-HPLC t_R	11.3 min
[DUPA-6-Ahx-(NODAGA)-5-Ava-BBN(7-14)NH_2] RP-HPLC t_R	12.2 min
[DUPA-6-Ahx-(^{nat}Cu-NODAGA)-5-Ava-BBN(7-14)NH_2] RP-HPLC t_R	11.6 min
IC_{50}, [DUPA-6-Ahx-(^{nat}Cu-NODAGA)-5-Ava-BBN(7-14)NH_2], PC-3	11.1 ± 0.46 nM
IC_{50}, [DUPA-6-Ahx-(^{nat}Cu-NODAGA)-5-Ava-BBN(7-14)NH_2], LNCaP	1.16 ± 1.35 nM

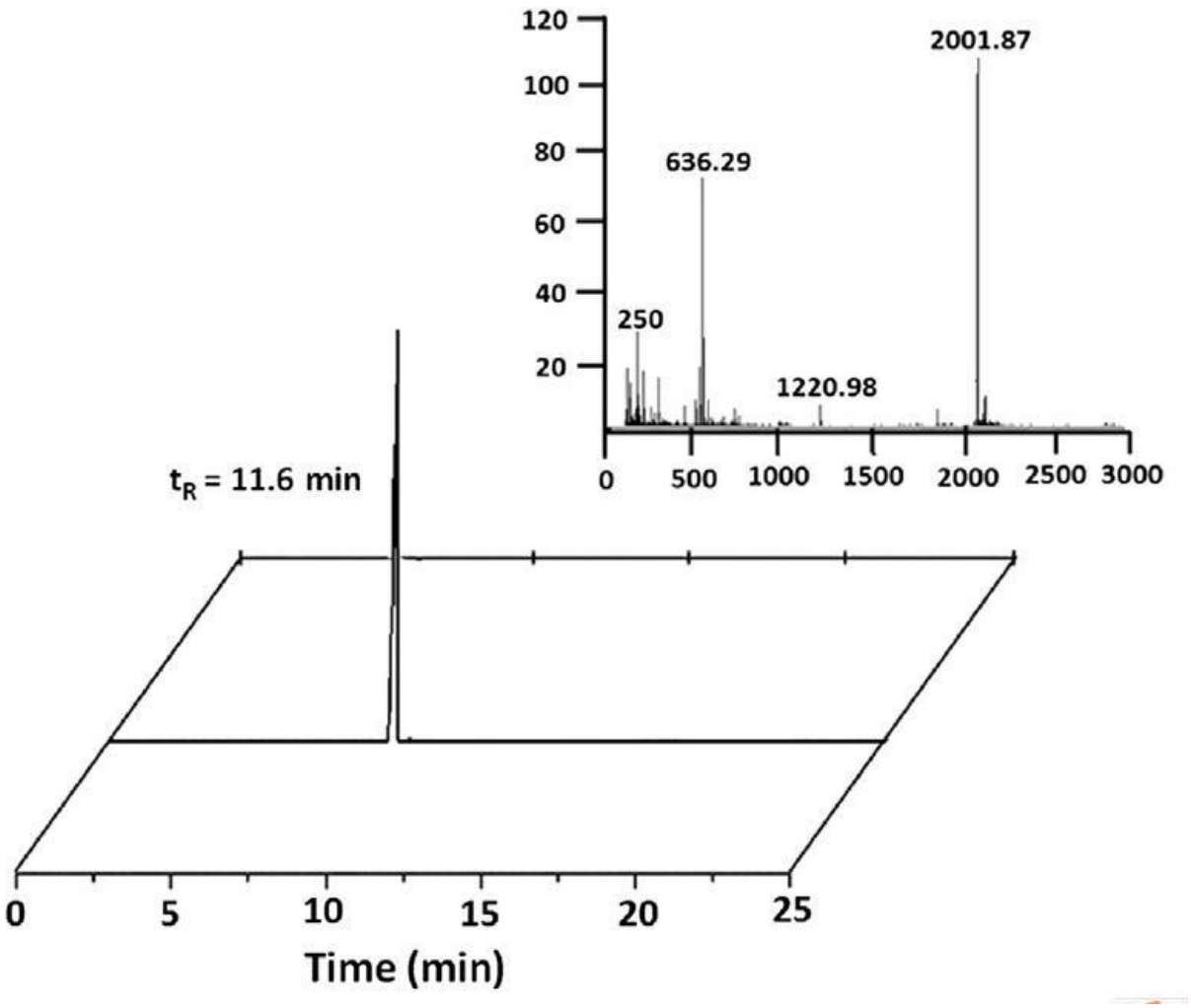

Fig. 2.2: HPLC chromatographic profiles of [DUPA-6-Ahx-(64Cu-NODAGA)-5-Ava-BBN(7-14)NH2] (tR = 11.6 min) and ESI mass spectrum ($M + H^+$ = 2001.87) for [DUPA-6-Ahx-(^{nat}Cu-NODAGA)-5-Ava-BBN(7-14)NH_2].

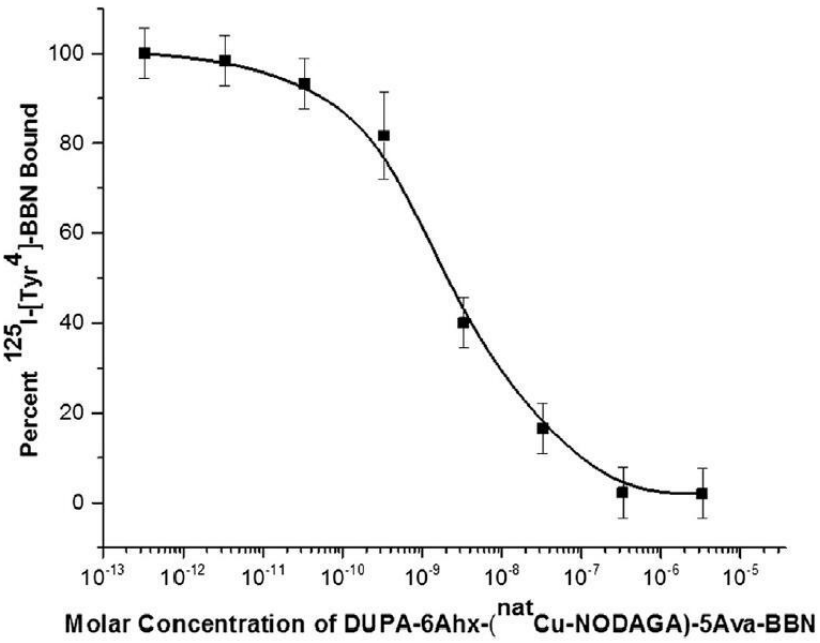

Fig. 2.3: Half-maximal inhibitory concentrations (IC_{50}) for [DUPA-6-Ahx-(^{nat}Cu-NODAGA)-5-Ava-BBN(7-14)NH_2] (IC_{50} = 11.1 ± 0.46 nM) in human, prostate, PC-3 cells.

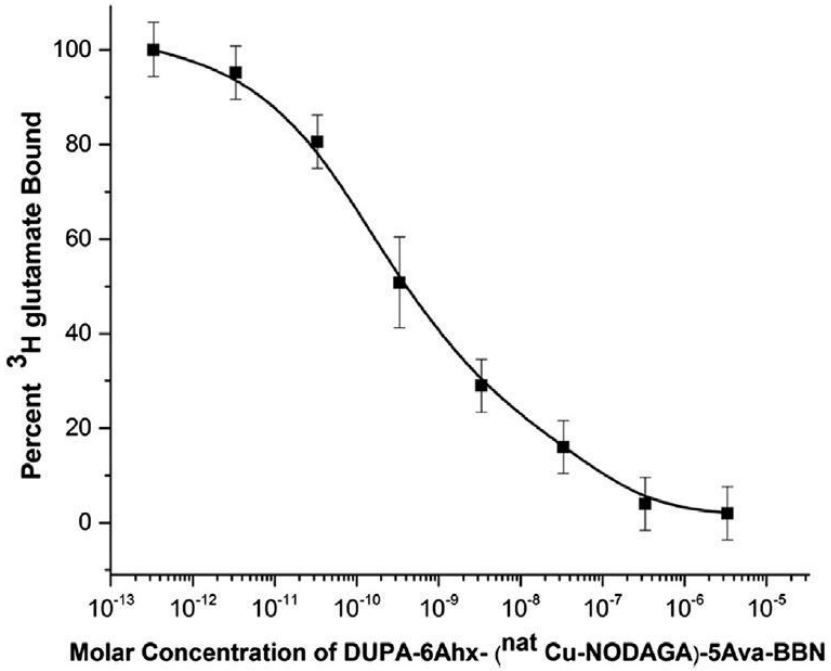

Fig. 2.4: Half-maximal inhibitory concentrations (IC_{50}) for [DUPA-6-Ahx-(^{nat}Cu-NODAGA)-5-Ava-BBN(7-14)NH_2] (IC50 = 1.16 ± 1.35 nM) in human, prostate, LNCaP cells.

A competitive displacement binding assay of [DUPA-6-Ahx-(^{nat}Cu-NODAGA)-5-Ava-BBN(7-14)NH_2] was performed in GRPR-positive PC-3 and PSMA-positive LNCaP cells using [^{125}I-(Tyr^4)-BBN] and [N-acetyl aspartyl ^{3}H-glutamate] (NAAG) as radioligands, and a typical sigmoidal curve demonstrating displacement of radioactive competitors from cells as a function of increasing concentration of the naturally metallated conjugate was generated (Fig. 2.3, Fig. 2.4). According to IC_{50} values (Table 2.1) obtained from the curves, the bivalent conjugate showed high affinity to both biomarkers expressed on cells (11.1 ± 0.46 nM for GRPR-expressing PC-3 cells, 1.16 ± 1.35 nM for PSMA-expressing LNCaP cells).

The results of microPET/microCT imaging studies for [DUPA-6-Ahx-(^{64}Cu-NODAGA)-5-Ava-BBN(7-14)NH_2] in PC-3 and LNCaP tumor-bearing SCID and nu/nu mice are shown in Fig. 2.5 and Fig. 2.6. The images were obtained at 18 h post-injection (p.i.) of the tracer through the tail vein. The two xenografted PC-3 tumors on both flanks are clearly observable in all images. However, the abdominal uptake and retention of the tracer are significant, probably due to the hydrophobicity of the molecule. Additionally, a big portion of the abdominal background is expected to result from the receptor-mediated accumulation and retention of the tracer in PSMA-positive kidney. For the microPET/microCT image of [DUPA-6-Ahx-(^{64}Cu-NODAGA)-5-Ava-BBN(7-14)NH_2] in an LNCaP tumor-bearing nude mouse model, only a single LNCaP tumor is observable also with great amounts of radioactivity uptake and retention in abdominal tissues, such as the liver, small intestine and kidneys.

As the first example of the bivalent ligand with the capability of targeting both GRPR and PSMA, [DUPA-6-Ahx-(^{64}Cu-NODAGA)-5-Ava-BBN(7-14)NH_2], despite of its strong binding affinity to GRPR and PSMA biomarkers in *in vitro* evaluations, the microPET images obtained in *in vivo* evaluations displayed its ability to effectively identify tumors but were not

superior to other tracers that were produced and evaluated in our laboratory. Preliminary biodistribution studies indicated the tracer in PC-3 tumor-bearing SCID mice underwent renal excretion meanwhile with great retention in abdominal tissues at 24 h p.i. The hydrophobicity of the tracer along with receptor-mediated binding in PSMA-positive kidney results in the similarly high abdominal background in microPET images of mice bearing PSMA-postive LNCaP tumors. Consequently, adjustments and alternatives for improving the metabolic profiles of the tracer and reducing background uptake of the tracer in non-target tissues are warranted. In addition to adjusting the linkers to decrease the hydrophobicity of the molecule, using an antagonist ligand such as [D-Phe-Gln-Trp-Ala-Val-Gly-His-Sta-Leu-NH2] (AR) is of great interest with reference to recent studies demonstrating that antagonists are superior to agonists in *in vivo* evaluations [16, 17]. As a result, a bivalent PSMA/GRPR-targeting ligand based on DUPA-AR can be a candidate of great potential to improve targeting ability of primary and metastatic prostate cancer.

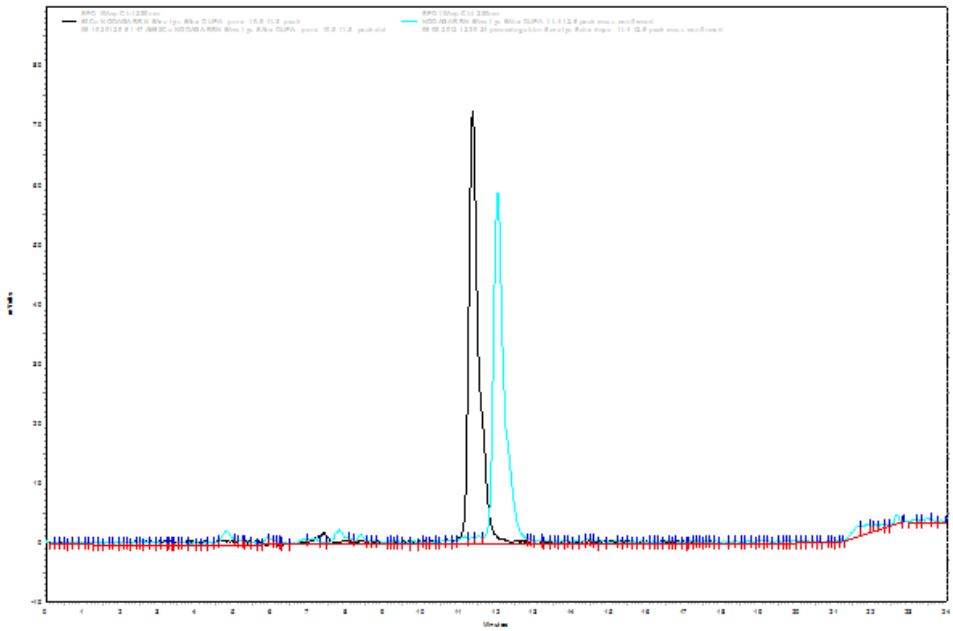

Fig. 2.7: The RP-HPLC profiles of [BBN-5-Ava-(^{nat}Cu-NODAGA)-6-Ahx-DUPA] and [BBN-5-Ava-(NODAGA)-6-Ahx-DUPA].

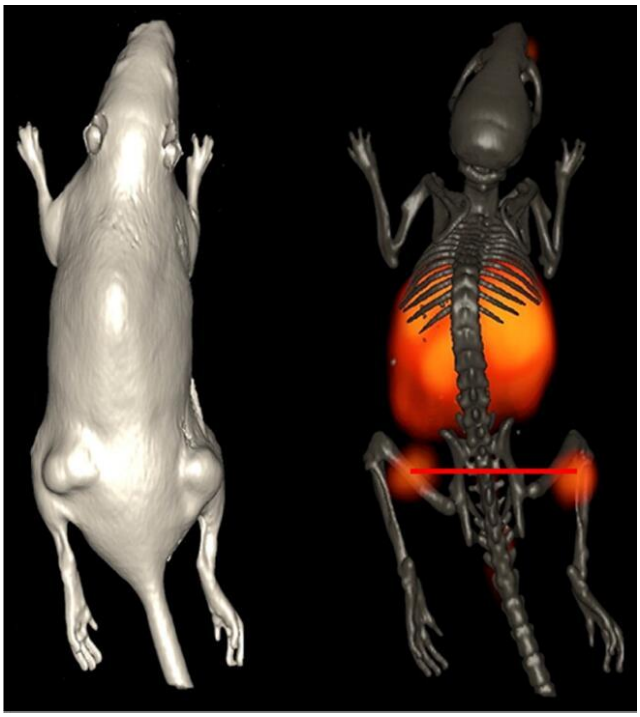

Fig. 2.5: Maximum intensity microPET tumor and microCT skeletal fusion coronal whole body image of a PC-3 tumor bearing SCID mouse at 18 h after tail vein injection of [DUPA-6-Ahx-(^{64}Cu-NODAGA)-5-Ava-BBN(7-14)NH_2].

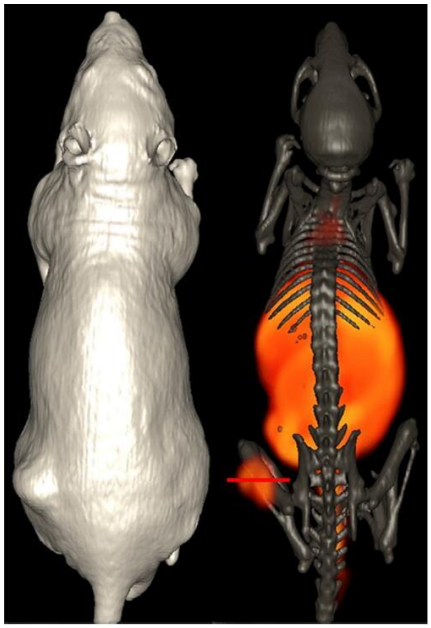

Fig. 2.6: Maximum intensity microPET tumor and microCT skeletal fusion coronal whole body image of an LNCaP tumor bearing SCID mouse at 18 h after tail vein injection of [DUPA-6-Ahx-(^{64}Cu-NODAGA)-5-Ava-BBN(7-14)NH_2].

2.4 CONCLUSION

This study herein demonstrated the synthesis, characterization, *in vitro*, *in vivo*, and microPET investigations of a new bivalent ligand, [DUPA-6-Ahx-(^{64}Cu-NODAGA)-5-Ava-BBN(7-14)NH_2], as a universal molecular imaging agent capable of targeting both the GRPR and PSMA for prostate cancer. *In vitro* and *in vivo* evaluations confirmed the targeting ability of the tracer for either biomarker. Although the microPET images for the tracer in PC-3 (GRPR-positive) and LNCaP (PSMA-positive) prostate cancer cells are not ideal, the development and future improvement of the tracer is warranted due to its potential to be a fundamental tool for early detection, progression staging, possible recurrence evaluation, and monitoring the effects of therapeutic intervention.

2.5 REFERENCES

1. Hillier, S. M., Maresca, K. P., Femia, F. J., Marquis, J. C., Foss, C. A., Nguyen, N., Zimmerman, C. N., Barrett, J. A., Eckelman, W. C., Pomper, M. G., Joyal, J. L., Babich, J. W., Preclinical evaluation of novel glutamate-urea-lysine analogues that target prostate-specific membrane antigen as molecular imaging pharmaceuticals for prostate cancer. Cancer Res, 2009. **69**: p. 6932–40.
2. Lane, S. R., Nanda, P., Rold, T. L., Sieckman, G. L., Figueroa, S. D., Hoffman, T. J., Jurisson, S. S., Smith, C. J., Optimization, biological evaluation and microPET imaging of copper-64-labeled bombesin agonists, [^{64}Cu-NO2A-(X)-BBN(7-14)NH_2], in a prostate tumor xenografted mouse model. Nucl Med Biol, 2010. **37**; p. 751–61.
3. Jensen, R. T., Battey, J. F., Spindel, E. R., Benya, R. V., International union of pharmacology. LXVIII. Mammalian bombesin receptors: nomenclature, distribution, pharmacology, signaling, and functions in normal and disease states. Pharmacol Rev, 2008. **60**: p. 1–42.
4. Cescato, R., Maina, T., Nock, B., Nikolopoulou, A., Charalambidis, D., Piccand, V., Reubi, J. C., Bombesin receptor antagonists may be preferable to agonists for tumor targeting. J Nucl Med, 2008. **49**: p. 318–26.
5. Thomas, R., Chen, J., Roudier, M. M., Vessella, R. L., Lantry, L. E., Nunn, A. D., In vitro binding evaluation of ^{177}Lu-AMBA, a novel ^{177}Lu-labeled GRP-R agonist for systemic radiotherapy in human tissues. Clin Exp Metastasis, 2009. **26**: p. 105–19.
6. Chang, S. S., Reuter, V. E., Heston, W. D., Bander, N. H., Grauer, L. S., Gaudin, P. B., Five different anti-prostate-specific membrane antigen (PSMA) antibodies confirm PSMA expression in tumor-associated neovasculature. Cancer Res, 1999. **59**: p. 3192–8.
7. Rajasekaran, A. K., Anilkumar, G., Christiansen, J. J., Is prostate-specific membrane antigen a multifunctional protein? Am J Physiol Cell, 2005. **288**: p. C975–81.
8. Chen, Y., Dhara, S., Banerjee, S. R., Byun, Y., Pullambhatla, M., Mease, R. C., Pomper, M. G., A low molecular weight PSMA-based fluorescent imaging agent for cancer. Biochem Biophys Res Commun, 2009. **390**: p. 624–9.
9. Banerjee, S. R., Foss, C. A., Castanares, M., Mease, R. C., Byun, Y., Fox, J. J., Hilton, J., Lupold, S. E., Kozikowski, A. P., Pomper, M. G., Synthesis and evaluation of technetium-99 m- and rhenium-labeled inhibitors of the prostate specific membrane antigen (PSMA). J Med Chem, 2008. **51**: p. 4504–17.
10. Foss, C. A., Mease, R. C., Fan, H., Wang, Y., Ravert, H. T., Dannals, R. F., Olszewski, R. T., Heston, W. D., Kozikowski, A. P., Pomper, M. G., Radiolabeled small-molecule ligands for prostate-specific membrane antigen: in vivo imaging in experimental models of prostate cancer. Clin Cancer Res, 2005. **11**: p. 4022–8.
11. Kularatne, S. A., Wang, K., Santhapuram, H. K., Low, P. S., Prostate-specific membrane antigen targeted imaging and therapy of prostate cancer using a PSMA inhibitor as a homing ligand. Mol Pharm, 2009. **6**: p. 780–9.
12. Kularatne, S. A., Zhou, Z., Yang, J., Post, C. B., Low, P. S., Design, synthesis, and preclinical evaluation of prostate-specific membrane antigen targeted ^{99m}Tc-radioimaging agents. Mol Pharm, 2009. **6**: p. 790–800.
13. Durkan, K., Jiang, Z., Rold, T. L., Sieckman, G. L., Hoffman, T. J., Bandari, R. P., Szczodroski, A. F., Liu, L., Miao, Y., Reynolds, T. S., Smith, C. J., A heterodimeric

[RGD-Glu-[^{64}Cu-NO2A]-6-Ahx-RM2] $\alpha_v\beta_3$/GRPr-targeting antagonist radiotracer for PET imaging of prostate tumors. Nucl Med Biol, 2014. **41**: p. 133–9.

14. Prasanphanich, A. F., Retzloff, L., Lane, S. R., Nanda, P. K., Sieckman, G. L., Rold, T. L., Ma, L., Figueroa, S. D., Sublett, S. V., Hoffman, T. J., Smith, C. J., In vitro and in vivo analysis of [^{64}Cu-NO2A-8-Aoc-BBN(7-14)NH_2]: a site-directed radiopharmaceutical for positron-emission tomography imaging of T-47D human breast cancer tumors. Nucl Med Biol, 2009. **36**: p. 171–81.
15. Graham, K., Lesche, R., Gromov, A. V., Böhnke, N., Schäfer, M., Hassfeld, J., Dinkelborg, L., Kettschau, G., Radiofluorinated derivatives of 2-(phosphonomethyl)pentanedioic acid as inhibitors of prostate specific membrane antigen (PSMA) for the imaging of prostate cancer. J Med Chem, 2012. **55**: p. 9510–20.
16. Mansi, R., Wang, X., Forrer, F., Waser, B., Cescato, R., Graham, K., Borkowski, S., Reubi, J. C., Maecke, H. R., Development of a potent DOTA-conjugated bombesin antagonist for targeting GRPr-positive tumours. Eur J Nucl Med Mol Imaging, 2011. **38**: p. 97–107.
17. Abiraj, K., Mansi, R., Tamma, M. L., Fani, M., Forrer, F., Nicolas, G., Cescato, R., Reubi, J. C., Maecke, H. R., Bombesin antagonist-based radioligands for translational nuclear imaging of gastrinreleasing peptide receptor-positive tumors. J Nucl Med, 2011. **52**: p. 1970–8.

Chapter 3: COPPER-64 NOTA RGD/RM2 BIVALENT LIGAND FOR POTENTIAL DIAGNOSTIC IMAGING OF PROSTATE CANCER

3.1 INTRODUCTION

The GRPR is a subtype of the BBN receptor superfamily with high expression in a variety of human cancers, such as breast, colon, pancreatic, and prostate cancer. Many of these cancers have been targeted with radiolabeled BBN derivatives for site-directed molecular imaging or therapy of disease [1-5]. BBN, a tetradecapeptide analogue of human GRP has very high binding affinity for GRPR and numerous BBN analogues have been synthesized and characterized for GRPR-positive tumor-targeted imaging and therapy [6-11]. RM2 is an antagonist analogue of BBN with high binding affinity to the GRPR and the research of BBN antagonists has shown superior biodistribution and imaging when compared to BBN agonists [12-16]. The $\alpha_v\beta_3$ integrin, a member of the integrin receptor family is another target of great interest due to its important roles in the modulation of cell migration and survival during angiogenesis, potentially facilitating metastatic invasion of the tumor cells across the blood vessels, and its moderate expression in a number of cancers such as malignant melanoma, glioblastoma, breast, and prostate tumors [17-19]. Monomeric and dimeric RGD peptides have attracted interest due to their ability to specifically target the $\alpha_V\beta_3$ integrin, which is expressed on several tumors such as malignant melanomas, glioblastoma, breast, and prostate tumors [20-22]. In this project, the BBN antagonist analogue, RM2 (Fig. 1.4), was used as the GRPR targeting motif, and a cyclic five amino acid moiety abbreviated as c(RGDyK), RGD (Fig. 1.6), with the strong binding affinity to $\alpha_v\beta_3$ was used as the $\alpha_v\beta_3$ integrin targeting motif for the bivalent ligand. ^{64}Cu was used to radiolabel the bivalent ligand to produce the tracer for biological evaluations. NOTA (Fig. 1.7) was used as the chelating agents for linking radionuclides to the bivalent ligand.

3.1.1 Specific Aims

The goal of the project was to produce, purify, characterize, and evaluate, both *in vitro* and *in vivo*, a GRPR/$\alpha_v\beta_3$ dual-targeting peptide conjugate ligand labeled with copper-64.

3.2 EXPERIMENTAL

3.2.1 Materials

[RGD-Glu-6-Ahx-RM2], [Cyclo(Arg-Gly-Asp-DTyr-Lys)-Glu-(6-Ahx-D-Phe-Gln-Trp-Ala-Val-Gly-His-Sta-Leu-NH_2], was purchased from CPC Scientific (Sunnyvale, CA, USA). $^{64}CuCl_2$ was purchased as a 0.1 M HCl solution from the University of Wisconsin-Madison (Madison, WI). All other reagents or solvents were purchased from Fisher Scientific (Pittsburgh, PA, USA) or Sigma-Aldrich Chemical Company (St. Louis, MO, USA) and used without further purification. ^{125}I-[Tyr^4]-BBN and ^{125}I-Echistatin were purchased from Perkin-Elmer (Waltham, MA, USA). PC-3 cells were obtained from American Type Culture Collection and were maintained by the University of Missouri Cell and Immunobiology Core Facility (Columbia, MO).

3.2.2 Synthesis of [RGD-Glu-(NO2A)-6-Ahx-RM2]

The NOTA derivative conjugates, [NO2A-(X)-BBN(7–14)NH_2], were produced by conjugating NOTA, 1,4,7-triazacyclononane-1,4,7-triacetic acid, to the peptide conjugate via an active ester as previously reported [23]. Briefly, 2-[morpholino]ethanesulfonic acid (MES) buffer (pH 4.7), NOTA, sulfo-NHS (N-hydroxysulfosuccinimide) and EDC (1-ethyl-3-[3-dimethylaminopropyl]carbodiimide hydrochloride) were stirred at room temperature. The desired peptide, dissolved in phosphate buffered solution, was then added to the active ester solution in MES buffer. The NO2A conjugate was purified by RP-HPLC and characterized by ESI-MS.

3.2.3 Metallation of [RGD-Glu-(NO2A)-6-Ahx-RM2] with ^{nat}Cu and ^{64}Cu

[RGD-Glu-[^{nat}Cu-NO2A]-6-Ahx-RM2] was produced by adding natural $CuCl_2 \bullet 2H_2O$ in 0.05 N HCl (90 nmol) to purified [RGD-Glu-[NO2A]-6-Ahx-RM2] peptide conjugate (89 nmol, 250 µl 0.4M ammonium acetate). The pH of the reaction mixture was adjusted to approximately 7.0 by the addition of 1% NaOH. The mixture was incubated for 1 h at 70 ℃ and then 50 µl of 10 mM DTPA solution was added to scavenge unbound metal. The metallated conjugate, [RGD-Glu-(^{nat}Cu-NO2A)-6-Ahx-RM2], was purified by RP-HPLC and characterized by ESI-MS prior to *in vitro* receptor binding assays.

The radiolabeled ligand, [RGD-Glu-(^{64}Cu-NO2A)-6-Ahx-RM2], was synthesized by the reaction of [RGD-Glu-(NO2A)-6-Ahx-RM2] (50 µg, 200 µl 0.4 M ammonium acetate) with $^{64}CuCl_2$ (74-111 MBq, 9.15×10^8 Bq/mol) in 0.05 N HCl for 1 h at 70 ℃ (pH = 7.0). Fifty µl of 10 mM DTPA solution was added to scavenge any remaining copper metal ion. The ^{64}Cu-radiolabeled peptide was purified via RP-HPLC and collected into 100 µl of 1mg/ml BSA prior to *in vitro, in vivo,* and imaging assays. Acetonitrile was removed under a steady stream of nitrogen and the radiochemical purity was assessed by RP-HPLC.

3.2.4 RP-HPLC and MS Analysis of Non-metallated and Metallated [RGD-Glu-(NO2A)-6-Ahx-RM2]

The unmetallated peptide conjugates and metallated complexes were purified via RP-HPLC performed on an SCL-10A HPLC system (Shimadzu, Kyoto, Japan) employing a binary gradient system [Solvent A=99.9% DI water with 0.1% trifluoroacetic acid (TFA); Solvent B=99.9% acetonitrile containing 0.1% TFA], programmed with a linear gradient of 25:75A/B to 35:65 A/B gradient over 15 min (followed by an additional 10 min at 5:95 A/B). Samples were eluted from an analytical C-18 reversed-phase column (Phenomenex Jupiter Proteo, 250 × 4.60

mm, 5 μm; Phenomenex, Torrance, CA, USA) maintained at 34 ℃ via an Eppendorf TC-50 column heater and observed using an in-line Shimadzu SPD-10A UV-vis tunable absorption detector (λ = 280 nm) and an in-line, EG&G Ortec NaI solid crystal scintillation detector (EG&G, Salem, MA, USA). EZStart software (7.4.3; Shimadzu, Kyoto, Japan) was used to accomplish data acquisition of both signals. Purified compounds were lyophilized in a CentriVap system (Labconco, Kansas City, MO, USA). ESI-MS analyses were performed in the laboratory of Dr. Fabio Gallazzi at the University of Missouri, Department of Chemistry, Columbia, MO, USA.

3.2.5 *In Vitro* Competitive Displacement Binding Assays of [RGD-Glu-(^{nat}Cu-NO2A)-6-Ahx-RM2] in GRPR-expressing PC-3 Cells and $\alpha_V\beta_3$-expressing U87-MG Cells

The IC_{50} value of [RGD-Glu-[^{nat}Cu-NO2A]-6-Ahx-RM2] was obtained by competitive displacement binding assays using GRPR-expressing, human PC-3 prostate cancer cells (~3 × 10^4 cells/tube, suspended in DMEM/F-12 K) incubated with ~20,000 cpm of ^{125}I-[Tyr^4]-BBN and increasing concentrations of each cold metal labeled conjugate (10^{-12} M to 10^{-5} M) for 1 h at 37 ℃ in a 5% CO_2-enriched atmosphere. The medium was aspirated after incubation, and the cells washed three times with cold cell medium (pH = 7, 0.2% BSA in DMEM + HEPES). A Packard Riastar multiwall gamma counting system was utilized to measure cell-associated radioactivity. The dissociation curves and IC_{50} values were generated via Origin 8.5 software. The experiments were carried out in triplicate, and the average of the trials was used as the final IC_{50} value.

Similarly, competitive displacement binding assays were also performed to determine the IC_{50} value of the conjugate for the $\alpha_v\beta_3$ integrin using $\alpha_v\beta_3$-expressing, human glioblastoma U87-MG cells and ^{125}I-Echistatin as the radioligand. Briefly, U87-MG cells (9 × 10^4 cells/well) were

seeded in Millipore 96-well filter multiscreen DV plates (0.65 μm pore size) and incubated at 25 ℃ for 2 h with approximately 30,000 cpm of ^{125}I-Echistatin in the presence of increasing concentrations (10^{-12} M to 10^{-5} M) of [RGD-Glu-[^{nat}Cu-NO2A]-6-Ahx-RM2] in 0.2 ml of binding medium. Following the incubation, plates were filtered through a multiscreen vacuum manifold and rinsed twice with 0.5 ml of ice cold pH 7.4, 0.2% BSA/0.01M PBS (phosphate buffered saline). The hydrophilic polyvinylidenedifluoride (PVDF) filters were collected and the radioactivity was measured in a Wallac 2480 automated gamma counter (PerkinElmer, NJ, USA). The IC_{50} value was calculated as previously described [23]. As a control, the IC_{50} of cyclo-RGD was also measured in U87-MG cells using ^{125}I-Echistatin as the radioligand.

3.2.6 *In Vivo* Assays of [RGD-Glu-(^{64}Cu-NO2A)-6-Ahx-RM2]

3.2.6.1 Biodistribution Studies of [RGD-Glu-(^{64}Cu-NO2A)-6-Ahx-RM2] in CF-1 Normal Mice and in PC-3 Tumor-bearing SCID Mice

All animal studies were conducted in compliance with the highest standards of care as outlined in the NIH Guide for the Care and Use of Laboratory Animals and the Policy and Procedures for Animal Research at the Truman VA Hospital, Columbia, MO, USA. Male, 4-5 week-old CF-1 mice and Institute of Cancer Research severe combined immunodeficient (ICR-SCID) mice were supplied by Taconic Farms (Germantown, NY, USA), housed four per cage in a ventilated rack system under temperature- and humidity-controlled environments with a 12 h light/12 h dark schedule, and fed *ad libitum* irradiated rodent chow (Ralston Purina 300 Company, St. Louis, MO, USA) and acidified water. For tumor inoculations, bilateral subcutaneous flank injections of approximately 5×10^6 PC-3 cells per 100 μl of Dulbecco's Phosphate-Buffered Saline (DPBS, Gibco) were performed on the SCID mice, which were anesthetized with isoflurane (Baxter Healthcare Corp., Deerfield, IL, USA) at a rate of 2.5% with

0.4 L oxygen supplied through a nonrebreathing anesthesia vaporizer first. Tumors were allowed to grow 2-3 weeks post inoculation and developed to range in mass from 0.03 g to 0.50 g. Biodistribution studies were performed in CF-1 and SCID mice after tail vein injection with ~20 μCi (~0.75 MBq, 8.08×10^{-14}-2.02×10^{-13} mol, 9.16×10^{18} Bq/mol) of [RGD-Glu-[^{64}Cu-NO2A]-6-Ahx-RM2] in 100 μl of 0.9% NaCl. Mice were sacrificed at 1 h, 4 h or 24 h post-injection (p.i.) and tissues, organs, and urine were collected, weighed, and counted in a NaI well counter. The percent injected dose (%ID) and the percent injected dose per gram (%ID/g) were calculated with the assumption that the whole blood volume was estimated to be 6.5% of the total body weight.

3.2.6.2 MicroPET/microCT Imaging Studies of [RGD-Glu-(^{64}Cu-NO2A)-6-Ahx-RM2] in PC-3 Tumor-bearing SCID Mice

Maximum intensity microPET coronal images were obtained on a Siemens INVEON small animal, dedicated PET/CT unit (Siemens, Nashville, TN, USA) at 4 h p.i. according to published procedure [23]. Micro-computed tomography (microCT) coronal images were also obtained on the Siemens INVEON small-animal CT unit following microPET imaging for fusing the anatomic and molecular data. The microCT images were acquired, and concurrent image reconstruction was achieved using a conebeam (Feldkamp) filtered, back-projection algorithm. The raw, reconstructed microSPECT datasets were imported into the INVEON Research Workstation software for subsequent image fusion with the microCT image data and 3D visualization.

3.3 RESULTS AND DISCUSSION

In this study, the bifunctional chelator, NOTA, was manually conjugated to the [RGD-Glu-6-Ahx-RM2] peptide to produce [RGD-Glu-(NO2A)-6-Ahx-RM2]. The bivalent ligand,

[RGD-Glu-(NO2A)-6-Ahx-RM2], was purified by RP-HPLC, characterized by ESI-MS and then metallated with $^{nat/64}CuCl_2$ to produce [RGD-Glu-($^{nat/64}$Cu-NO2A)-6-Ahx-RM2], the structure of which is shown in Fig. 3.1. The metallated conjugates were also purified by RP-HPLC and characterized by ESI-MS. The mass spectrometry results of each [RGD-Glu-6-Ahx-RM2] derivative, shown in Table 3.1, were consistent with the calculated molecular weights, which confirmed the identity of the expected products. The ^{64}Cu-radiolabeled conjugate was synthesized in high radiochemical yield (> 95%). According to the RP-HPLC chromatographic profiles of [RGD-Glu-($^{nat/64}$Cu-NO2A)-6-Ahx-RM2] (Fig. 3.2, Table 3.1), the ^{64}Cu-conjugate has similar retention time (t_R = 12.35 min) to ^{nat}Cu-conjugate (t_R = 12.27 min), indicating structural similarity between the tracer and the cold ligand.

In vitro competitive binding assays of [RGD-Glu-[^{nat}Cu-NO2A]-6-Ahx-RM2] were performed in GRPR-positive, human androgen-independent prostate cancer PC-3 cells and $\alpha_v\beta_3$-expressing, human glioblastoma U87-MG cells using [^{125}I-(Tyr^4)-BBN] and ^{125}I-Echistatin as radioligands, and the typical sigmoidal curves demonstrating displacement of radioactive competitors from cells as a function of increasing concentration of the naturally metallated conjugate were generated (Fig. 3.3). The IC_{50} value of the heterodimer in PC-3 was determined to be 3.09 $\pm$ 0.34 nM (Table 3.1) and is similar to the reported NO2A-RGD-BBN agonist [23]. The IC_{50} value of the heterodimer in U87-MG was determined to be 518 $\pm$ 37.5 nM, indicating only moderate specific binding to the $\alpha_v\beta_3$ receptor compared to cyclo-RGD (IC_{50} = 162 $\pm$ 5.5 nM, U87-MG). However, this does not necessarily indicate inferior behavior of the tracer in *in vivo* investigations. The IC_{50} of a ^{99m}Tc-radiolabeled dual-targeting MC1/$\alpha_V\beta_3$ ligand previously studied was found to be 403 nM for the $\alpha_V\beta_3$ integrin receptor in an M21 human, melanoma cell

line, while successful molecular imaging results were obtained due to high binding affinity of the tracer to the MC1 receptor [24].

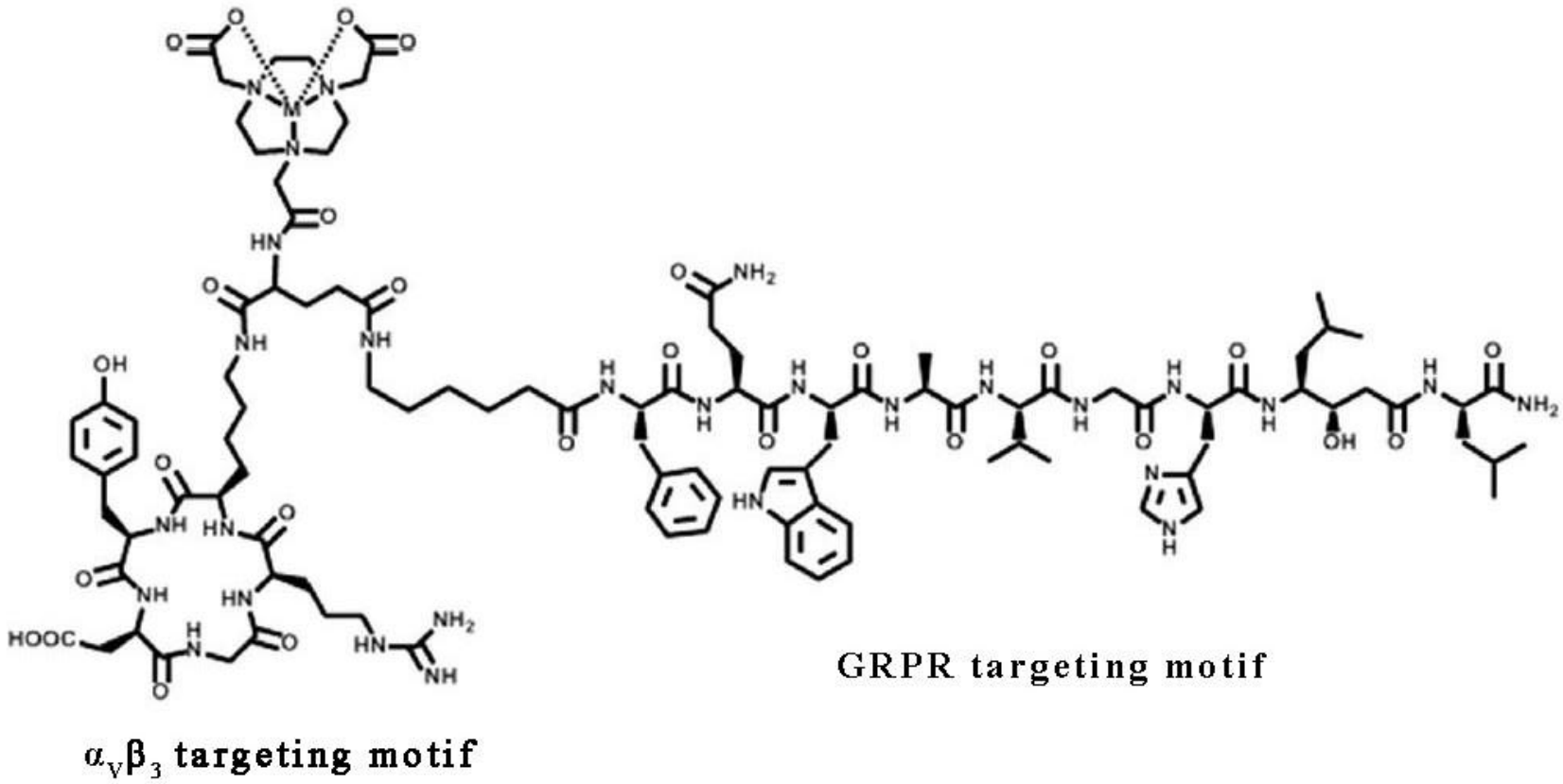

Fig. 3.1: Chemical structure of [RGD-Glu-($^{nat/64}$Cu-NO2A)-6-Ahx-RM2]

Table 3.1. Mass spectrometry, IC_{50}, and RP-HPLC data for [RGD-Glu-(NO2A)-6-Ahx-RM2], and [RGD-Glu-($^{nat/64}$Cu-NO2A)-6-Ahx-RM2]

Molecular formula [RGD-Glu-(NO2A)-6-Ahx-RM2]	$C_{105}H_{156}N_{28}O_{27}$
Molecular formula [RGD-Glu-(Cu-NO2A)-6-Ahx-RM2]	$C_{105}H_{154}CuN_{28}O_{27}$
Calculated molecular mass, [RGD-Glu-(NO2A)-6-Ahx-RM2]	2241.17 Da
Calculated molecular mass, [RGD-Glu-(^{nat}Cu-NO2A)-6-Ahx-RM2]	2302.08 Da
ESI-MS molecular mass ($M + H^+$), [RGD-Glu-(Cu-NO2A)-6-Ahx-RM2]	2242.39 Da
ESI-MS molecular mass ($M + H^+$), [RGD-Glu-(^{nat}Cu-NO2A)-6-Ahx-RM2]	2303.64 Da
[RGD-Glu-(^{nat}Cu-NO2A)-6-Ahx-RM2] RP-HPLC t_R	12.27 min
[RGD-Glu-(^{64}Cu-NO2A)-6-Ahx-RM2] RP-HPLC t_R	12.35 min
IC_{50}, [RGD-Glu-(^{nat}Cu-NO2A)-6-Ahx-RM2], PC-3	3.09 ± 0.34 nM
IC_{50}, [RGD-Glu-(^{nat}Cu-NO2A)-6-Ahx-RM2], U87-MG	518 ± 37.5 nM

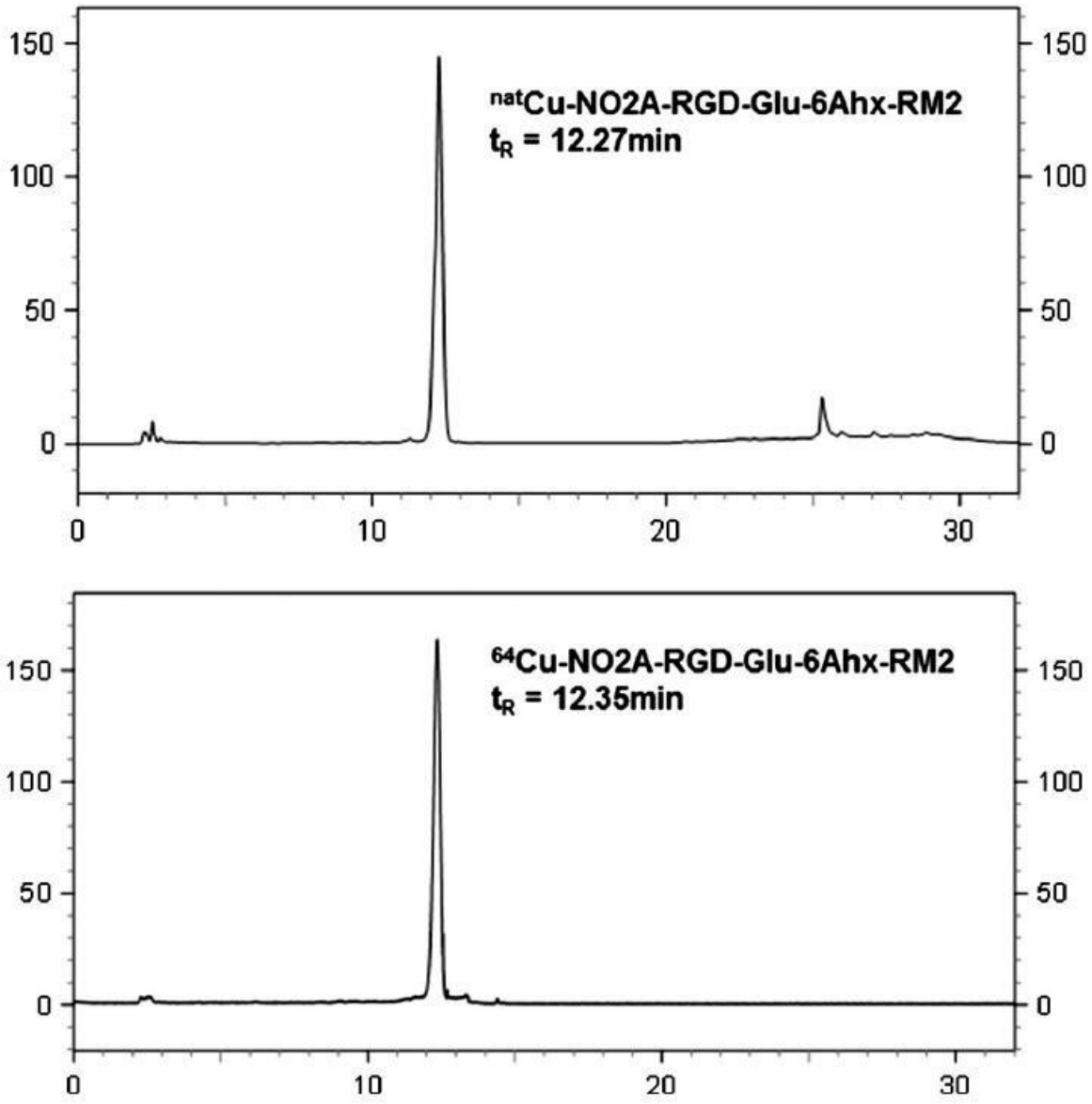

Fig. 3.2: HPLC chromatographic profiles of [RGD-Glu-(^{nat}Cu-NO2A)-6-Ahx-RM2] (t_R = 12.27 min) and [RGD-Glu-(^{64}Cu-NO2A)-6-Ahx-RM2] (t_R = 12.35 min).

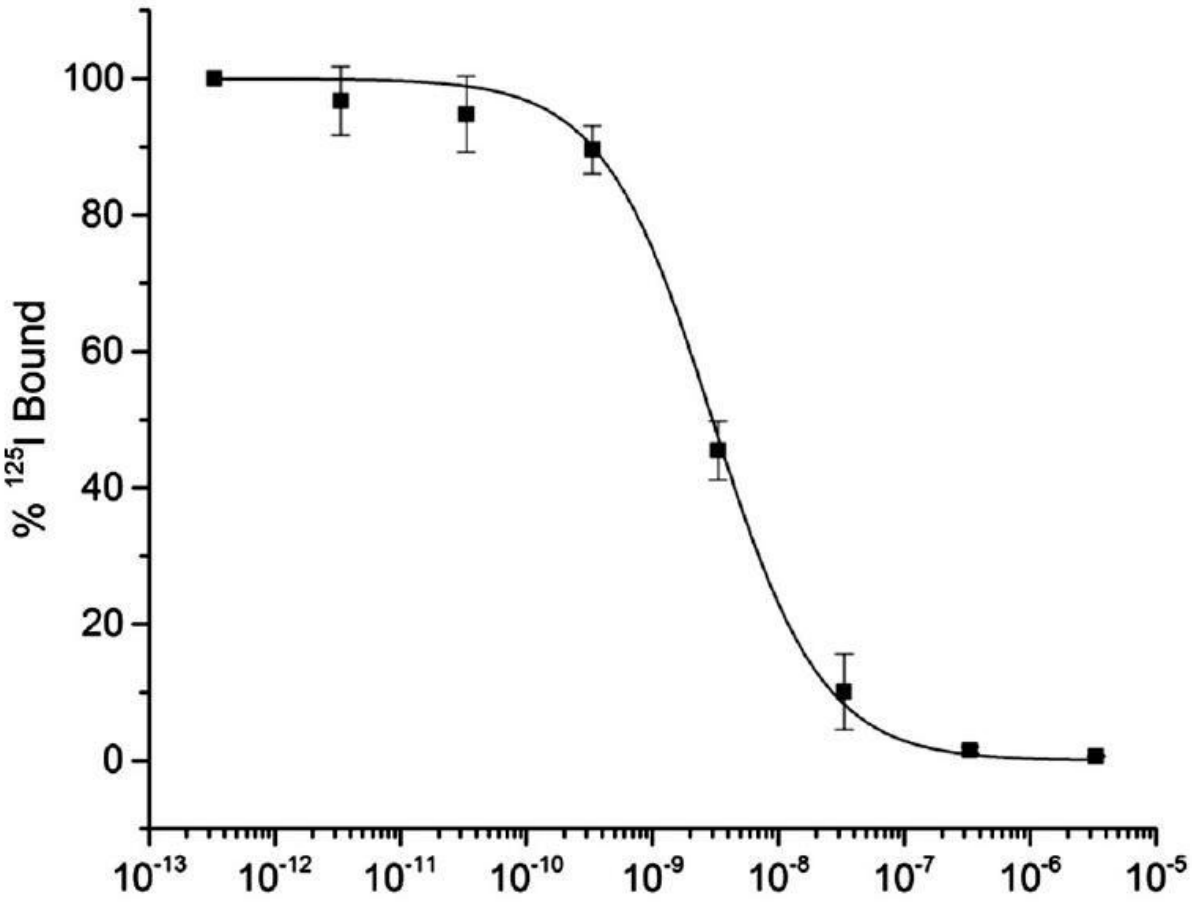

Fig. 3.3: Inhibitory concentration half maximum (IC_{50}) [RGD-Glu-(^{nat}Cu-NO2A)-6-Ahx-RM2] IC_{50} = 3.09 ± 0.34 nM) in human, prostate, PC-3 cells.

Biodistribution studies of [RGD-Glu-[^{64}Cu-NO2A]-6-Ahx-RM2] were performed in both CF-1 normal mice and PC-3 tumor bearing mice at 1, 4, and 24 h p.i., and the results are listed in Tables 3.2 and Table 3.3. For the CF-1 normal mice (Table 3.2), the tracer showed quick clearance from the blood, with 0.09 ± 0.03% ID remaining at 4 h p.i. The tracer was voided primarily through renal-urinary excretion pathway, which was confirmed by the high urine clearances of 75% ID at 1 h p.i. Quick clearance of the tracer from GRPR-negative tissues and minimal uptake in hepatic were observed. The uptake of [RGD-Glu-[^{64}Cu-NO2A]-6-Ahx-RM2] in pancreas was 4.70 ± 1.04% ID/g at 1 h p.i. and decreased to 0.71 ± 0.08 % ID/g at 4 h p.i. The high pancreatic accumulation of the tracer at 1 h p.i. was expected due to the high density of GRPR in mouse pancreatic tissue. Consequently, the pancreatic uptake of the tracer indicated effective GRPR targeting for the tracer. Low liver uptake and accumulation were also observed with 1.32 ± 0.27% ID/g at 1 h p.i. and 1.42 ± 0.17% ID/g at 4 h p.i., indicating effective *in vivo* stability of the tracer.

Biodistribution data for [RGD-Glu-[^{64}Cu-NO2A]-6-Ahx-RM2] in PC-3 tumor bearing mice are listed in Tables 3.3. The tracer presented efficient clearance from the bloodstream, with only 0.55 ± 0.13% ID remaining in whole blood at 1 h p.i. With the same primary route of excretion that was comparable to that seen in the normal CF-1 mice, the uptake of the tracer in renal tissue was determined to be 5.06 ± 1.13, 4.76 ± 1.92, and 2.43 ± 0.81% ID/g, at 1, 4 and 24 h p.i., respectively. The tracer showed moderately high accumulation and retention in liver as compared to that observed in normal CF-1 mice, with 2.65 ± 0.55% ID/g at 1 h p.i. and 2.44 ± 0.39% ID/g at 24 p.i. Additionally, the pancreatic uptake of the tracer in PC-3 tumor bearing mice at 1 h p.i. was 8.09 ± 1.29% ID/g, which nearly doubled the pancreatic uptake of the tracer in normal CF-1 mice at 1 h p.i. The uptake of the tracer was found to be high in the xenografted

PC-3 tumors, achieving maximum of 6.37 ± 1.23% ID/g at 4 h p.i. and remaining 4.26 ± 1.23% ID/g at 24 h p.i. The retention of the dose in the tumors surpassed that of all normal tissues including those GRPR-positive organs such as the pancreas and intestines. [RGD-Glu-[^{64}Cu-NO2A]-6-Ahx-RM2] showed larger portion of dose (~ 87%) remained in tumor at 24 h p.i. as compared to the agonist ^{64}Cu-NO2A-RGD-Glu-6-Ahx-BBN conjugate (~60%) studied previously, while only ~6% of the radioactively was retained in normal pancreas at the same time interval as compared to the agonist (~24%). These results indicate that the antagonist-based ligands have superior behavior in faster clearance from normal tissues, higher tumor uptake and retention.

The results of microPET/microCT imaging studies of [RGD-Glu-[^{64}Cu-NO2A]-6-Ahx-RM2] in PC-3 tumor-bearing, SCID mice are presented in Fig. 3.4. PC-3 xenografted tumors were clearly observable from all other tissues at 4 h p.i., producing high-quality, high-contrast microPET images with excellent tumor-to-background ratios. In comparison, many of the high-quality microPET images in our laboratory were obtained at the 15–18 h time-point. Minimal collateral radioactivity in non-target tissues was shown at 4 h p.i., indicating the propensity of the RGD sequence to possibly facilitate excretion and clearance from these tissues to create high-quality, high-contrast images at an earlier time-point.

Table 3.2. Biodistribution studies of [RGD-Glu-(^{64}Cu-NO2A)-6-Ahx-RM2] in CF-1 normal mice at 1, 4 and 24 h p.i. (%ID/g ± SD, n=5).

	1 h	4 h	24 h
Heart	0.35 ± 0.12	0.54 ± 0.40	0.39 ± 0.04
Lung	0.98 ± 0.17	0.83 ± 0.35	0.78 ± 0.19
Liver	1.32 ± 0.27	1.42 ± 0.17	1.38 ± 0.19
Kidneys	3.54 ± 0.56	2.53 ± 0.37	1.15 ± 0.07
Spleen	1.00 ± 0.27	0.69 ± 0.12	0.61 ± 0.15
Stomach	1.63 ± 0.41	1.08 ± 0.47	0.64 ± 0.22
S. Intestine	2.20 ± 0.56	1.43 ± 0.55	0.72 ± 0.20
L. Intestine	1.01 ± 0.14	2.30 ± 0.40	0.91 ± 0.20
Muscle	0.32 ± 0.11	0.15 ± 0.05	0.10 ± 0.03
Bone	0.88 ± 0.26	0.71 ± 0.16	0.39 ± 0.11
Brain	0.05 ± 0.02	0.04 ± 0.01	0.08 ± 0.03
Pancreas	4.70 ± 1.04	0.71 ± 0.08	0.38 ± 0.08
Blood*	0.24 ± 0.04	0.09 ± 0.03	0.13 ± 0.02
Urine*	75.2 ± 3.47	82.5 ± 2.86	84.7 ± 2.68
Bladder	2.34 ± 1.15	1.31 ± 0.46	0.39 ± 0.36

*Data presented as % ID

Table 3.3. Biodistribution studies of [RGD-Glu-(^{67}Ga-DO3A)-6-Ahx-RM2] in PC-3 tumor-bearing SCID mice at 1, 4 and 24 h p.i. (%ID/g ± SD, n=5).

	1 h	4 h	24 h
Heart	0.99 ± 0.53	0.73 ± 0.26	0.79 ± 0.11
Lung	1.65 ± 0.29	1.56 ± 0.26	1.21 ± 0.22
Liver	2.65 ± 0.55	3.22 ± 0.92	2.44 ± 0.39
Kidneys	5.06 ± 1.13	4.76 ± 1.92	2.43 ± 0.81
Spleen	2.56 ± 0.90	3.13 ± 1.65	2.17 ± 0.72
Stomach	2.21 ± 0.47	2.04 ± 1.29	0.74 ± 0.47
S. Intestine	3.64 ± 0.61	3.12 ± 1.62	2.17 ± 0.72
L. Intestine	1.39 ± 0.47	4.20 ± 1.55	2.37 ± 2.13
Muscle	0.44 ± 0.11	0.45 ± 0.21	0.26 ± 0.13
Bone	0.89 ± 0.14	0.84 ± 0.41	0.68 ± 0.50
Brain	0.08 ± 0.02	0.09 ± 0.05	0.08 ± 0.03
Pancreas	8.09 ± 1.29	1.95 ± 0.93	0.64 ± 0.26
Blood*	0.55 ± 0.13	0.30 ± 0.08	0.36 ± 0.08
Urine*	69.4 ± 5.28	76.1 ± 6.48	79.1 ± 2.66
Tumor	4.86 ± 1.01	6.37 ± 1.68	4.26 ± 1.23

*Data presented as % ID

Fig. 3.4: Maximum intensity microPET tumor and microCT skeletal fusion coronal whole body image of a PC-3 tumor bearing SCID mouse at 4 h after tail vein injection of [RGD-Glu-(^{64}Cu-NO2A)-6-Ahx-RM2].

3.4 CONCLUSION

In this study, [RGD-Glu-(^{64}Cu-NO2A)-6-Ahx-RM2], a bivalent ligand with the capability of recognizing both GRPR and integrin $\alpha_V\beta_3$ biomarkers that are co-expressed on the surface of most prostate cancer cells, was produced, characterized, evaluated *in vitro* and *in vivo*. MicroPET imaging investigations at 4 h p.i. produced high-quality, high-contrast, whole body images with minimal tracer present in surrounding, collateral, abdominal tissues. The high selectivity and retention of this tracer for tumor tissue support previous studies that suggest the superiority of radiolabeled antagonists over agonists to be used for molecular imaging of human cancers.

3.5 REFERENCES

1. Markwalder, R., Reubi, J. C., Gastrin-releasing peptide receptors in the human prostate: Relation to neoplastic transformation. Cancer Res, 1999. **59**: p. 1152.
2. Smith, C. J., Volkert, W. A., Hoffman, T. J., Gastrin releasing peptide (GRP) receptor targeted radiopharmaceuticals: a concise update. Nucl Med Biol, 2003. **30**: p. 861.
3. Varvarigou, A., Bouziotis, P., Zikos, C., Scopinaro, F., De Vincentis, G., Gastrin-releasing peptide (GRP) analogues for cancer imaging. Cancer Biother Radiopharm, 2004. **19**: p. 219.
4. Schroeder, R. P., Bouziotis, P., Zikos, C., Scopinaro, F., De Vincentis, G., Gastrin-releasing peptide receptor-based targeting using bombesin analogues is superior to metabolism-based targeting using choline for in vivo imaging of human prostate cancer xenografts. Eur J Nucl Med Mol Imaging, 2011. **38**: p. 1257.
5. Yu, Z., Ananias, H. J., Carlucci, G., Hoving, H. D., Helfrich, W., Dierckx, R. A., Wang, F., de Jong, I. J., Elsinga, P. H., An update of radiolabeled bombesin analogs for gastrin-releasing peptide receptor targeting. Curr Pharm Des, 2013. **19**: p. 3329.
6. Chen X., Park, R., Hou, Y., Tohme, M., Shahinian, A. H., Bading, J. R., Conti, P. S., MicroPET and autoradiographic imaging of GRP receptor expression with ^{64}Cu-DOTA-[Lys^3] bombesin in human prostate adenocarcinoma xenografts. J Nucl Med, 2004. **45**: p. 1390–7.
7. Smith, C. J., Sieckman, G. L., Owen, N. K., Hayes, D. L., Mazuru, D. G., Kannan, R., Volkert, W. A., Hoffman, T. J., Radiochemical investigations of gastrin-releasing peptide receptor-specific [^{99m}Tc(X)(CO)3-Dpr-Ser-Ser-Ser-Gln-Trp-Ala-Val-Gly-His-Leu-Met-(NH_2)] in PC-3, tumor-bearing, rodent models: syntheses, radiolabeling, and in vitro/in vivo studies where Dpr = 2,3-diaminopropionic acid and X = H_2O or $P(CH2OH)_3$. Cancer Res, 2003. **63**: p. 4082–8.
8. Prasanphanich A. F., Retzloff, L., Lane, S. R., Nanda, P. K., Sieckman, G. L., Rold, T. L., Ma, L., Figueroa, S. D., Sublett, S. V., Hoffman, T. J., Smith, C. J., In vitro and in vivo analysis of [^{64}Cu-NO2A-8-Aoc-BBN(7-14)NH_2]: a site-directed radiopharmaceutical for positron-emission tomography imaging of T-47D human breast cancer tumors. Nucl Med Biol, 2009. **36**: p. 171–81.
9. Yang Y-S., Zhang X., Xiong Z., Chen X., Comparative in vitro and in vivo evaluation of two ^{64}Cu-labeled bombesin analogues in a mouse model of human prostate adenocarcinoma. Nucl Med Biol, 2006. **33**: p. 371–80.
10. Gourni, E., Bouziotis, P., Benaki, D., Loudos, G., Xanthopoulos, S., Paravatou-Petsotas, M., Mavri-Vavagianni, M., Pelecanou, M., Archimandritis, S. C., Varvarigou, A. D., Structural assessment and biological evaluation of two N3S bombesin derivatives. J Med Chem, 2009. **52**: p. 4234–46.
11. Scopinaro F., De Vincentis, G., Varvarigou, A. D., Laurenti, C., Iori, F., Remediani, S., Chiarini, S., Stella S., ^{99m}Tc-bombesin detects prostate cancer and invasion of pelvic lymph nodes. Eur J Nucl Med Mol Imaging, 2003. **30**: p. 1378–82.
12. Abiraj, K., Mansi, R., Tamma, M. L., Fani, M., Forrer, F., Nicolas, G., Cescato, R., Reubi, J. C., Maecke, H. R., Bombesin antagonist based radioligands for translational nuclear imaging of gastrin-releasing peptide receptor-positive tumors. J Nucl Med, 2011. **52**: p. 1970.

13. Dumont, R. A., Tamma, M., Braun, F., Borkowski, S., Reubi, J. C., Maecke, H., Weber, W. A., Mansi, R., Targeted radiotherapy of prostate cancer with a gastrin-releasing peptide receptor antagonist is effective as monotherapy and in combination with rapamycin. J Nucl Med, 2013. **54**: p. 762.
14. Cescato, R., Maina, T., Nock, B., Nikolopoulou, A., Charalambidis, D., Piccand, V., Reubi, J. C., Bombesin receptor antagonists may be preferable to agonists for tumor targeting. J Nucl Med, 2008. **49**: p. 318.
15. Ginj, M., Zhang, H., Waser, B., Cescato, R., Wild, D., Wang, X., Erchegyi, J., Rivier, J., Mäcke, H. R., Reubi, J. C., Radiolabeled somastostatin receptor antagonists are preferable to agonists for in vivo peptide receptor targeting of tumors. Proc Natl Acad Sci USA, 2006. **103**: p. 16436.
16. Anderson, C. J., Welch, M. J., Radiometal-labeled agents (non-technetium) for diagnostic imaging. Chem. Rev, 1999. **99**: p. 2219.
17. Ruoslahti, E., Pierschbacher, M. D., New perspectives in cell adhesion: RGD and integrins. Science, 1987. **238**: p. 491.
18. Romanov, V. I., Goligorsky, M. S., RGD-recognizing integrin mediate interactions of human prostate carcinoma cells with endothelial cells in vitro. Prostate, 1999. **39**: p. 108.
19. Gladson, C. L., Cheresh, D. A., Glioblastoma expression of vitronectin and the αvβ3 integrin. Adhesion mechanism for transformed glial cells. J Clin Invest, 1991. **88**: p. 1924.
20. Schottelius M., Laufer, B., Kessler, H., Wester, H. J., Ligands for mapping $\alpha_v\beta_3$-integrin expression in vivo. Acc Chem Res, 2009. **42**: p. 969–80.
21. Fani, M., Maecke, H. R., Okarvi, S. M., Radiolabeled peptides: valuable tools for the detection and treatment of cancer. Theranostics, 2012. **2**: p. 481–501.
22. Liu, S., Radiolabeled multimeric cyclic RGD peptides as Integrin $\alpha_v\beta_3$ targeted radiotracers for tumor imaging. Mol Pharm, 2006. **3**: p. 472–87.
23. Jackson, A. B., Nanda, P. K., Rold, T. L., Sieckman, G. L., Szczodroski, A. F., Hoffman, T. J., Chen, X., Smith, C. J., ^{64}Cu-NO2A-RGD-Glu-6-Ahx-BBN(7-14)NH2: a heterodimeric targeting vector for positron emission tomography imaging of prostate cancer. Nucl Med Biol, 2012. **39**: p. 377.
24. Yang, J., Guo, H., Miao, Y., Technetium-99 m-labeled Arg-Gly-Asp-conjugated alpha-melanocyte stimulating hormone hybrid peptides for human melanoma imaging. Nucl Med Biol, 2010. **37**: p. 873–83.

Chapter 4: GALLIUM-67/GALLIUM-68/COPPER-64 DOTA RGD/RM2 BIVALENT LIGAND FOR POTENTIAL DIAGNOSTIC IMAGING OF PROSTATE CANCER

4.1 INTRODUCTION

The mammalian gastrin releasing peptide receptor (GRPR), as a subtype of the BBN receptor family, is found to be highly expressed in a variety of human cancers including pancreatic, breast, colon, and prostate cancer [1-5]. BBN, bombesin, is a tetradecapeptide analogue of human GRP and thus has high binding affinity for the GRPR [6]. RM2 is an antagonist analogue of BBN with high binding affinity to the GRPR and the research of BBN antagonists has shown superior biodistribution and imaging when compared to BBN agonists [7-11]. The $\alpha_v\beta_3$ integrin, a member of the integrin receptor family is another target of great interest due to its important roles in the modulation of cell migration and survival during angiogenesis, potentially facilitating metastatic invasion of the tumor cells across the blood vessels, and its moderate expression in a number of cancers such as malignant melanoma, glioblastoma, breast, and prostate tumors [12-14]. In this project, the BBN antagonist analogue, RM2 (Fig. 1.4), was used as the GRPR targeting motif, and a cyclic five amino acid moiety abbreviated as c(RGDyK), RGD (Fig. 1.6), with the strong binding affinity to $\alpha_v\beta_3$ was used as the $\alpha_v\beta_3$ integrin targeting motif for the bivalent ligand. ^{64}Cu and $^{68/67}$Ga was used to radiolabel the bivalent ligand to produce the tracer for biological evaluations. DOTA (Fig. 1.9) was used as the chelating agents for linking radionuclides to the bivalent ligand.

4.1.1 Specific Aims

The goal of this project was to produce, purify, characterize, and evaluate, both *in vitro* and *in vivo*, a GRPR/$\alpha_v\beta_3$ dual-targeting peptide conjugate ligand labeled with copper-64 and

Gallium-68. A comparative study was conducted with the copper-64 DOTA and the Gallium-67 DOTA conjugate in terms of *in vitro* and *in vivo* stabilities.

4.2 EXPERIMENTAL

4.2.1 Materials

[RGD-Glu-(DO3A)-6-Ahx-RM2], [Cyclo(Arg-Gly-Asp-DTyr-Lys)-(DO3A)-Glu-(6-Ahx-D-Phe-Gln-Trp-Ala-Val-Gly-His-Sta-Leu-NH_2], was purchased from CPC Scientific (Sunnyvale, CA, USA). $^{67}GaCl_3$ in 0.1 M HCl solution was purchased from MDS Nordion (Ottawa, Canada). $^{64}CuCl_2$ was purchased as a 0.1 M HCl solution from the University of Wisconsin-Madison (Madison, WI). All other reagents or solvents were purchased from Fisher Scientific (Pittsburgh, PA, USA) or Sigma-Aldrich Chemical Company (St. Louis, MO, USA) and used without further purification. ^{125}I-[Tyr^4]-BBN and ^{125}I-Echistatin were purchased from Perkin-Elmer (Waltham, MA, USA). PC-3 cells were obtained from American Type Culture Collection and were maintained by the University of Missouri Cell and Immunobiology Core Facility (Columbia, MO).

4.2.2 Metallation of [RGD-Glu-(DO3A)-6-Ahx-RM2] with $^{nat/67/68}$Ga and $^{nat/64}$Cu

The metallation of each conjugate was performed following the procedure in a previously published paper [15] with some modifications. Briefly, [RGD-Glu-(^{nat}Ga-DO3A)-6-Ahx-RM2] was produced by adding natural $GaCl_3$ in 0.05 N HCl (90 nmol) to purified [RGD-Glu-(DO3A)-6-Ahx-RM2] peptide conjugate (89 nmol) which was dissolved in 0.1M sodium acetate (250 µl). The pH of the reaction mixture was adjusted to approximately 5.0 by the addition of 1% NaOH. The mixture was incubated for 15 min at 90 ℃ and then 50 µl of 10 mM diethylenetriaminepentaacetic acid (DTPA) solution was added to scavenge unbound metal. The

metallated conjugate, [RGD-Glu-(^{nat}Ga-DO3A)-6-Ahx-RM2], was purified by RP-HPLC and characterized by ESI-MS prior to *in vitro* receptor binding assays.

The radiolabeled ligand, [RGD-Glu-(^{67}Ga-DO3A)-6-Ahx-RM2], was synthesized by the reaction of [RGD-Glu-(DO3A)-6-Ahx-RM2] (50 µg, 200 µl 0.1 M sodium acetate) with $^{67}GaCl_3$ (~92.5 MBq, ~2.5 mCi) in 0.05 N HCl for 30 min at 90 ℃ (pH = 5.0). Fifty µl of 10 mM DTPA solution was added to scavenge any remaining gallium metal ion. The ^{67}Ga-radiolabeled peptide was purified via RP-HPLC and collected into 100 µl of 1 mg/ml bovine serum albumin (BSA) prior to *in vitro*, *in vivo*, and imaging assays. Acetonitrile was removed under a steady stream of nitrogen and the radiochemical purity was assessed by RP-HPLC.

[RGD-Glu-(^{nat}Cu-DO3A)-6-Ahx-RM2] was produced by adding natural $CuCl_2 \bullet 2H_2O$ in 0.05 N HCl (90 nmol) to purified [RGD-Glu-(DO3A)-6-Ahx-RM2] peptide conjugate (89 nmol, 250 µl 0.4M ammonium acetate). The pH of the reaction mixture was adjusted to approximately 7.0 by the addition of 1% NaOH. The mixture was incubated for 1 h at 70 ℃ and then 50 µl of 10 mM DTPA solution was added to scavenge unbound metal. The metallated conjugate, [RGD-Glu-(^{nat}Cu-DO3A)-6-Ahx-RM2], was purified by RP-HPLC and characterized by ESI-MS prior to *in vitro* receptor binding assays.

The radiolabeled ligand, [RGD-Glu-(^{64}Cu-DO3A)-6-Ahx-RM2], was synthesized by the reaction of [RGD-Glu-(DO3A)-6-Ahx-RM2] (50 µg, 200 µl 0.4 M ammonium acetate) with $^{64}CuCl_2$ (~92.5 MBq, ~2.5 mCi) in 0.05 N HCl for 1 h at 70 ℃ (pH = 7.0). Fifty µl of 10 mM DTPA solution was added to scavenge any remaining copper metal ion. The ^{64}Cu-radiolabeled peptide was purified via RP-HPLC and collected into 100 µl of 1 mg/ml BSA prior to *in vitro*, *in vivo*, and imaging assays. Acetonitrile was removed under a steady stream of nitrogen and the radiochemical purity was assessed by RP-HPLC.

4.2.3 RP-HPLC and MS Analysis of Non-metallated and Metallated [RGD-Glu-(DO3A)-6-Ahx-RM2]

The unmetallated peptide conjugates and metallated complexes were purified via RP-HPLC performed on an SCL-10A HPLC system (Shimadzu, Kyoto, Japan) employing a binary gradient system [Solvent A=99.9% DI water with 0.1% trifluoroacetic acid (TFA); Solvent B=99.9% acetonitrile containing 0.1% TFA], programmed with a linear gradient of 25:75 A/B to 35:65 A/B gradient over 15 min (followed by an additional 10 min at 5:95 A/B). Samples were eluted from an analytical C-18 reversed-phase column (Phenomenex Jupiter Proteo, 250 × 4.60 mm, 5 μm; Phenomenex, Torrance, CA, USA) maintained at 34 ℃ via an Eppendorf TC-50 column heater and observed using an in-line Shimadzu SPD-10A UV-vis tunable absorbance detector (λ = 280 nm) and an in-line, EG&G Ortec NaI solid crystal scintillation detector (EG&G, Salem, MA, USA). EZStart software (7.4.3; Shimadzu, Kyoto, Japan) was used to accomplish data acquisition of both signals. Purified compounds were lyophilized in a CentriVap system (Labconco, Kansas City, MO, USA). ESI-MS analyses were performed in the laboratory of Dr. Fabio Gallazzi at the University of Missouri, Department of Chemistry, Columbia, MO, USA.

4.2.4 *In Vitro* Competitive Displacement Binding Assays of [RGD-Glu-(^{nat}Ga/^{nat}Cu-DO3A)-6-Ahx-RM2] in GRPR-expressing PC-3 Cells and $\alpha_V\beta_3$-expressing U87-MG Cells

The IC_{50} values of [RGD-Glu-(^{nat}Ga/^{nat}Cu-DO3A)-6-Ahx-RM2] were obtained by competitive displacement binding assays using GRPR-expressing, human PC-3 prostate cancer cells (~3 × 10^4 cells/tube, suspended in DMEM/F-12 K) incubated with ~20,000 cpm of ^{125}I-[Tyr^4]-BBN and increasing concentrations of each cold metal labeled conjugate (10^{-12} M to 10^{-5}

M) for 1 h at 37 ℃ in a 5% CO_2-enriched atmosphere. The medium was aspirated after incubation, and the cells washed three times with cold cell medium (pH = 7, 0.2% BSA in DMEM + HEPES). A Packard Riastar multiwall gamma counting system was utilized to measure cell-associated radioactivity. The dissociation curves and IC_{50} values were generated via Origin 8.5 software. The experiments were carried out in triplicate, and the average of the trials was used as the final IC_{50} value.

Similarly, competitive displacement binding assays were also performed to determine the IC_{50} values of each conjugate for the $\alpha_v\beta_3$ integrin using $\alpha_v\beta_3$-expressing, human glioblastoma U87-MG cells and ^{125}I-Echistatin as the radioligand. Briefly, U87-MG cells (9×10^4 cells/well) were seeded in Millipore 96-well filter multiscreen DV plates (0.65 μm pore size) and incubated at 25 ℃ for 2 h with approximately 30,000 cpm of ^{125}I-Echistatin in the presence of increasing concentrations (10^{-12} M to 10^{-5} M) of [RGD-Glu-(^{nat}Ga/^{nat}Cu-DO3A)-6-Ahx-RM2] in 0.2 ml of binding medium. Following the incubation, plates were filtered through a multiscreen vacuum manifold and rinsed twice with 0.5 ml of ice cold pH 7.4, 0.2% BSA/0.01M PBS. The hydrophilic polyvinylidenedifluoride (PVDF) filters were collected and the radioactivity was measured in a Wallac 2480 automated gamma counter (PerkinElmer, NJ, USA). The IC_{50} values were calculated as previously described [15, 16]. As a control, the IC_{50} of cyclo-RGD was also measured in U87-MG cells using ^{125}I-Echistatin as the radioligand.

4.2.5 *In Vivo* Assays of [RGD-Glu-(^{67}Ga/^{64}Cu-DO3A)-6-Ahx-RM2]

4.2.5.1 Biodistribution Studies of [RGD-Glu-(^{67}Ga/^{64}Cu-DO3A)-6-Ahx-RM2] in CF-1 Normal Mice and in PC-3 Tumor-bearing SCID Mice

All animal studies were conducted in compliance with the highest standards of care as outlined in the NIH Guide for the Care and Use of Laboratory Animals and the Policy and

Procedures for Animal Research at the Truman VA Hospital, Columbia, MO, USA. Male, 4-5 week-old CF-1 mice and Institute of Cancer Research severe combined immunodeficient (ICR-SCID) mice were received from Taconic Farms (Germantown, NY, USA), housed four per cage in a ventilated rack system under temperature- and humidity-controlled environments with a 12 h light/12 h dark schedule, and fed *ad libitum* irradiated rodent chow (Ralston Purina 300 Company, St. Louis, MO, USA) and acidified water. For tumor inoculations, bilateral subcutaneous flank injections of approximately 5×10^6 PC-3 cells per 100 µl of Dulbecco's Phosphate-Buffered Saline (DPBS, Gibco) were performed on the SCID mice which were anesthetized with isoflurane (Baxter Healthcare Corp., Deerfield, IL, USA) at a rate of 2.5% with 0.4 L oxygen supplied through a nonrebreathing anesthesia vaporizer first. Tumors were allowed to grow 2-3 weeks post inoculation and developed to range in mass from 0.03 g to 0.50 g. Biodistribution studies were performed in CF-1 and SCID mice after tail vein injection with ~8.5 µCi (~0.31 MBq) of [RGD-Glu-(^{67}Ga-DO3A)-6-Ahx-RM2] or ~37.5 µCi (~1.39 MBq) of [RGD-Glu-(^{64}Cu-DO3A)-6-Ahx-RM2] in 100 µl of 0.9% NaCl. Mice were sacrificed at 1 h, 4 h or 24 h post-injection (p.i.) and tissues, organs, and urine were collected, weighed, and counted in a NaI well counter. The percent injected dose (%ID) and the percent injected dose per gram (%ID/g) were calculated with the assumption that the whole blood volume was estimated to be 6.5% of the total body weight.

4.2.5.2 MicroSPECT/microCT Imaging Studies of [RGD-Glu-(^{67}Ga-DO3A)-6-Ahx-RM2] and MicroPET/microCT Imaging Studies of [RGD-Glu-(^{64}Cu-DO3A)-6-Ahx-RM2] in PC-3 Tumor-bearing SCID Mice

Maximum intensity microSPECT coronal and axial images were obtained on a Siemens INVEON small animal, dedicated SPECT/CT unit (Siemens, Nashville, TN, USA) at 18 h p.i.

according to published procedures [15, 16]. ~850 μCi (~31.45 MBq) of [RGD-Glu-(^{67}Ga-DO3A)-6-Ahx-RM2] in 100-200 μl of 0.9% NaCl was delivered to each PC-3 tumor-bearing mouse via tail vein injection. Micro-computed tomography (microCT) coronal images were also obtained on the Siemens INVEON small-animal CT unit following microSPECT imaging for fusing the anatomic and molecular data. The microCT images were acquired, and concurrent image reconstruction was achieved using a conebeam (Feldkamp) filtered, back-projection algorithm. The raw, reconstructed microSPECT datasets were imported into the INVEON Research Workstation software for subsequent image fusion with the microCT image data and 3D visualization.

Maximum intensity microPET coronal and axial images were obtained on a Siemens INVEON small animal, dedicated PET/CT unit (Siemens, Nashville, TN, USA) at 18 h p.i. according to published procedure [15, 16]. ~950 μCi (~35.15 MBq) of [RGD-Glu-(^{64}Cu-DO3A)-6-Ahx-RM2] in 100-200 μl of 0.9% NaCl was delivered to each PC-3 tumor-bearing mouse through the tail vein injection. Micro-computed tomography (microCT) coronal images were also obtained on the Siemens INVEON small-animal CT unit following microPET imaging for fusing the anatomic and molecular data. The microCT images were acquired, and concurrent image reconstruction was achieved using a conebeam (Feldkamp) filtered, back-projection algorithm. The raw, reconstructed microSPECT datasets were imported into the INVEON Research Workstation software for subsequent image fusion with the microCT image data and 3D visualization.

4.3 RESULTS AND DISCUSSION

In this study, [RGD-Glu-(^{nat}Ga/^{nat}Cu-DO3A)-6-Ahx-RM2] were synthesized via metallation of [RGD-Glu-(DO3A)-6-Ahx-RM2] (Fig. 4.1) with natural Ga/Cu, purified by RP-HPLC, and characterized by ESI-MS. The mass spectrometry results of each conjugate were consistent with the calculated molecular weights (Table 4.1), which verified the identity of the expected complexes. The ^{67}Ga- or ^{64}Cu- radiolabeled conjugates were produced in high radiochemical yield (>95%), which was determined by RP-HPLC analysis. There existed only slight differences in retention times between the non-metallated ligand (10.8 min) and the corresponding metallated ligands (~11.5 min), presumably due to similarities in the structures of the compounds as well as slight change in charge density and atomic mass after coordinating different metals via the DOTA chelator. The RP-HPLC profiles of [RGD-Glu-(^{67}Ga/^{64}Cu-DO3A)-6-Ahx-RM2] (Fig. 4.2) showed no significant changes in the traces of either compound for the 0-24 h time points and thus indicated sufficiently good serum stability for further in vivo investigations.

In vitro competitive binding assays for [RGD-Glu-(^{nat}Ga/^{nat}Cu-DO3A)-6-Ahx-RM2] were carried out in PC-3 cells and U87-MG cells, and typical sigmoidal curves demonstrating displacement of radioactive competitors from cells as a function of increasing concentration of naturally metallated conjugates were generated (Fig. 4.3 and Fig. 4.4). The IC_{50} values of nonmetallated and metallated conjugates are listed in Table 4.1. Both metallated conjugates, [RGD-Glu-(^{nat}Ga/^{nat}Cu-DO3A)-6-Ahx-RM2], exhibited high binding affinity towards the GRPR with slightly superior IC_{50} values in the nanomolar range (7.78 $\pm$ 2.42 nM for ^{nat}Ga-conjugate; 8.64 $\pm$ 2.16 nM for ^{nat}Cu-conjugate) when compared to the nonmetallated conjugate (IC_{50} of 9.26 $\pm$ 0.01 nM). Consequently, the binding affinities of the complexes for the $\alpha_v\beta_3$ integrin were

tested in U87-MG cells, which express a high level of the $\alpha_v\beta_3$ integrin [17]. The results from the studies on U87-MG showed IC_{50} values of 307 ± 0.00 nM for the ^{nat}Ga-conjugate and 308 ± 42.6 nM for the ^{nat}Cu-conjugate, suggesting only moderate specific binding to the $\alpha_v\beta_3$ integrin. This was not unexpected according to the IC_{50} values of other reported targeting vectors towards the integrin receptor in U87-MG cells [15, 16].

Biodistribution studies of [RGD-Glu-(^{67}Ga/^{64}Cu-DO3A)-6-Ahx-RM2] were performed in both CF-1 normal mice and PC-3 tumor bearing mice at 1, 4, and 24 h p.i., and the results are listed in Tables 4.2, Table 4.3, Table 4.4 and Table 4.5. For the CF-1 normal mice (Tables 4.2 and Table 4.3), the ^{67}Ga-labeled ligand showed quick clearance from the blood, with 0.10 ± 0.09 %ID remaining at 4 h p.i. and 0.02 ± 0.02 %ID at 24 h p.i. However, the ^{64}Cu-labeled ligand, by comparison, displayed slower washout from the blood, with 0.25 ± 0.04 %ID remaining at 4 h p.i. and 0.25 ± 0.09 %ID at 24 h p.i. High urine clearances of 65.82 ± 3.34 %ID and 69.67 ± 3.34 %ID at 1 h p.i. confirmed that both radiolabeled ligands were voided through renal excretion. High uptake of [RGD-Glu-(^{67}Ga-DO3A)-6-Ahx-RM2] in pancreas at 1 h p.i. was observed due to high expression of the GRPR in mouse pancreas, indicating binding specificity of the ligand for the GRPR. Rapid clearance from pancreas occurred subsequently with 11.11 ± 1.37 %ID/g at 1 h p.i. and 0.79 ± 0.20 %ID/g at 4 h p.i. Uptake of [RGD-Glu-(^{64}Cu-DO3A)-6-Ahx-RM2] in pancreas was only 2.68 ± 0.37 %ID/g at 1 h p.i. and decreased to 0.58 ± 0.04 %ID/g at 4 h p.i. The ^{67}Ga-peptide exhibited low hepatic uptake and retention, while [RGD-Glu-(^{64}Cu-DO3A)-6-Ahx-RM2] exhibited accumulation in liver with 2.29 ± 0.31 %ID/g at 1 h p.i., increasing to 2.52 ± 0.32 %ID/g at 4 h p.i., and remaining at 2.30 ± 0.50 %ID/g at 24 h p.i. The high uptake and prolonged retention of ^{64}Cu-ligand in liver was not unexpected due to the low *in vivo* stability of ^{64}Cu-DOTA complex. Although DOTA forms a thermodynamically

stable complex with the copper (II) cation, studies have demonstrated that the Cu(II)-DOTA complex does not have sufficiently strong kinetic inertness [18]. Consequently, loss of ^{64}Cu from the ligand can occur *in vivo* due to transchelation by proteins such as superoxide dismutase (SOD), which can result in ^{64}Cu accumulation in liver [19].

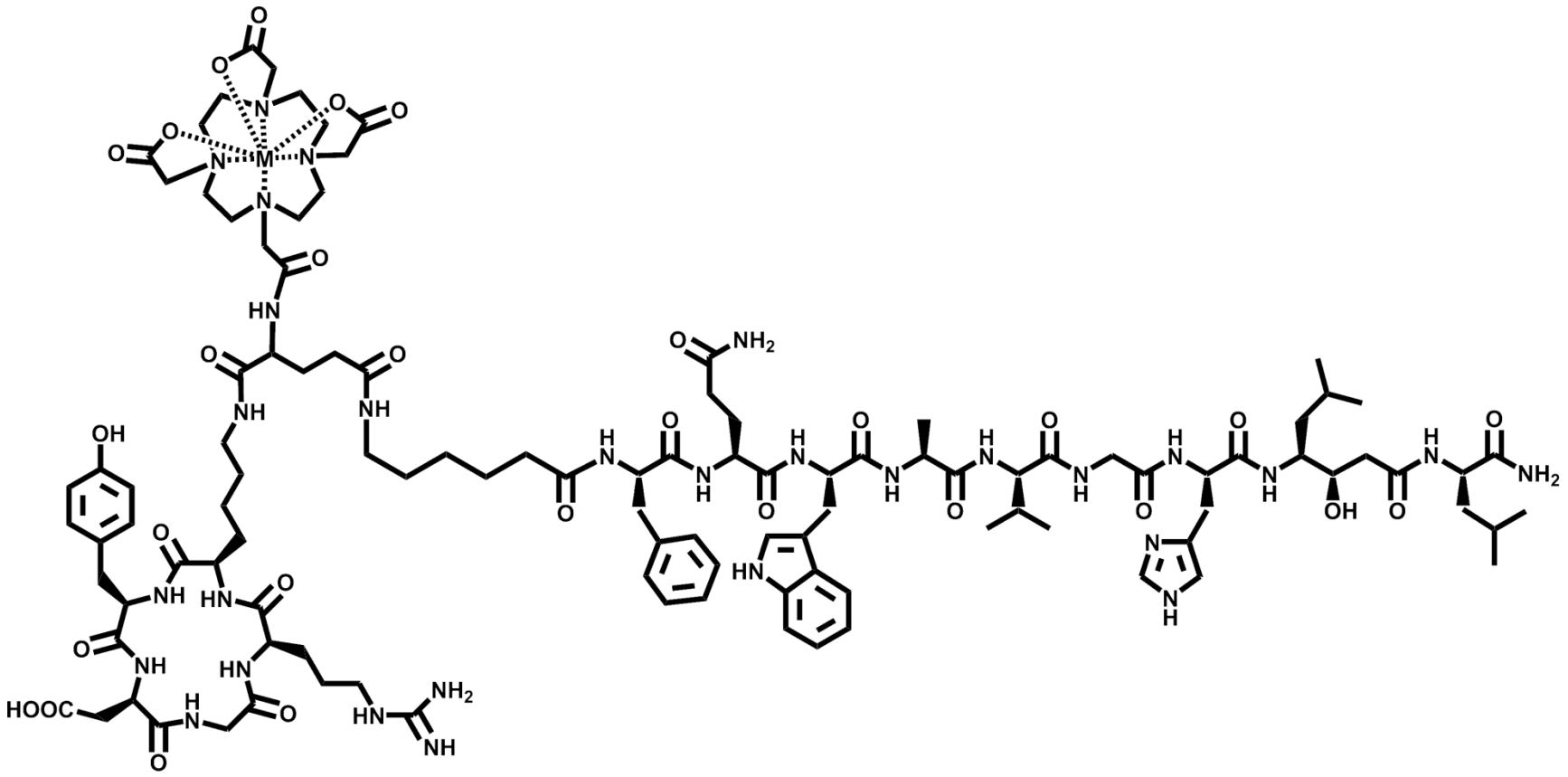

Fig. 4.1: Chemical structure of [RGD-Glu-(Ga/Cu-DO3A)-6-Ahx-RM2] antagonist.

Table 4.1. Mass spectrometry, IC_{50}, and RP-HPLC data for [RGD-Glu-(DO3A)-6-Ahx-RM2], [RGD-Glu-($^{nat/64}$Cu-DO3A)-6-Ahx-RM2], and [RGD-Glu-($^{nat/67/68}$Ga-DO3A)-6-Ahx-RM2].

Molecular formula [RGD-Glu-[DO3A]-6-Ahx-RM2]	$C_{109}H_{163}N_{29}$
Molecular formula [RGD-Glu-[Cu-DO3A]-6-Ahx-RM2]	$C_{109}H_{163}CuN_{29}$
Molecular formula [RGD-Glu-[Ga-DO3A]-6-Ahx-RM2]	$C_{109}H_{163}GaN_{29}$
Calculated molecular mass, [RGD-Glu-[DO3A]-6-Ahx-RM2]	2343.64 Da
Calculated molecular mass, [RGD-Glu-[^{nat}Cu-DO3A]-6-Ahx-RM2]	2405.17 Da
Calculated molecular mass, [RGD-Glu-[^{nat}Ga-DO3A]-6-Ahx-RM2]	2411.34 Da
ESI-MS molecular mass ($M + H^+$), [RGD-Glu-[DO3A]-6-Ahx-RM2]	2344.86 Da
ESI-MS molecular mass ($M + H^+$), [RGD-Glu-[^{nat}Cu-DO3A]-6-Ahx-RM2]	2405.47 Da
ESI-MS molecular mass ($M + H^+$), [RGD-Glu-[^{nat}Ga-DO3A]-6-Ahx-RM2]	2411.81 Da
[RGD-Glu-[DO3A]-6-Ahx-RM2] RP-HPLC t_R	10.8 min
[RGD-Glu-[^{nat}Cu-DO3A]-6-Ahx-RM2] RP-HPLC t_R	11.3 min
[RGD-Glu-[^{64}Cu-DO3A]-6-Ahx-RM2] RP-HPLC t_R	11.4 min
[RGD-Glu-[^{nat}Ga-DO3A]-6-Ahx-RM2] RP-HPLC t_R	11.2 min
[RGD-Glu-[$^{67/68}$Ga-DO3A]-6-Ahx-RM2] RP-HPLC t_R	11.3 min
IC_{50}, [RGD-Glu-[DO3A]-6-Ahx-RM2], PC-3	9.26 ± 0.01 nM
IC_{50}, [RGD-Glu-[^{nat}Cu-DO3A]-6-Ahx-RM2], PC-3	8.64 ± 2.16 nM
IC_{50}, [RGD-Glu-[^{nat}Ga-DO3A]-6-Ahx-RM2], PC-3	7.78 ± 2.42 nM
IC_{50}, [RGD-Glu-[DO3A]-6-Ahx-RM2], U87-MG	321 ± 82.0 nM
IC_{50}, [RGD-Glu-[^{nat}Cu-DO3A]-6-Ahx-RM2], U87-MG	308 ± 0.0 nM
IC_{50}, [RGD-Glu-[^{nat}Ga-DO3A]-6-Ahx-RM2], U87-MG	307 ± 0.0 nM

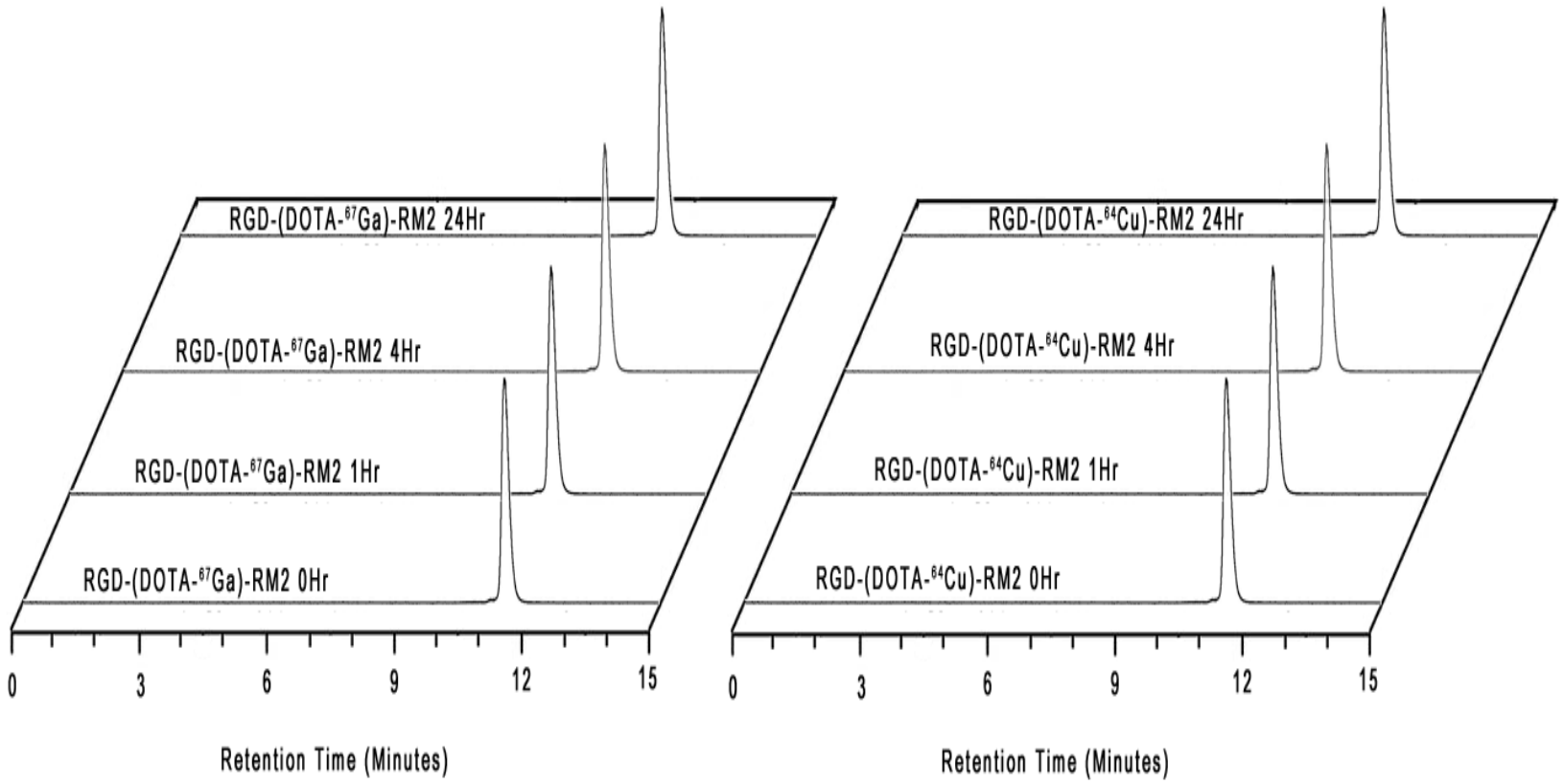

Fig. 4.2: HPLC chromatographic profiles of serum stability studies for [RGD-Glu-(^{67}Ga-DO3A)-6-Ahx-RM2] and [RGD-Glu-(^{64}Cu-DO3A)-6-Ahx-RM2

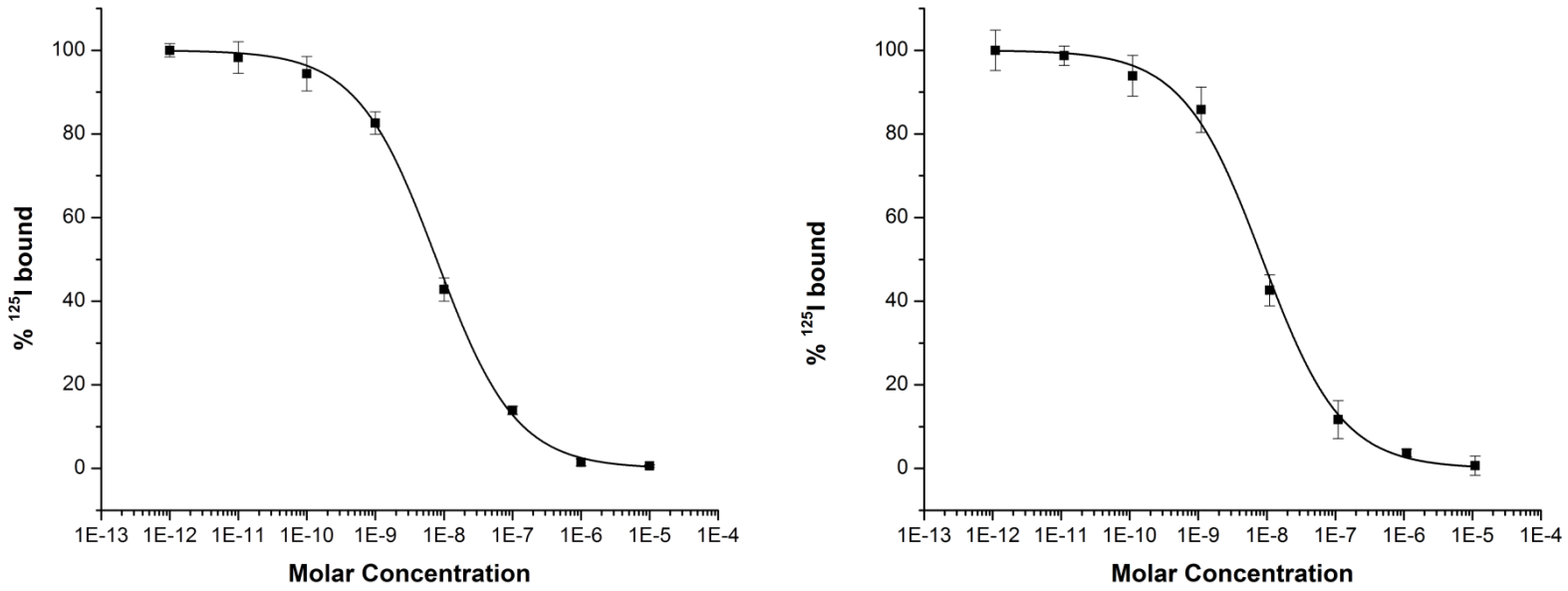

Fig. 4.3: Half-maximal inhibitory concentrations (IC_{50}) for [RGD-Glu-(^{nat}Ga-DO3A)-6-Ahx-RM2] (IC_{50} = 7.78 ± 2.42 nM, left) and [RGD-Glu-(^{nat}Cu-DO3A)-6-Ahx-RM2] (IC_{50} = 8.64 ± 2.16 nM, right) in human prostate PC-3 cells (n = 4).

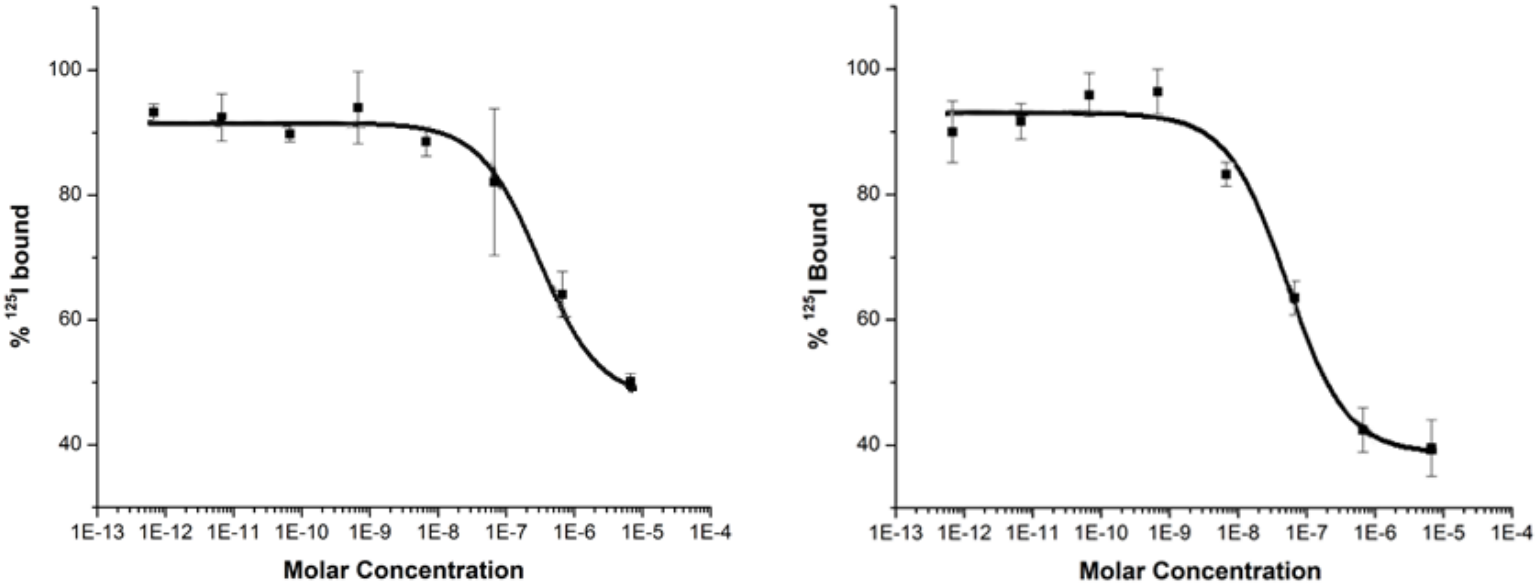

Fig. 4.4: Half-maximal inhibitory concentrations (IC_{50}) for [RGD-Glu-(^{nat}Ga-DO3A)-6-Ahx-RM2] (IC_{50} = 307 ± 0.0 nM, left) and [RGD-Glu-(^{nat}Cu-DO3A)-6-Ahx-RM2] (IC_{50} = 308 ± 0.0 nM, right) in human glioblastoma U87-MG cells (n = 4).

Biodistribution data for [RGD-Glu-(^{67}Ga/^{64}Cu-DO3A)-6-Ahx-RM2] in PC-3 tumor bearing mice are listed in Tables 4.4 and Table 4.5. Both the ^{67}Ga-labeled and the ^{64}Cu-labeled conjugates were cleared from the blood rapidly via the renal-urinary pathway. The uptake of [RGD-Glu-(^{67}Ga/^{64}Cu-DO3A)-6-Ahx-RM2] was found to be high in the implanted tumors, with 7.44 ± 1.09 %ID/g for the ^{67}Ga-ligand and 10.85 ± 4.02 %ID/g for the ^{64}Cu-ligand at 1 h p.i. Moreover, good retention in tumors was also achieved with 7.23 ± 1.12 %ID/g and 4.89 ± 1.11 %ID/g at 4 h p.i. and 24 h p.i. for the ^{67}Ga-ligand. In spite of the higher uptake in tumor at 1 h p.i., the ^{64}Cu-ligand exhibited similarly favorable retentions in tumors, with 6.89 ± 2.00 %ID/g and 4.09 ± 0.96 %ID/g at 4 h p.i. and 24 h p.i., respectively. The radioactivity washed out from normal tissues rapidly with the exception of the liver. Retention of ^{64}Cu-ligand in liver tissue remained at 1.46 ± 0.39 %ID/g and 1.75 ± 0.35 %ID/g, 4 h p.i. and 24 h p.i., respectively. Furthermore, an increase of radioactivity accumulation in the large intestine was obtained using the ^{64}Cu-ligand as the radiotracer, with 0.87 ± 0.21 %ID/g at 1 h p.i., increasing to 1.73 ± 0.58 %ID/g and 1.50 ± 0.26 %ID/g for 4 and 24 h p.i., respectively. In contrast, the ^{67}Ga-ligand possessed significantly lower uptake in the liver throughout the study and superior clearance from non-target tissues. Additionally, the ^{67}Ga-ligand complex showed lower kidney uptake (3.70 ± 0.42 %ID/g) at 1 h p.i. than the ^{64}Cu-ligand complex (4.92 ± 0.92 %ID/g), but the residual dose in the kidney decreased to low levels for both radioligands, with 1.06 ± 0.26 %ID/g and 1.15 ± 0.09 %ID/g at 24 h p.i., respectively. Table 4.6 shows tumor-to-non-target tissue ratios. The tumor-to-liver ratio of [RGD-Glu-(^{64}Cu-DO3A)-6-Ahx-RM2], with an initial value of 4.30 at 1 h p.i., reached its highest value of 5.33 at 4 h p.i. and decreased to 2.46 at 24 h p.i. By comparison, with a much higher initial value of 9.90 at 1 h p.i., [RGD-Glu-(^{67}Ga-DO3A)-6-Ahx-RM2] possessed its highest value of 10.90 at 4 h p.i. and maintained at a satisfactory ratio of 8.71

at 24 h p.i. The same trend was also observed in the tumor-to large intestine ratio. The tumor-to-L.intestine of [RGD-Glu-(^{64}Cu-DO3A)-6-Ahx-RM2] reached its highest value of 11.39 at 1 h p.i., and decreased to 4.42 and 2.81 at 4 and 24 h p.i., respectively. However, the tumor-to-large intestine value of [RGD-Glu-(^{67}Ga-DO3A)-6-Ahx-RM2], with an initial value of 7.54 at 1 h p.i., decreased to 5.41 at 4 h p.i. and reached its highest value of 8.18 at 24 h p.i. The much lower tumor to non-target tissue ratios, such as the large intestine and liver ratios of the ^{64}Cu-ligand as compared to the ^{67}Ga-ligand, offer additional strong support that ^{64}Cu(II)-DOTA complex is not as stable in vivo as the ^{67}Ga(III)-DOTA complex, probably due to its relatively low kinetic stability and the comparatively loose fitting of DOTA to the Cu (II) ion.

The results of microSPECT/microCT imaging studies for [RGD-Glu-(^{67}Ga-DO3A)-6-Ahx-RM2] in PC-3 tumor-bearing, SCID mice are presented in Fig. 4.5. The results of microPET/microCT imaging studies for [RGD-Glu-(^{64}Cu-DO3A)-6-Ahx-RM2] in PC-3 tumor-bearing, SCID mice are also presented in Fig. 4.6. Compared to the ^{64}Cu-ligand, the ^{67}Ga-ligand provided lower background retention in non-tumor tissue. Xenografted tumors were clearly observable from all other tissues at 18 h p.i. The results of imaging studies are consistent with the results of the biodistribution studies. Higher non-target abdominal tissue uptake and retention of the ^{64}Cu-ligand complex consequently decrease the corresponding tumor to non-target normal tissue ratios, thus increasing background noise in the microPET/microCT image. Additionally, [RGD-Glu-(^{64}Cu-DO3A)-6-Ahx-RM2], compared to [RGD-Glu-(^{64}Cu-NO2A)-6-Ahx-RM2] discussed in the last chapter, displayed much larger abdominal radiation, which provided strong evidence of the instability of ^{64}Cu-DOTA complex in vivo, indicating NOTA is superior to DOTA as a suitable chelating agent for ^{64}Cu.

Table 4.2. Biodistribution studies of [RGD-Glu-(^{67}Ga-DO3A)-6-Ahx-RM2] in CF-1 normal mice at 1, 4 and 24 h p.i. (%ID/g ± SD, n=5).

	1 h	4 h	24 h
Heart	0.35 ± 0.09	0.23 ± 0.21	0.11 ± 0.13
Lung	0.70 ± 0.12	0.45 ± 0.12	0.29 ± 0.16
Liver	0.77 ± 0.12	0.75 ± 0.12	0.32 ± 0.05
Kidneys	4.10 ± 1.31	2.45 ± 0.23	0.67 ± 0.09
Spleen	1.06 ± 0.61	0.96 ± 0.49	0.56 ± 0.17
Stomach	1.99 ± 1.74	0.75 ± 0.22	0.34 ± 0.06
S. Intestine	2.84 ± 1.43	0.91 ± 0.18	0.64 ± 0.10
L. Intestine	1.05 ± 0.27	1.54 ± 0.21	0.45 ± 0.15
Muscle	0.25 ± 0.20	0.13 ± 0.12	0.15 ± 0.03
Bone	0.71 ± 0.28	0.52 ± 0.16	0.27 ± 0.18
Brain	0.04 ± 0.04	0.08 ± 0.05	0.03 ± 0.03
Pancreas	11.11 ± 1.37	0.79 ± 0.20	0.42 ± 0.13
Blood*	0.60 ± 0.22	0.10 ± 0.09	0.02 ± 0.02
Urine*	65.82 ± 3.34	73.57 ± 5.05	92.40 ± 3.29

*Data presented as % ID

Table 4.3. Biodistribution studies of [RGD-Glu-(^{64}Cu-DO3A)-6-Ahx-RM2] in CF-1 normal mice at 1, 4 and 24 h p.i. (%ID/g ± SD, n=5).

	1 h	4 h	24 h
Heart	0.63 ± 0.12	0.45 ± 0.11	0.43 ± 0.04
Lung	1.28 ± 0.30	1.23 ± 0.26	1.00 ± 0.19
Liver	2.29 ± 0.31	2.52 ± 0.32	2.30 ± 0.50
Kidneys	6.03 ± 1.77	3.98 ± 0.77	1.16 ± 0.21
Spleen	0.95 ± 0.19	0.98 ± 0.19	0.66 ± 0.13
Stomach	2.06 ± 0.75	1.52 ± 0.39	0.70 ± 0.15
S. Intestine	2.15 ± 0.09	1.84 ± 0.44	1.06 ± 0.19
L. Intestine	1.19 ± 0.22	5.29 ± 3.31	1.26 ± 0.49
Muscle	0.32 ± 0.05	0.15 ± 0.04	0.14 ± 0.03
Bone	1.43 ± 0.64	0.63 ± 0.11	0.40 ± 0.28
Brain	0.07 ± 0.02	0.05 ± 0.01	0.07 ± 0.01
Pancreas	2.68 ± 0.37	0.58 ± 0.04	0.37 ± 0.06
Blood*	0.78 ± 0.20	0.25 ± 0.04	0.25 ± 0.09
Urine*	69.67 ± 3.34	73.57 ± 5.05	73.07 ± 3.29

*Data presented as % ID

Table 4.4. Biodistribution studies of [RGD-Glu-(^{67}Ga-DO3A)-6-Ahx-RM2] in PC-3 tumor-bearing SCID mice at 1, 4 and 24 h p.i. (%ID/g ± SD, n=5).

	1 h	4 h	24 h
Heart	0.63 ± 0.47	0.39 ± 0.18	0.14 ± 0.04
Lung	0.97 ± 0.21	0.54 ± 0.31	0.41 ± 0.10
Liver	0.84 ± 0.11	0.68 ± 0.14	0.58 ± 0.12
Kidneys	3.70 ± 0.42	2.34 ± 0.73	1.06 ± 0.26
Spleen	2.19 ± 0.78	1.73 ± 1.34	1.91 ± 2.51
Stomach	1.02 ± 0.35	0.48 ± 0.19	0.48 ± 0.20
S. Intestine	2.75 ± 0.24	0.92 ± 0.14	0.66 ± 0.14
L. Intestine	1.05 ± 0.23	1.56 ± 0.73	0.63 ± 0.11
Muscle	0.36 ± 0.11	0.17 ± 0.05	0.55 ± 0.85
Bone	1.48 ± 0.57	1.01 ± 0.90	0.54 ± 0.56
Brain	0.07 ± 0.04	0.05 ± 0.03	0.06 ± 0.09
Pancreas	15.84 ± 3.10	1.17 ± 0.32	0.33 ± 0.06
Blood*	0.77 ± 0.11	0.08 ± 0.07	0.03 ± 0.02
Urine*	71.29 ± 9.10	84.96 ± 0.79	85.53 ± 1.29
Tumor	7.44 ± 1.09	7.23 ± 1.12	4.89 ± 1.11

*Data presented as % ID

Table 4.5. Biodistribution studies of [RGD-Glu-(^{64}Cu-DO3A)-6-Ahx-RM2] in PC-3 tumor-bearing SCID mice at 1, 4 and 24 h p.i. (%ID/g ± SD, n=5).

	1 h	4 h	24 h
Heart	0.62 ± 0.11	0.41 ± 0.10	0.35 ± 0.14
Lung	1.54 ± 0.11	1.00 ± 0.30	0.74 ± 0.16
Liver	2.26 ± 0.30	1.46 ± 0.39	1.75 ± 0.35
Kidneys	4.92 ± 0.92	2.37 ± 0.18	1.15 ± 0.09
Spleen	2.43 ± 2.02	1.57 ± 0.71	0.79 ± 0.21
Stomach	0.77 ± 0.32	0.28 ± 0.10	0.56 ± 0.25
S. Intestine	2.01 ± 0.44	0.98 ± 0.27	0.77 ± 0.08
L. Intestine	0.87 ± 0.21	1.73 ± 0.58	1.50 ± 0.26
Muscle	0.31 ± 0.07	0.16 ± 0.07	0.14 ± 0.03
Bone	0.77 ± 0.28	0.43 ± 0.13	0.39 ± 0.11
Brain	0.06 ± 0.01	0.04 ± 0.01	0.05 ± 0.00
Pancreas	2.10 ± 0.29	0.41 ± 0.09	0.39 ± 0.05
Blood*	0.65 ± 0.20	0.21 ± 0.08	0.35 ± 0.20
Urine*	72.67 ± 26.72	84.61 ± 1.01	79.95 ± 0.95
Tumor	10.85 ± 4.02	6.89 ± 2.00	4.09 ± 0.96

*Data presented as % ID

Table 4.6. Tumor-to-non-target tissue ratios for [RGD-Glu-[^{64}Cu-DO3A]-6-Ahx-RM2] and [RGD-Glu-[^{67}Ga-DO3A]-6-Ahx-RM2] in PC-3 tumor bearing SCID mice at 1, 4, 24 h p.i. (% ID/g, n=5).

	[RGD-Glu-[^{64}Cu-DO3A]-6-Ahx-RM2]			[RGD-Glu-[^{67}Ga-DO3A]-6-Ahx-RM2]		
	1 hr	4 hr	24 hr	1 hr	4 hr	24 hr
Liver	4.30	5.33	2.46	9.09	10.90	8.71
Kidney	2.03	2.90	3.61	2.04	3.26	4.84
S. Intestine	5.03	7.37	5.29	2.73	8.03	7.86
L. Intestine	11.39	4.42	2.81	7.54	5.41	8.18
Muscle	33.80	49.54	29.11	22.46	46.61	25.90
Bone	14.58	18.30	10.91	5.91	14.69	8.45
Pancreas	4.63	17.79	10.88	0.49	6.52	14.77
Blood*	28.38	80.25	27.82	19.35	132.06	591.26

*Data based upon % ID

4.4 CONCLUSION

In this study, [RGD-Glu-(DO3A)-6-Ahx-RM2], which is a bivalent ligand with the capability of targeting either the integrin $\alpha_v\beta_3$ or GRPR biomarkers expressed on prostate cancer, was radiolabeled with ^{67}Ga/^{64}Cu to produce [RGD-Glu-(^{67}Ga/^{64}Cu-DO3A)-6-Ahx-RM2]. The new radiotracers were investigated via *in vitro* and *in vivo* studies in normal and tumor-bearing SCID mice and by microSPECT/CT and microPET/CT at 18 h p.i. of the radiotracers in tumor-bearing SCID mice. The results indicate that [RGD-Glu-(^{67}Ga/^{64}Cu-DO3A)-6-Ahx-RM2] exhibit high binding affinity for GRPR and specific targeting of prostate tumors that co-express both GRPR and $\alpha_v\beta_3$. Meanwhile, the comparative analysis indicates that the ^{67}Ga-labeled ligand shows superior *in vivo* behavior and imaging results compared to the ^{64}Cu-labeled complex despite the fact that the *in vitro* studies reflect similarly high binding affinities of corresponding cold metal coordinated ligands for GRPR and $\alpha_v\beta_3$. This is consistent with the studies of other ^{64}Cu-labeled DOTA conjugates of peptides as a result of poor stability of ^{64}Cu-DOTA *in vivo* [20-22]. It can be clearly shown when comparing [RGD-Glu-(^{64}Cu-DO3A)-6-Ahx-RM2] with a

previously studied ligand of similar structure but with a different chelator in our lab, [RGD-Glu-(^{64}Cu-NO2A)-6-Ahx-RM2], that the NOTA conjugate exhibited lower hepatic uptake than the DOTA conjugate. However, the SPECT/CT images of the ^{67}Ga-DOTA conjugate shows similarly good uptake and retention of the dose in tumors and low hepatic background compared to the ^{64}Cu-NOTA conjugate. ^{67}Ga was used as a substitute of ^{68}Ga in this study. Therefore, we anticipate similarly good microPET molecular images, albeit at shorter time-points p.i., for the ^{68}Ga labeled analogue. . In conclusion, despite similar binding affinities *in vitro*, [RGD-Glu-(^{67}Ga-DO3A)-6-Ahx-RM2] demonstrates more favorable pharmacokinetics *in vivo* than [RGD-Glu-(^{64}Cu-DO3A)-6-Ahx-RM2], which consequently indicates $^{67/68}$Ga is better choices than ^{64}Cu for the bivalent ligand, [RGD-Glu-(DO3A)-6-Ahx-RM2] due to the instability of Cu-DOTA complex *in vivo*. NOTA is superior to DOTA as a chelating agent for ^{64}Cu due to the instability of Cu-DOTA complex *in vivo*.

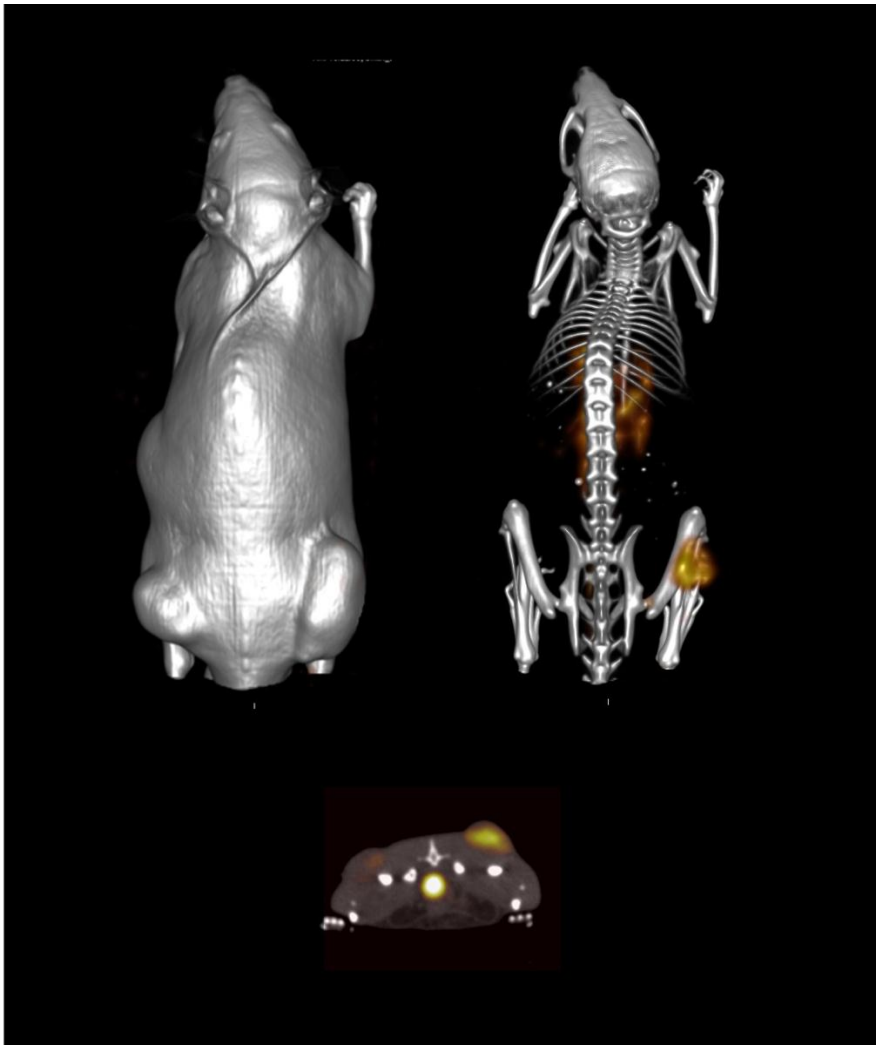

Fig. 4.5. Maximum-intensity microSPECT tumor and microCT skeletal fusion coronal whole-body image (right) and soft tissue image (left) of a PC-3 tumor-bearing SCID mouse at 18 h after tail vein injection of [RGD-Glu-(^{67}Ga-DO3A)-6-Ahx-RM2]. Axial fused microSPECT/CT image shown below.

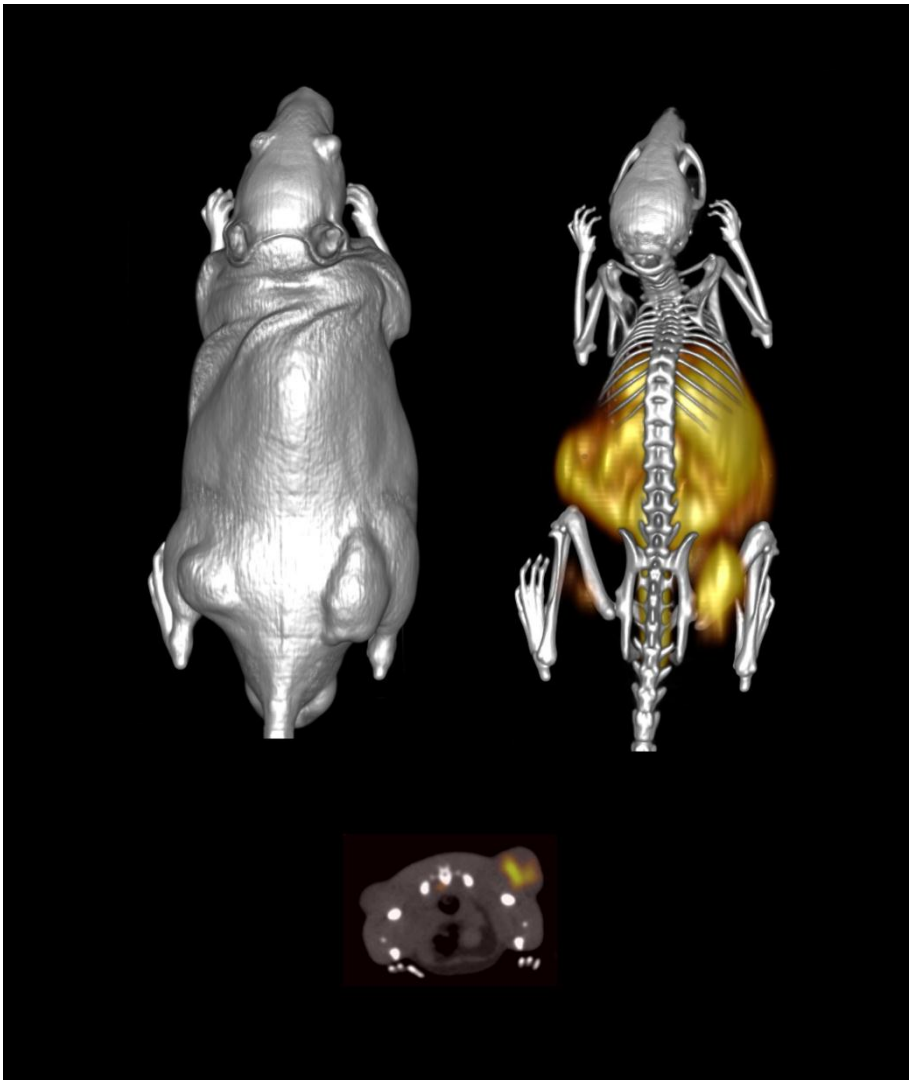

Fig. 4.6. Maximum-intensity microPET tumor and microCT skeletal fusion coronal whole-body image (right) and soft tissue image (left) of a PC-3 tumor-bearing SCID mouse at 18 h after tail vein injection of [RGD-Glu-(^{64}Cu-DO3A)-6-Ahx-RM2]. Axial fused microPET/CT image shown below.

4.5 REFERENCES

1. Markwalder, R., Reubi, J. C., Gastrin-releasing peptide receptors in the human prostate: Relation to neoplastic transformation. Cancer Res, 1999. **59**: p. 1152.
2. Smith, C. J., Volkert, W. A., Hoffman, T. J., Gastrin releasing peptide (GRP) receptor targeted radiopharmaceuticals: a concise update. Nucl Med Biol, 2003. 30: p. 861.
3. Varvarigou, A., Bouziotis, P., Zikos, C., Scopinaro, F., De Vincentis, G., Gastrin-releasing peptide (GRP) analogues for cancer imaging. Cancer Biother Radiopharm, 2004. **19**: p. 219.
4. Schroeder, R. P., Bouziotis, P., Zikos, C., Scopinaro, F., De Vincentis, G., Gastrin-releasing peptide receptor-based targeting using bombesin analogues is superior to metabolism-based targeting using choline for in vivo imaging of human prostate cancer xenografts. Eur J Nucl Med Mol Imaging, 2011. 38: p. 1257.
5. Yu, Z., Ananias, H. J., Carlucci, G., Hoving, H. D., Helfrich, W., Dierckx, R. A., Wang, F., de Jong, I. J., Elsinga, P. H., An update of radiolabeled bombesin analogs for gastrin-releasing peptide receptor targeting. Curr Pharm Des, 2013. **19**: p. 3329.
6. Thomas, R., Chen, J., Roudier, M. M., Vessella, R. L., Lantry, L. E., Nunn, A. D., In vitro binding evaluation of ^{177}Lu-AMBA, a novel ^{177}Lu-labeled GRP-R agonist for systemic radiotherapy in human tissues. Clin Exp Metastasis, 2009. **26**: p. 105–19.
7. Abiraj, K., Mansi, R., Tamma, M. L., Fani, M., Forrer, F., Nicolas, G., Cescato, R., Reubi, J. C., Maecke, H. R., Bombesin antagonist based radioligands for translational nuclear imaging of gastrin-releasing peptide receptor-positive tumors. J Nucl Med, 2011. **52**: p. 1970.
8. Dumont, R. A., Tamma, M., Braun, F., Borkowski, S., Reubi, J. C., Maecke, H., Weber, W. A., Mansi, R., Targeted radiotherapy of prostate cancer with a gastrin-releasing peptide receptor antagonist is effective as monotherapy and in combination with rapamycin. J Nucl Med, 2013. **54**: p. 762.
9. Cescato, R., Maina, T., Nock, B., Nikolopoulou, A., Charalambidis, D., Piccand, V., Reubi, J. C., Bombesin receptor antagonists may be preferable to agonists for tumor targeting. J Nucl Med, 2008. **49**: p. 318.
10. Ginj, M., Zhang, H., Waser, B., Cescato, R., Wild, D., Wang, X., Erchegyi, J., Rivier, J., Mäcke, H. R., Reubi, J. C., Radiolabeled somastostatin receptor antagonists are preferable to agonists for in vivo peptide receptor targeting of tumors. Proc Natl Acad Sci USA, 2006. **103**: p. 16436.
11. Anderson, C. J., Welch, M. J., Radiometal-labeled agents (non-technetium) for diagnostic imaging. Chem. Rev, 1999. **99**: p. 2219.
12. Ruoslahti, E., Pierschbacher, M. D., New perspectives in cell adhesion: RGD and integrins. Science, 1987. **238**: p. 491.
13. Romanov, V. I., Goligorsky, M. S., RGD-recognizing integrin mediate interactions of human prostate carcinoma cells with endothelial cells in vitro. Prostate, 1999. **39**: p. 108.
14. Gladson, C. L., Cheresh, D. A., Glioblastoma expression of vitronectin and the $\alpha_v\beta_3$ integrin. Adhesion mechanism for transformed glial cells. J Clin Invest, 1991. **88**: p. 1924.
15. Durkan, K., Jiang, Z., Rold, T. L., Sieckman, G. L., Hoffman, T. J., Bandari, R. P., Szczodroski, A. F., Liu, L., Miao, Y., Reynolds, T. S., Smith, C. J., A heterodimeric [RGD-Glu-[^{64}Cu-NO2A]-6-Ahx-RM2] $\alpha_V\beta_3$/GRPr-targeting antagonist radiotracer for PET imaging of prostate tumors. Nucl Med Biol, 2014. **41**: p. 133.

16. Stott Reynolds, T. J., Schehr, R., Liu, D., Xu, J., Miao, Y., Hoffman, T. J., Rold, T. L., Lewis, M. R., Smith, C. J., Characterization and evaluation of DOTA-conjugated Bombesin/RGD-antagonist for prostate cancer tumor imaging and therapy. Nucl Med Biol, 2015. **42**: p. 99.
17. Jackson, A. B., Nanda, P. K., Rold, T. L., Sieckman, G. L., Szczodroski, A. F., Hoffman, T. J., Chen, X., Smith, C. J., ^{64}Cu-NO2A-RGD-Glu-6-Ahx-BBN(7-14)NH_2: a heterodimeric targeting vector for positron emission tomography imaging of prostate cancer. Nucl Med Biol, 2012. **39**: p. 377.
18. Jackson, A. B., Nanda, P. K., Rold, T. L., Sieckman, G. L., Szczodroski, A. F., Hoffman, T. J., Chen, X., Smith, C. J., ^{64}Cu-NO2A-RGD-Glu-6-Ahx-BBN(7-14)NH_2: a heterodimeric targeting vector for positron emission tomography imaging of prostate cancer. Nucl Med Biol, 2012. **39**: p. 377.
19. Cutler, C. S., Hennkens, H. M., Sisay, N., Huclier-Markai, S., Jurisson, S. S., Radiometals for combined imaging and therapy. Chem Rev, 2013. **113**: p. 858.
20. Garrison, J. C., Rold, T. L., Sieckman, G. L., Figueroa, S. D., Volkert, W. A., Jurisson, S. S., Hoffman, T. J., In vivo evaluation and small-animal PET/CT of a prostate cancer mouse model using ^{64}Cu bombesin analogs: side-by-side comparison of the CB-TE2A and DOTA chelation system. J Nucl Med, 2007. **48**: p. 1327.
21. Bass, L. A., Wang, M., Welch, M. J., Anderson, C. J., In vivo transchelation of copper-64 from TETA-octreotide to superoxide dismutase in rat liver. Bioconjug Chem, 2000. **11**: p. 527.
22. Boswell, C. A., Sun, X., Niu, W., Weisman, G. R., Wong, E. H., Rheingold, A. L., Anderson, C. J., Comparative in vivo stability of copper-64-labeled cross-bridged and conventional tetraazamacrocyclic complexes. J Med Chem, 2004. **47**: p. 1465.

Chapter 5: FUTURE STUDIES

5.1 INTRODUCTION

In the GRPR/PSMA dual targeting project, the microPET imaging studies of the ^{64}Cu-labeled ligand, [DUPA-6-Ahx-(^{64}Cu-NODAGA)-5-Ava-BBN(7-14)NH_2], showed obvious background radiation in non-target tissues, although the xenografted tumors were discernible. As a result, further optimizations are necessary to improve pharmacokinetics of the ligand. A new ligand precursor, [DUPA-6-Ahx-K-6-Ahx-RM2], has been synthesized and characterized. As compared to [DUPA-6-Ahx-K-5-Ava-BBN(7-14)NH_2], the new ligand used RM2 as the targeting motif for GRPR and replaced 5-aminovaleric acid with 6-aminohexanoic acid in the structure. In this chapter, preliminary data and future plans of the study on the DOTA conjugate of [DUPA-6-Ahx-K-6-Ahx-RM2] will be described.

5.2 PRELIMINARY WORK

5.2.1 Synthesis of [DUPA-6-Ahx-(DO3A)-6-Ahx-RM2]

First of all, the bivalent ligand precursor, [DUPA-6-Ahx-K-6-Ava-RM2], was synthesized via a combination of solid phase and manual peptide synthesis using traditional F-moc chemistry. Then, DOTA was conjugated onto the ε-amine of lysine (K) on the bivalent peptide precursor, [DUPA-6-Ahx-K-6-Ahx-RM2], via an active ester using a modified procedure that has been previously described. Briefly, [DUPA-6-Ahx-K-6-Ava-RM2] (2.7 μmol) was dissolved in 0.1 M sodium phosphate buffer and the pH was adjusted to 7.4 using 10% NaOH. DOTA-NHS (27 μmol), dissolved in 200 μL of 0.1 M sodium phosphate buffer (pH = 7.0), was mixed with the peptide solution. The reaction mixture was stirred for 6 h at 5–10 ℃, followed by stirring overnight at ambient temperature. The bivalent DOTA conjugate was purified by RP-HPLC and then characterized via ESI-MS.

5.2.2 Metallation of [DUPA-6-Ahx-(DO3A)-5-Ava-BBN(7-14)NH_2] with ^{nat}Ga

The ^{nat}Ga-metallated DOTA conjugates were produced by adding natural $GaCl_3$ in 0.05 N HCl (90 nmol) to purified [DUPA-6-Ahx-(DO3A)-6-Ahx-RM2] peptide conjugate (80 nmol, 250 µl 0.4 M ammonium acetate). The pH of the reaction mixture was adjusted to approximately 5.0 by the addition of 1% NaOH. The mixtures were incubated for 1 h at 90 ℃ and then 50 µl of 10 mM DTPA (diethylenetriaminepentaacetic acid) solution was added to scavenge unbound metal. The metallated conjugates, [DUPA-6-Ahx-(^{nat}Ga-DO3A)-6-Ahx-RM2], were purified by RP-HPLC and characterized by ESI-MS.

5.3 PRELIMINARY DATA

[DUPA-6-Ahx-K-6-Ahx-RM2] was synthesized by solid-phase peptide synthesis (SPPS) combined with manual peptide synthesis using F-moc chemistry. [DUPA-6-Ahx-(DO3A)-6-Ahx-RM2] was produced via conjugation reaction of the precursor with the active DOTA-ester, and then metallated with the natural metals of interest ^{nat}Ga. The chemical structure of the DOTA conjugate is shown in Fig. 5.1. The mass spectrometry results of [DUPA-6-Ahx-(DO3A)-6-Ahx-RM2] and [DUPA-6-Ahx-(^{nat}Ga-DO3A)-6-Ahx-RM2] is shown in Fig. 5.2 and Fig. 5.3.

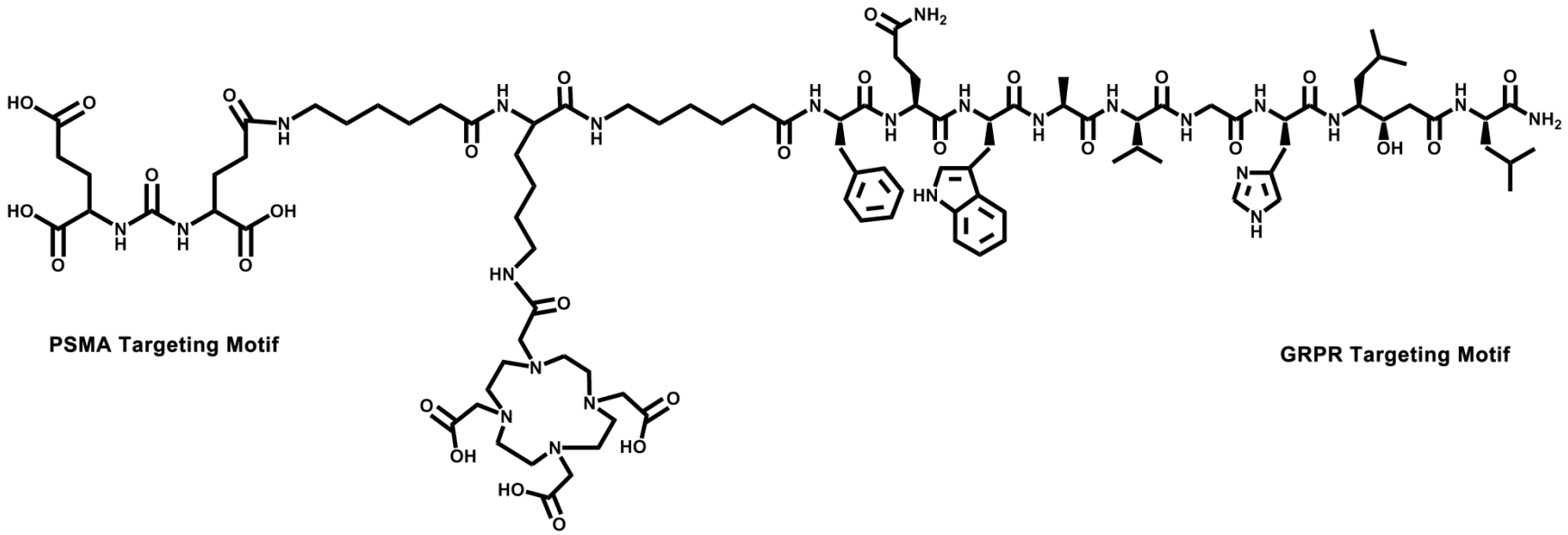

Fig. 5.1: Chemical structure of [DUPA-6-Ahx-(DO3A)-6-Ahx-RM2].

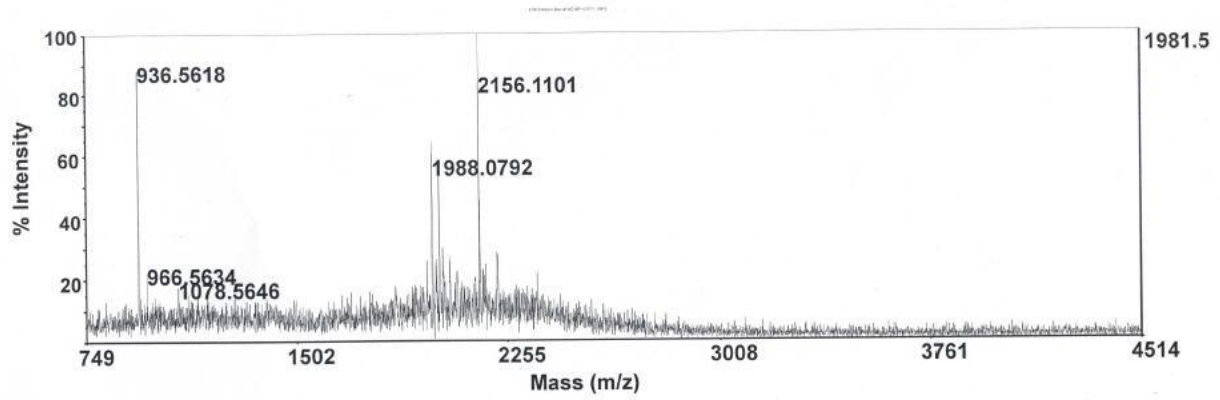

Fig.5.2: ESI mass spectrum (M + H^+ = 2056.11) for [DUPA-6-Ahx-(DO3A)-6-Ahx-RM2] (Calculated Mass = 2155.13).

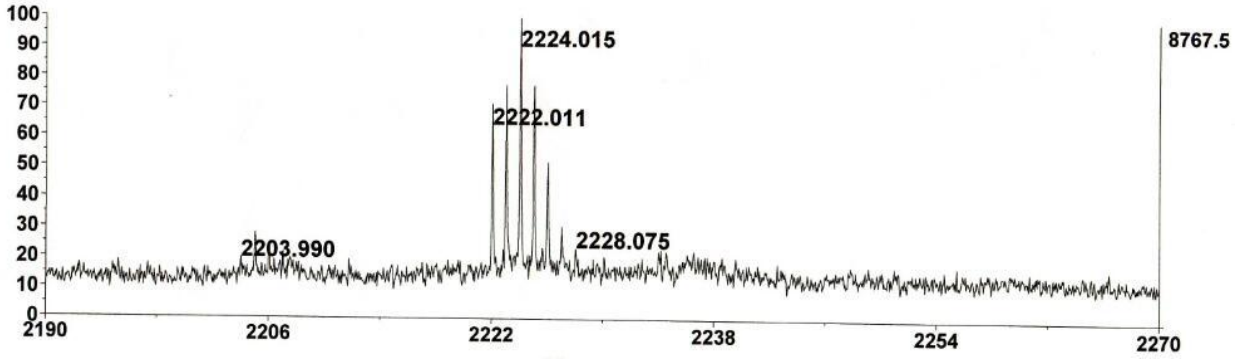

Fig.5.3: ESI mass spectrum for [DUPA-6-Ahx-(^{nat}Ga-DO3A)-6-Ahx-RM2] (Calculated Mass = 2222.37).

5.4 FUTURE WORK

The bivalent DOTA conjugate can be metallated with other natural metals of interest (^{nat}Lu, ^{nat}In). The bivalent DOTA conjugate can be radiolabeled with the radiometals of interest ($^{67/68}$Ga, ^{177}Lu, ^{111}In). Afterwards, for *in vitro* investigations of the ligands, the stability of the tracers labeled with the radioactive metals of interest can be evaluated via RP-HPLC analysis at 0, 4, 24 h post-radiolabeling. The IC_{50} values of natural metal (^{nat}Ga, ^{nat}Lu, ^{nat}In) metallated ligands can be obtained by the competitive displacement binding assays in GRPR-positive, human PC-3 prostate cancer cells and PSMA-positive LNCaP homogenized cell membranes using [^{125}I-(Tyr^4)-BBN] and [$^{+}$N-acetyl aspartyl ^{3}H-glutamate] (NAAG) as the radioligands. The IC_{50} values will indicate the binding affinity of the ligands to GRPR and PSMA, respectively.

For *in vivo* investigations, biodistribution studies of the DOTA conjugates metallated with the radioactive metals of interest ($^{67/68}$Ga, ^{177}Lu, ^{111}In) can be conducted in CF-1 normal mice, GRPR tumor-bearing SCID mice, and LNCaP tumor-bearing athymic nude mice. MicroPET/CT or microSPECT/CT studies of each tracer can be also performed in GRPR tumor-bearing SCID mice and LNCaP tumor-bearing athymic nude mice.

VITA

Zongrun Jiang was born on June 16, 1988, in Zhejiang, China. He graduated from Shanghai High School in July, 2007. He earned a Bachelor degree in Chemistry from the Shanghai Jiao Tong University in June, 2011. He received a Ph.D. in Chemistry with a specialization in Radiopharmaceutical Chemistry from the University of Missouri-Columbia (2015). He is planning to continue his research in the area of radiochemistry.